

GSI-Preprint-01-30, December 2001

Scattering of vector mesons off nucleons

M.F.M. Lutz^{a,b}, Gy. Wolf^c and B. Friman^{a,b}

^a *GSI, Planckstr. 1, D-64291 Darmstadt, Germany*

^b *Institut für Kernphysik, TU Darmstadt
D-64289 Darmstadt, Germany*

^c *KFKI RMKI, H-1525 Budapest POB. 49, Hungary*

Abstract

We construct a relativistic and unitary approach to 'high' energy pion- and photon-nucleon reactions taking the $\pi N, \pi\Delta, \rho N, \omega N, \eta N, K\Lambda, K\Sigma$ final states into account. Our scheme dynamically generates the s- and d-wave nucleon resonances $N(1535)$, $N(1650)$ and $N(1520)$ and isobar resonances $\Delta(1620)$ and $\Delta(1700)$ in terms of quasi-local interaction vertices. The description of photon-induced processes is based on a generalized vector-meson dominance assumption which directly relates the electromagnetic quasi-local 4-point interaction vertices to the corresponding vertices involving the ρ and ω fields. We obtain a satisfactory description of the elastic and inelastic pion- and photon-nucleon scattering data in the channels considered. The resulting s-wave ρ - and ω -nucleon scattering amplitudes are presented. Using these amplitudes we compute the leading density modification of the ρ and ω energy distributions in nuclear matter. We find a repulsive energy shift for the ω meson at small nuclear density but predict considerable strength in resonance-hole like ω -meson modes. Compared to previous calculations our result for the ρ -meson spectral function shows a significantly smaller in-medium effect. This reflects a fairly small coupling strength of the $N(1520)$ resonance to the ρN channel.

1 Introduction

The decay of vector mesons into e^+e^- and $\mu^+\mu^-$ pairs offers a unique tool to explore the properties of dense and hot matter in nuclear collisions. The lepton pairs provide virtually undistorted information on the current-current correlation function $\langle j_\mu j_\nu \rangle$ in the medium [1]. At invariant masses in the range 500 – 1000 MeV, $\langle j_\mu j_\nu \rangle$ is sensitive to in-medium modifications of the mass distribution of the light vector mesons ρ and ω . Indeed, the observed enhancement of the di-lepton yield at small invariant masses in ultra relativistic heavy ion collisions [2] is presently interpreted in terms of in-medium modifications

of the mass and width of the ρ meson [3–14]. To leading orders in the baryon density, modifications of the mass distribution are determined by the vector-meson nucleon scattering amplitudes. Since these amplitudes are not directly constrained by data, there are presently large theoretical ambiguities in predictions of the vector-meson spectral densities in nuclear matter.

This work is an attempt to overcome this problem by using the constraints from data on pion- and photon-nucleon reactions considering in particular the ω and ρ production data in a systematic way. We develop a coupled-channel approach for meson-baryon and photon-baryon scattering, including the $\gamma N, \pi N, \rho N, \omega N, \pi\Delta, \eta N, K\Lambda$ and $K\Sigma$ channels where the interaction kernel is approximated by quasi-local 4-point interaction vertices. The description of photon-induced reactions is based on a vector-meson dominance type assumption which directly relates the electromagnetic quasi-local 4-point interaction vertices to the corresponding vertices involving the ρ and ω fields. In such a scheme the amplitudes for experimentally non-accessible processes like ρN and ωN scattering are constrained by the data on elastic πN scattering and inelastic reactions like the pion-and photon-induced production of vector mesons. Our primary goal is to derive the vector-meson nucleon scattering amplitudes close to threshold, which in turn determine the self energy of a vector-meson at rest in nuclear matter to leading order in density. Thus it is sufficient to consider only s-wave scattering in the ρN and ωN channels. As a consequence of parity conservation, this implies that in the πN and $\pi\Delta$ channels we need only s- and d-waves. In particular, we consider the S_{11}, S_{31}, D_{13} and D_{33} partial waves of πN scattering. To derive systematically the momentum dependence of the vector-meson self energy, vector-meson nucleon scattering in higher partial waves would have to be considered in addition. We concentrate on the energy window $1.4 \text{ GeV} < \sqrt{s} < 1.8 \text{ GeV}$ and base our analysis on the conjecture that all baryon resonances except the baryon octet and decuplet ground states are generated by coupled channel dynamics. Under these assumptions the application of quasi-local interaction terms is justified, because in all considered channels the interaction kernel is slowly varying in energy.

In this paper we expand the scope of existing coupled channel calculations [15–17,19] in several ways. First, we attempt a comprehensive description of pion and photon induced reactions, including for the first time the $\rho N, \omega N$ photon-nucleon channels on equal footing. Thus, we describe elastic πN scattering as well as pion and photon induced production cross sections within the same model. Second, our approach is consistent with analyticity and causality, i.e. the amplitudes satisfy dispersion relations. This is not the case for models that employ the K-matrix approximation or extensions thereof [15,16,19]. Analyticity is a fundamental property of the S-matrix and the analytic structure of the scattering amplitude plays an important role e.g. close to thresholds (see e.g. [18]). Since we are addressing the physics in an energy range where several

production thresholds are located, this is an important feature of our model. Finally, in our approach, which applies and generalizes the covariant projector technique of [20], baryon resonances can be generated by coupled channel dynamics. This offers an appropriate framework for testing the conjecture of dynamical generation of resonances [20]. If this conjecture is correct, a more economical description of the scattering amplitude follows, since there is no need for introducing explicit baryon resonances in the interaction kernel. We note that in the K-matrix approximation, the lack of analyticity prohibits the dynamical generation of resonances. Thus, in such an approach the baryon resonances must be explicitly included in the interaction kernel,

We obtain a satisfactory description of the elastic and inelastic πN and γN reaction data in the channels considered. The s- and d-wave nucleon resonances $N(1535)$, $N(1650)$ and $N(1520)$ and isobar resonances $\Delta(1620)$ and $\Delta(1700)$ are generated dynamically in our approach. Whereas we predict considerable strength for the $N(1520)$ nucleon-hole component of the ω meson in nuclear matter, our analysis suggests only a moderate importance of the $N(1520)$ nucleon-hole states in the in-medium spectral function of the ρ meson.

In section 2 we first present the general hadronic coupled channel approach within the framework of the covariant projector operator technique of [20]. We first introduce the projection operators for elastic πN scattering and subsequently generalize the scheme to include inelastic reactions between the different coupled channels. In the following section the specifics of the ρN and $\pi \Delta$ channels are presented, while in section 4 we give the framework for the treatment of electromagnetic interactions. There we also motivate our choice for the vector meson dominance assumption. Readers who are not interested in the technical details of the calculation may skip sections 2-4 and jump to the results, which are presented in section 5. There the basic ingredients of our approach are recalled with appropriate references to the central equations in sections 2-4.

2 Relativistic coupled-channel dynamics

In this section we present the theoretical framework for our analysis of the meson-baryon scattering process. We construct an effective Lagrangian with quasi-local four-point meson-baryon contact interactions. Within this framework, the Bethe-Salpeter equation for the coupled-channel system reduces to a matrix equation. The justification of our approximation strategy follows from two assumptions. First, we conjecture that all baryon resonances except the baryon octet and decuplet ground states are dynamically generated by coupled channel dynamics. And second, we aim at a description of elastic and inelastic pion-nucleon scattering in an energy window $1400 \text{ MeV} < \sqrt{s} < 1800 \text{ MeV}$

only, where the interaction kernel is slowly varying in energy in all channels considered. This will be explained in detail later.

In order to keep the discussion transparent, we first restrict ourselves to the pion-nucleon sector. Consider the general pion-nucleon four-point interaction in momentum space

$$\mathcal{L}_{\pi N}(\bar{k}, k; w) = \frac{1}{2} \sum_{ijkl} \pi_i^\dagger(\bar{q}) \bar{N}_j(\bar{p}) K_{ijkl}(\bar{k}, k; w) N_k(p) \pi_l(q), \quad (1)$$

where i, j, k, l are isospin indices, and K is a matrix in spinor space, which in general is a function of the relative momenta in the initial and final states $k = \frac{1}{2}(p - q)$ and $\bar{k} = \frac{1}{2}(\bar{p} - \bar{q})$ as well as the total momentum $w = p + q = \bar{p} + \bar{q}$. Here we use a generic two-body interaction kernel K at tree-level as to specify the conventions applied throughout this work. The relation of the momentum-space object (1) to the Lagrangian density $\mathcal{L}(x)$ is obtained by defining the action,

$$\begin{aligned} \int d^4x \mathcal{L}(x) &= \int \frac{d^4k}{(2\pi)^4} \frac{d^4\bar{k}}{(2\pi)^4} \frac{d^4w}{(2\pi)^4} \mathcal{L}(\bar{k}, k; w), \\ \pi(q) &= \int d^4x e^{i q \cdot x} \pi(x), \quad \pi^\dagger(\bar{q}) = \int d^4x e^{-i \bar{q} \cdot x} \pi(x), \\ N(p) &= \int d^4x e^{i p \cdot x} N(x), \quad \bar{N}(\bar{p}) = \int d^4x e^{-i \bar{p} \cdot x} \bar{N}(x). \end{aligned} \quad (2)$$

Without loss of generality we may assume a crossing symmetric interaction kernel with

$$K_{ijkl}(\bar{k}, k; w) = K_{l j k i}((\bar{p} + q)/2, (p - \bar{q})/2; p - \bar{q}), \quad (3)$$

simplifying the identification of any exchange term contribution. The fact that the effective interaction $\mathcal{L}(\bar{k}, k; w)$ depends only on three combinations of the four 4-momenta introduced in (2) is a consequence of the invariance of the coordinate-space interaction kernel under time- and space-translation. Note for instance that the momenta q and \bar{q} of the $\pi(q)$ and $\pi^\dagger(\bar{q})$ fields do not represent the 4-momenta of the physical pion states. This interpretation is legitimate only after the pion field is decomposed into positive and negative frequency parts¹

$$\pi_i^{(+)}(x) = \int \frac{d^3p}{(2\pi)^3 2p_0} a_i(p) e^{-ipx},$$

¹ We use the normalization of Itzykson and Zuber [21].

$$\pi_i^{(-)}(x) = \int \frac{d^3 p}{(2\pi)^3 2p_0} a_i^\dagger(p) e^{ipx}. \quad (4)$$

In order to construct the isospin projectors, it is useful to split also the nucleon field into positive and negative frequency parts, defined by

$$\begin{aligned} N^{(+)}(x) &= \sum_s \int \frac{d^3 p}{(2\pi)^3} \frac{m_N}{p_0} u(p, s) b(p, s) e^{-ipx}, \\ N^{(-)}(x) &= \sum_s \int \frac{d^3 p}{(2\pi)^3} \frac{m_N}{p_0} v(p, s) d^\dagger(p, s) e^{ipx}, \end{aligned} \quad (5)$$

where $u(p, s)$ and $v(p, s)$ are the positive and negative energy spinors, respectively. Here, $a_i(p)$ and $a_i^\dagger(p)$ are the pion annihilation and creation operators, while $b(p, s)$ is the nucleon annihilation operator and $d^\dagger(p, s)$ is the anti-nucleon creation operator.

For the construction of the Bethe-Salpeter kernel, it is convenient to rearrange the interaction Lagrangian, $\mathcal{L}_{\pi N}(\bar{k}, k; w)$, which is considered in momentum space, as a sum of terms that project onto states of good isospin²

$$\begin{aligned} \mathcal{L}_{\pi N}(\bar{k}, k; w) &= \frac{1}{3} \bar{N}^{(+)}(\bar{p}) [\vec{\tau} \cdot \vec{\pi}^{(-)}(\bar{q})] K^{(\frac{1}{2})}(\bar{k}, k; w) [\vec{\pi}^{(+)}(q) \cdot \vec{\tau}] N^{(+)}(p) \\ &\quad + \bar{N}^{(+)}(\bar{p}) [\vec{T} \cdot \vec{\pi}^{(-)}(\bar{q})] K^{(\frac{3}{2})}(\bar{k}, k; w) [\vec{\pi}^{(+)}(q) \cdot \vec{T}] N^{(+)}(p) + \dots, \end{aligned} \quad (6)$$

where τ_i is a Pauli matrix in isospin space and T_i an isospin 1/2 to 3/2 transition matrix and $K^{(I)}$ the interaction kernel for states with isospin I . The normalization of the isospin transition matrices is such that $T_i^\dagger T_j = \delta_{ij} - \tau_i \tau_j / 3$. In (6) we have only written the terms that explicitly contribute to pion-nucleon scattering in the Born approximation. These are sufficient to specify the tree-level Bethe-Salpeter kernel. The additional terms, indicated by the dots in (6), contribute to the production and absorption of two pions and are uniquely determined by covariance.

It is straightforward to generalize this scheme to the coupled-channel problem at hand. The interaction Lagrangian can thus be written in the form

$$\mathcal{L}(\bar{k}, k; w) = \sum_I R^{(I)\dagger}(\bar{q}, \bar{p}) \gamma_0 K^{(I)}(\bar{k}, k; w) R^{(I)}(q, p) + \dots \quad (7)$$

where again we show only those terms that contribute to meson-baryon scattering in the Born approximation. The state vectors $R^{(I)}(q, p)$ are given by

² We assume perfect isospin symmetry.

$$R^{(\frac{1}{2})} = \begin{pmatrix} \frac{1}{\sqrt{3}} (\vec{\pi}^{(+)} \cdot \vec{\tau}) N^{(+)} \\ \frac{1}{\sqrt{2}} (\vec{\pi}^{(+)} \cdot \vec{T}^\dagger) \Delta_\mu^{(+)} \\ \frac{1}{\sqrt{3}} (\vec{\rho}_\mu^{(+)} \cdot \vec{\tau}) N^{(+)} \\ \omega_\mu^{(+)} N^{(+)} \\ \eta^{(+)} N^{(+)} \\ K^{(+)} \Lambda^{(+)} \\ \frac{1}{\sqrt{3}} (\vec{\Sigma}^{(+)} \cdot \vec{\tau}) K^{(+)} \end{pmatrix}, \quad R^{(\frac{3}{2})} = \begin{pmatrix} (\pi^{(+)} \cdot T) N^{(+)} \\ \sqrt{\frac{3}{5}} T_i (\vec{\pi}^{(+)} \cdot \vec{\tau}) T_i^\dagger \Delta_\mu^{(+)} \\ (\vec{\rho}_\mu^{(+)} \cdot \vec{T}) N^{(+)} \\ (\vec{\Sigma}^{(+)} \cdot \vec{T}) K^{(+)} \end{pmatrix} \quad (8)$$

Note that the spin and isospin structure of the states is implicit in (8). Thus, ρ_μ is an isovector and ω_μ an isoscalar vector field, while e.g. the nucleon is an isospin doublet Dirac spinor field. Similarly, the Δ_μ is a Rarita-Schwinger isospin 3/2 field. These fields combine with the corresponding elements of the kernel $K^{(I)}(\bar{k}, k, w)$ and the isospin operators in (8). For instance, the vector index of the ρ_μ and ω_μ fields are contracted with a vector index of the corresponding term in the kernel.

The coupled-channel Bethe-Salpeter equation ³ projected onto a given isospin then reads

$$T_{ab}^{(I)}(\bar{k}, k; w) = K_{ab}^{(I)}(\bar{k}, k; w) + \sum_{c,d} \int \frac{d^4 l}{(2\pi)^4} K_{ac}^{(I)}(\bar{k}, l; w) G_{cd}^{(I)}(l; w) T_{db}^{(I)}(l, k; w),$$

$$G_{cd}^{(I)}(l; w) = -i D_{\Phi(I,c)\Phi(I,d)}\left(\frac{1}{2}w - l\right) S_{B(I,c)B(I,d)}\left(\frac{1}{2}w + l\right), \quad (9)$$

where $D_{\Phi(I,c)\Phi(I,d)}(q)$ and $S_{B(I,c)B(I,d)}(p)$ denote the meson and baryon propagators in a given channel. Evidently the interaction kernel $K_{ab}^{(I)}(\bar{k}, k; w)$ in the Bethe-Salpeter equation (9) is not necessarily restricted to the tree-level expressions discussed in detail above. It encompasses all Feynman diagrams which are two-particle irreducible in the s-channel. Off-diagonal components of $G^{(I)}$ are due to the matrix structure of the vector-meson and isobar propagators. A convenient labelling of the channels is obtained by defining

$$\begin{aligned} \Phi\left(\frac{1}{2}, a\right) &= (\pi, \pi, \rho_\mu, \omega_\mu, \eta, K, K)_a, & B\left(\frac{1}{2}, a\right) &= (N, \Delta_\mu, N, N, N, \Lambda, \Sigma)_a, \\ \Phi\left(\frac{3}{2}, a\right) &= (\pi, \pi, \rho_\mu, K)_a, & B\left(\frac{3}{2}, a\right) &= (N, \Delta_\mu, N, \Sigma)_a. \end{aligned} \quad (10)$$

The meson and baryon propagators $D_{\Phi(I,c)\Phi(I,d)}(q)$ and $S_{B(I,c)B(I,d)}(p)$ in (9) are

³ We apply here the conventions of Itzykson and Zuber [21] where the 'amputated' Greens function $G_{X \rightarrow Y}^{\text{amp}}$ defines the scattering amplitudes with $G_{\pi N \rightarrow \pi N}^{\text{amp}} = i T_{\pi N \rightarrow \pi N}$, $G_{VN \rightarrow VN}^{\text{amp}} = -i T_{VN \rightarrow VN}$ but $G_{\pi N \rightarrow VN}^{\text{amp}} = T_{\pi N \rightarrow VN}$ and $G_{VN \rightarrow \pi N}^{\text{amp}} = T_{VN \rightarrow \pi N}$. The analogous convention is chosen for the $\pi\Delta$ channel.

$$\begin{aligned}
D_{\pi\pi}(q) &= \frac{1}{q^2 - m_\pi^2 + i\epsilon}, & S_{NN}(q) &= \frac{1}{q^2 - m_N^2 + i\epsilon}, \\
D_{\rho^\mu\rho^\nu}(q) &= \int_{4m_\pi^2}^{\infty} \frac{d m^2}{\pi} \left(g^{\mu\nu} - \frac{q^\mu q^\nu}{m^2} \right) \frac{\rho_\rho(m^2)}{q^2 - m^2 + i\epsilon}, \\
S_{\Delta^\mu\Delta^\nu}(q) &= \int_{(m_N+m_\pi)^2}^{\infty} \frac{d m^2}{\pi} \left(g^{\mu\nu} \left(\not{q} + \sqrt{m^2} \right) + \frac{1}{3} \gamma^\mu \left(\not{q} - \sqrt{m^2} \right) \gamma^\nu \right. \\
&\quad \left. + \frac{1}{3\sqrt{m^2}} \left(q^\mu \left(\not{q} - \sqrt{m^2} \right) \gamma^\nu + \gamma^\mu \left(\not{q} - \sqrt{m^2} \right) q^\nu \right) \right. \\
&\quad \left. - \frac{2}{3} \frac{q^\mu q^\nu}{m^2} \left(\not{q} + 2\sqrt{m^2} \right) \right) \frac{\rho_\Delta(m^2)}{q^2 - m^2 + i\epsilon}. \tag{11}
\end{aligned}$$

The spectral distributions of the vector mesons, ρ_ρ and ρ_ω , and that of the isobar-resonance, ρ_Δ , will be specified in the subsequent section, where the pion-induced vector-meson and isobar production processes are discussed. The propagators of the η and K mesons as well as of the Λ and Σ baryons are, except for the mass, identical to the pion and nucleon propagators, respectively.

A convenient way to perform the partial-wave expansion is offered by the covariant projector formalism introduced in [20]. A detailed discussion of the underlying strategy leading to the projector formulation can be found in that paper. Here we generalize this approach in order to include the $\rho_\mu N$, $\omega_\mu N$ and $\pi\Delta_\mu$ channels. The interaction kernel $K_{ab}^{(I)}$ is expanded in a series of channel-dependent projectors $[Y_n^{(\pm)}(\bar{q}, q; w)]_{ab}$,

$$\begin{aligned}
K_{ab}^{(I)}(\bar{q}, q; w) &= \sum_{n=0}^{\infty} V_{ab}^{(I+)}(\sqrt{s}; n) [Y_n^{(+)}(\bar{q}, q; w)]_{ab} \\
&\quad + \sum_{n=0}^{\infty} V_{ab}^{(I-)}(\sqrt{s}; n) [Y_n^{(-)}(\bar{q}, q; w)]_{ab}, \tag{12}
\end{aligned}$$

with $s = w^2$, $n = J - \frac{1}{2}$ and a set of energy-dependent effective interaction kernels $V_{ab}^{(I\pm)}(\sqrt{s}; n)$. The projectors are constructed in a way that states corresponding to different projectors with given total angular momentum $J = n + \frac{1}{2}$ do not couple in the Bethe-Salpeter equation (9). Any given projector $Y_n^{(+)}(\bar{q}, q; w)$ is a finite polynomial in the Dirac matrices γ_5 and γ_μ and the four-momenta $q_\mu, \bar{q}_\mu, w_\mu$. A further crucial property of the projectors is that they are free of any kinematical singularities in $q \cdot w$, $\bar{q} \cdot q$, q^2 and \bar{q}^2 . Only then the set of projectors decouples in the Bethe-Salpeter equation (9) in any frame.

In general the Bethe-Salpeter interaction kernel $K_{ab}^{(I)}(\bar{q}, q; w)$ may have additional contributions not of the form (12). Such terms do not lead to s-channel unitarity cuts if iterated in the Bethe-Salpeter equation, since, by construc-

tion of the projectors, they vanish for on-shell kinematics. In [20] it is shown explicitly that these terms may be considered as part of the irreducible loop corrections of an effective interaction kernel $\bar{K}_{ab}^{(I)}(\bar{q}, q; w)$. Note that the form of the projectors implies a particular off-shell behavior of the interaction kernel. From a field theoretical point of view the off-shell structure of the interaction kernel and also that of the scattering amplitude is not defined because it may be changed at will by redefining the hadronic interpolating fields [22,23]. However, as was emphasized in [20] the proper treatment of the Bethe-Salpeter equation requires a systematic on-shell reduction as to avoid an unphysical and uncontrolled dependence on the choice of chiral coordinates or the choice of interpolating fields. A covariant on-shell reduction can be defined unambiguously with respect to the covariant set of projectors that solve the Bethe-Salpeter equation for any choice of quasi-local interaction terms. The systematic on-shell reduction of the Bethe-Salpeter interaction kernel then leads to an effective interaction kernel of the form imposed in (12).

Given an interaction kernel of the form (12), the coupled-channel scattering amplitudes $T_{ab}^{(I)}(\bar{k}, k; w)$ can be decomposed accordingly:

$$T_{ab}^{(I)}(\bar{q}, q; w) = \sum_{n=0}^{\infty} M_{ab}^{(I+)}(\sqrt{s}; n) [Y_n^{(+)}(\bar{q}, q; w)]_{ab} + \sum_{n=0}^{\infty} M_{ab}^{(I-)}(\sqrt{s}; n) [Y_n^{(-)}(\bar{q}, q; w)]_{ab}. \quad (13)$$

The reduced amplitudes $M_{ab}^{(I\pm)}(\sqrt{s}; n)$ are given by

$$M_{ab}^{(I\pm)}(\sqrt{s}; n) = \left[\left(1 - V^{(I\pm)}(\sqrt{s}; n) J^{(I\pm)}(\sqrt{s}; n) \right)^{-1} V^{(I\pm)}(\sqrt{s}; n) \right]_{ab}, \quad (14)$$

where the loop matrix $J_{ab}^{(I\pm)}(\sqrt{s}; n)$ is defined by

$$J_{ab}^{(\pm)}(\sqrt{s}; n) [Y_n^{(\pm)}(\bar{q}, q; w)]_{ab} = -i \int \frac{d^4 l}{(2\pi)^4} [Y_n^{(\pm)}(\bar{q}, l; w)]_{ac} \times S_{B(c)B(d)}(w - l) D_{\Phi(c)\Phi(d)}(l) [Y_n^{(\pm)}(l, q; w)]_{db}. \quad (15)$$

We stress that the definition of the loop functions in (15) is consistent only because the projectors are constructed to carry good total angular momentum J . A priori it is unclear that the left hand side of (15) does not involve additional terms not proportional to $Y_n^{(\pm)}$. Furthermore, since the integral in (15) diverges, the loop functions are defined only in conjunction with a suitable renormalization scheme, to be discussed below. The consistency of (15) is verified by explicit calculations.

Before we proceed with the presentation of the projectors and loop functions, we first discuss the general form of the interaction kernel used in this work. It may be obtained from a meson exchange model or more systematically from the chiral Lagrangian. Here we use the concept of an effective field theory in a sense that differs somewhat from common practice. Usually this concept is used to describe the physics close to threshold, like e.g. in chiral perturbation theory, which is based on a systematic expansion in powers of the momentum [24]. In this paper we construct an effective field theory for meson-nucleon scattering in the resonance region. The philosophy of this approach is to approximate the slowly varying interaction kernels K_{ab} with simple coupling functions, and to treat rescattering in the s-channel explicitly. By allowing an arbitrary energy dependence of K_{ab} , one could certainly describe the phase shifts at any energy, as long as all open channels are included. However, such a model has essentially no predictive power. In our scheme, the predictive power results from the assumption that the interaction kernel is slowly varying in energy in the relevant window $1.4 \text{ GeV} < \sqrt{s} < 1.8 \text{ GeV}$.

This assumption is based on the following observation. A small scale, which implies a strong energy dependence of the scattering amplitude, is a reflection of nearby singularities. In general the partial-wave amplitudes have an analytic structure which is more complicated than the s-channel singularities generated by rescattering. There are left-hand cuts generated by t - and u -channel exchanges of mesons and baryons, which are not treated explicitly in our approach. These cuts are located in an unphysical region, but the exchange of light mesons, e.g. the pion, may give rise to a rapid energy variation close to threshold because the branch point is located relatively close to the physical region. However, far above threshold, the energy variation due to the left-hand cuts is unimportant, and the interaction kernel can be approximated by slowly varying function. We have checked by explicit calculation that, for the partial waves considered, this is the case in the energy region of interest here. Consequently, we employ the following simple ansatz for the interaction kernel:

$$V_{ab}^{(\pm)}(\sqrt{s}; n) \simeq \frac{s}{m_N^2} g_{n,ab}^{(\pm)}, \quad (16)$$

where the linear dependence in (16) on s is imposed in order to guarantee a regular behaviour of the scattering amplitude at $\sqrt{s} = 0$ (see (17)). The linear dependence in s removes an unphysical kinematical singularity of the scattering amplitudes at $s = 0$, which is due to the form of the projectors⁴ [20]. Although this simple interpolation perhaps does not yield an accurate

⁴ An alternative, equally viable, way to eliminate this singularity is to include a factor proportional to s in the definition of the projection operators and take the interaction kernel independent of s .

representation of the scattering amplitude outside the window of applicability, because it does not account for e.g. the t - and u -channel singularities, we expect at least a qualitative description also there.

In this context, one may worry that the s-channel contributions of baryon ground states and resonance to the interaction kernel may lead to a rapid energy variation in our energy window $1.4 \text{ GeV} < \sqrt{s} < 1.8 \text{ GeV}$. Our ansatz (16) is justified by the following observations. In this work we consider only s-wave interactions in the vector-meson nucleon channels. Because of parity conservation these couple only to the s- and d-wave pion-nucleon channels. In these channels the large N_c baryon ground-state states, the positive parity baryon octet and decuplet states, do not lead to pole structures in the corresponding kernels⁵, $V_{ab}^{(+)}(\sqrt{s}; 0)$ and $V_{ab}^{(-)}(\sqrt{s}; 1)$. Furthermore, the large N_c excited states are not explicitly included in (16) since we aim to generate those as resonances of the ground-state degrees of freedom [20]. The basis for this strategy is the hypothesis that large N_c counting rules can be applied to the interaction kernel but not to the scattering amplitude. This is supported by the following argument. The reducible diagrams summed by the Bethe-Salpeter equation are typically enhanced by a factor 2π compared to irreducible diagrams. Thus, a reducible diagram, which in the large N_c expansion is suppressed by a factor $1/N_c$, acquires a total factor $2\pi/N_c$. For $N_c = 3$ this factor is about 2, which indicates that the large N_c expansion is not useful for reducible diagrams. Consequently, it is unclear whether baryon resonances are already present in the interaction kernel, i.e. included in the irreducible diagrams, or generated by coupled-channel dynamics, i.e. by including reducible diagrams. The fact that baryon resonances typically have large decay widths we take as an indication that indeed the coupled-channel dynamics is the driving mechanism for the creation of baryon resonances.

We return to the set of projectors and recall those that are relevant for elastic pion-nucleon scattering [20]

$$\begin{aligned}
[Y_n^{(\pm)}(\bar{q}, q; w)]_{11} &= \frac{1}{2} \left(\frac{\psi}{\sqrt{w^2}} \pm 1 \right) \bar{Y}_{n+1}(\bar{q}, q; w) \\
&\quad - \frac{1}{2} \left(\not{q} - \frac{w \cdot \bar{q}}{w^2} \psi \right) \left(\frac{\psi}{\sqrt{w^2}} \mp 1 \right) \left(\not{q} - \frac{w \cdot q}{w^2} \psi \right) \bar{Y}_n(\bar{q}, q; w) , \\
\bar{Y}_n(\bar{q}, q; w) &= \sum_{k=0}^{[(n-1)/2]} \frac{(-)^k (2n-2k)!}{2^n k! (n-k)! (n-2k-1)!} Y_{\bar{q}\bar{q}}^k Y_{\bar{q}q}^{n-2k-1} Y_{qq}^k , \\
Y_{\bar{q}\bar{q}} &= \frac{(w \cdot \bar{q})(\bar{q} \cdot w)}{w^2} - \bar{q} \cdot \bar{q} , \quad Y_{qq} = \frac{(w \cdot q)(q \cdot w)}{w^2} - q \cdot q ,
\end{aligned}$$

⁵ The partial wave content of the various projectors will be identified below.

$$Y_{\bar{q}q} = \frac{(w \cdot \bar{q})(q \cdot w)}{w^2} - \bar{q} \cdot q . \quad (17)$$

We list the leading order projectors $[Y_n^{(\pm)}]_{11}$ for s-,p- and d-wave scattering with total angular momentum $J = \frac{1}{2}, \frac{3}{2}$ explicitly

$$\begin{aligned} [Y_0^{(\pm)}(\bar{q}, q; w)]_{11} &= \frac{1}{2} \left(\frac{\psi}{\sqrt{w^2}} \pm 1 \right) , \\ [Y_1^{(\pm)}(\bar{q}, q; w)]_{11} &= \frac{3}{2} \left(\frac{\psi}{\sqrt{w^2}} \pm 1 \right) \left(\frac{(\bar{q} \cdot w)(w \cdot q)}{w^2} - (\bar{q} \cdot q) \right) \\ &\quad - \frac{1}{2} \left(\not{q} - \frac{w \cdot \bar{q}}{w^2} \psi \right) \left(\frac{\psi}{\sqrt{w^2}} \mp 1 \right) \left(\not{q} - \frac{w \cdot q}{w^2} \psi \right) . \end{aligned} \quad (18)$$

As demonstrated in [20] these projectors indeed lead to reduced scattering amplitudes $M_{ab}^{(I\pm)}(\sqrt{s}; n)$ of the form (14). The loop functions are

$$J_{11}^{(I\pm)}(\sqrt{s}; n) = p_{\pi N}^2 I_{\pi N}(\sqrt{s}) \left(\frac{\sqrt{s}}{2} + \frac{m_N^2 - m_\pi^2}{2\sqrt{s}} \pm m_N \right) , \quad (19)$$

with the master function $I_{\pi N}(\sqrt{s})$ given by

$$\begin{aligned} I_{\pi N}(\sqrt{s}) &= -i \int \frac{d^4 l}{(2\pi)^4} \frac{1}{l^2 - m_\pi^2} \frac{1}{(l - w)^2 - m_N^2} \\ &= \frac{1}{16\pi^2} \left(\frac{p_{\pi N}}{\sqrt{s}} \left(\ln \left(1 - \frac{s - 2p_{\pi N}\sqrt{s}}{m_\pi^2 + m_N^2} \right) - \ln \left(1 - \frac{s + 2p_{\pi N}\sqrt{s}}{m_\pi^2 + m_N^2} \right) \right) \right. \\ &\quad \left. + \left(\frac{1}{2} \frac{m_\pi^2 + m_N^2}{m_\pi^2 - m_N^2} - \frac{m_\pi^2 - m_N^2}{2s} \right) \ln \left(\frac{m_\pi^2}{m_N^2} \right) + 1 \right) + I_{\pi N}(0) , \\ p_{\pi N}^2 &= \frac{s}{4} - \frac{m_N^2 + m_\pi^2}{2} + \frac{(m_N^2 - m_\pi^2)^2}{4s} . \end{aligned} \quad (20)$$

We recall [20] that the projectors $Y_n^{(\pm)}$ with $J = n + \frac{1}{2}$ require a physical mass dependent renormalization procedure with vanishing renormalized tadpole contributions, $I_\pi \rightarrow 0$ and $I_N \rightarrow 0$. The loop-orthogonality of projectors with different total angular momenta J and J' follows only in a renormalization scheme where tadpole contributions vanish effectively. Moreover, we observe that the pion and nucleon tadpole diagrams I_π and I_N determine the master-loop function $I_{\pi N}(\sqrt{s})$ at $s = 0$ via the algebraic identity

$$I_{\pi N}(\sqrt{s} = 0) = \frac{-1}{m_N^2 - m_\pi^2} (I_N - I_\pi) . \quad (21)$$

The identity (21), which can be verified in dimensional regularization, then leads to $I_{\pi N}(0) = 0$ in (20). We conclude that the renormalization prescription, to drop tadpole contributions in reducible diagrams, leads to finite expressions for all loop functions defined by the set of covariant projectors (15).

The reduced amplitudes⁶ $M_{11}^{(\pm)}(\sqrt{s}; n)$ of (13) have a unique interpretation in terms of the pion-nucleon scattering phase shifts $\delta_{J=l\pm\frac{1}{2}}^{(l)}$ and inelasticity parameter $\eta_{J=l\pm\frac{1}{2}}^{(l)}$ [20]. The matching can be carried out in a straightforward manner by identifying the s-channel unitarity cut of $M_{11}^{(\pm)}(\sqrt{s}; n)$ and the partial-wave amplitudes $f_{\pm}^{(J)}(s)$

$$\begin{aligned} p_{\pi N} f_{\pm}^{(J)}(s) &= \frac{1}{2i} \left(\eta_{J=l\pm\frac{1}{2}}^{(l)}(s) e^{2i\delta_{J=l\pm\frac{1}{2}}^{(l)}(s)} - 1 \right), \\ f_{\pm}^{(J)}(s) &= \frac{(p_{\pi N})^{2J-1}}{8\pi\sqrt{s}} \left(\frac{\sqrt{s}}{2} + \frac{m_N^2 - m_{\pi}^2}{2\sqrt{s}} \pm m_N \right) M^{(\pm)}(\sqrt{s}; J - \frac{1}{2}). \end{aligned} \quad (22)$$

The angular momentum l of a given projector can be inferred from the threshold behavior of the associated loop function. From (19) it follows that $\Im J_{\pi N}^{(+)}(\sqrt{s}; n) \sim p_{\pi N}^{2n+1}$ but $\Im J_{\pi N}^{(-)}(\sqrt{s}; n) \sim p_{\pi N}^{2n+3}$. This confirms the angular momentum assignment implicit in (22). In the presence of inelastic channels the inelasticity parameter is smaller than the value for elastic scattering, $\eta = 1$.

The projectors of the ηN , $K\Lambda$ and $K\Sigma$ channels are identical to the ones of the pion-nucleon channels. Therefore they need not to be specified separately. For example in the isospin $\frac{1}{2}$ channel one has $[Y_n^{(\pm)}]_{11} = [Y_n^{(\pm)}]_{xy}$ for $x, y \in \{1, 5, 6, 7\}$. In order to arrive at a convenient notation for the pion-induced pseudo-scalar meson production cross sections it is useful to generalize the notation of (22). Take as an example the pion-induced η production amplitude for which we write

$$\begin{aligned} N_{\pi N}^{(\pm)} &= \frac{\sqrt{s}}{2} + \frac{m_N^2 - m_{\pi}^2}{2\sqrt{s}} \pm m_N, & N_{\eta N}^{(\pm)} &= \frac{\sqrt{s}}{2} + \frac{m_{\eta}^2 - m_N^2}{2\sqrt{s}} \pm m_N, \\ f_{\pm, \pi N \rightarrow \eta N}^{(\frac{1}{2}J)}(\sqrt{s}) &= \frac{\sqrt{N_{\pi N}^{(\pm)} N_{\eta N}^{(\pm)}}}{8\pi\sqrt{s}} (p_{\eta N} p_{\pi N})^{J-\frac{1}{2}} M_{15}^{(\frac{1}{2}\pm)}(\sqrt{s}, J - \frac{1}{2}), \end{aligned} \quad (23)$$

with $\sqrt{s} = \sqrt{m_N^2 + p_{\eta N}^2} + \sqrt{m_{\eta}^2 + p_{\eta N}^2}$. The expressions for the pion-induced pseudo-scalar meson production cross sections have the simple form

$$\sigma_{\pi^- p \rightarrow \eta n} = 4\pi \frac{p_{\eta N}}{p_{\pi N}} \frac{2}{3} \left| f_{+, \pi N \rightarrow \eta N}^{(\frac{1}{2}\frac{1}{2})} \right|^2, \quad (24)$$

⁶ For simplicity we suppress the isospin index in this paragraph.

$$\begin{aligned}
\sigma_{\pi^- p \rightarrow K^0 \Sigma^0} &= 4\pi \frac{p_{K\Sigma}}{p_{\pi N}} \frac{2}{9} \left| f_{+, \pi N \rightarrow K\Sigma}^{(\frac{1}{2}\frac{1}{2})} - f_{+, \pi N \rightarrow K\Sigma}^{(\frac{3}{2}\frac{1}{2})} \right|^2, \\
\sigma_{\pi^- p \rightarrow K^+ \Sigma^-} &= 4\pi \frac{p_{K\Sigma}}{p_{\pi N}} \frac{1}{9} \left| 2f_{+, \pi N \rightarrow K\Sigma}^{(\frac{1}{2}\frac{1}{2})} + f_{+, \pi N \rightarrow K\Sigma}^{(\frac{3}{2}\frac{1}{2})} \right|^2, \\
\sigma_{\pi^+ p \rightarrow K^+ \Sigma^+} &= 4\pi \frac{p_{K\Sigma}}{p_{\pi N}} \left| f_{+, \pi N \rightarrow K\Sigma}^{(\frac{3}{2}\frac{1}{2})} \right|^2, \quad \sigma_{\pi^- p \rightarrow K^0 \Lambda} = 4\pi \frac{p_{K\Lambda}}{p_{\pi N}} \frac{2}{3} \left| f_{+, \pi N \rightarrow K\Lambda}^{(\frac{1}{2}\frac{1}{2})} \right|^2,
\end{aligned}$$

where we have adopted a notation for the $K\Lambda$ and $K\Sigma$ production amplitudes, which is analogous to (23). We do not consider d-wave contribution in the ηN , $K\Lambda$ or $K\Sigma$ channels. Only with improved quality of the differential cross section data it would be possible to determine those channels reliably in our present approach. Moreover we do not address effects from isospin violation. We use the approximate mass parameters $m_N = 939$ MeV, $m_\Lambda = 1116$ MeV, $m_\Sigma = 1195$ MeV, $m_\pi = 139$ MeV, $m_\eta = 547$ MeV and $m_K = 494$ MeV throughout this work.

3 Pion-induced vector meson and isobar production

Pion-nucleon scattering at energies larger than $\sqrt{s} > m_N + 2m_\pi$ is complicated by the coupling to inelastic 2-pion channels. In our approach we approximate the three-body final state by including the ρN and $\Delta\pi$ channels [19]. The decay of the ρ meson and Δ isobar are taken into account by incorporating their energy-dependent widths. We do not consider the σN channel since it would be difficult to discriminate its effects from the $\pi\Delta$ channel which in our scheme is constrained by data only rather indirectly. The latter channel is viewed as an effective channel that takes into account some residual effects from the σN channel. We, however, consider the ωN channel because its mass is almost degenerate with that of the ρ meson and the ω meson is expected to couple strongly to baryons.

Before constructing the appropriate projectors required in (12) it is useful to describe the general framework within which our expressions should be considered. We assume that the vector-meson fields satisfy the Proca equation which follows from the Lagrangian density

$$\begin{aligned}
\mathcal{L} = & -\frac{\zeta_\rho^{(0)}}{4} \left(\partial_\mu \vec{\rho}_\nu - \partial_\nu \vec{\rho}_\mu \right) \left(\partial^\mu \vec{\rho}^\nu - \partial^\nu \vec{\rho}^\mu \right) + \frac{1}{2} \overset{\circ}{m}_\rho^2 \vec{\rho}_\mu \vec{\rho}^\mu \\
& - \frac{\zeta_\omega^{(0)}}{4} \left(\partial_\mu \omega_\nu - \partial_\nu \omega_\mu \right) \left(\partial^\mu \omega^\nu - \partial^\nu \omega^\mu \right) + \frac{1}{2} \overset{\circ}{m}_\omega^2 \omega_\mu \omega^\mu,
\end{aligned} \tag{25}$$

where we, for later convenience, allow for a wave-function renormalization. As is well known, the corresponding Feynman propagator sustains only (4-dimensionally) transverse modes. When interactions of the ρ meson with other fields are taken into account, its propagator is modified by the polarization

tensor $\Pi_{\mu\nu}^{(\rho)}(q)$, which in vacuum has two independent components, $\Pi_L^{(\rho)}(q)$ and $\Pi_T^{(\rho)}(q)$. The ρ -meson propagator is then given by

$$D_{\mu\nu}^{(\rho)}(q) = \left(g_{\mu\nu} - \frac{q_\mu q_\nu}{q^2} \right) \frac{1}{\zeta_\rho^{(0)} q^2 - \mathring{m}_\rho^2 - \Pi_T^{(\rho)}(q^2)} + \frac{q_\mu q_\nu}{q^2} \frac{1}{\mathring{m}_\rho^2 - \Pi_L^{(\rho)}(q^2)} \quad (26)$$

The first term is the transverse component of the propagator, while the second one is the longitudinal one. In a scheme, where the vector meson couples to a conserved current, the vector-meson nucleon scattering amplitude is transverse, i.e. $\bar{q}_\mu T_{\rho N \rightarrow \rho N}^{\mu\nu}(\bar{q}, q; w) = T_{\rho N \rightarrow \rho N}^{\mu\nu}(\bar{q}, q; w) q_\nu = 0$ vanish [25,26]. However, in an approximation scheme, where the corresponding current is not conserved, the longitudinal self energy differs from zero and the longitudinal propagator may exhibit singularities, which correspond to the propagation of unphysical degrees of freedom. Thus it is preferable to work in a scheme with conserved currents, when possible. Nevertheless, in non-perturbative approximations, like the present one, there is no systematic way of implementing current conservation. We therefore employ an alternative scheme, which deals with this in a pragmatic way.

From a practical point of view, the minimal requirement a model should satisfy is that a possible longitudinal mode should have a mass large enough so that it does not lead to cut structures within the domain of applicability of the model. The idea is to start with the most general interaction terms which then allows one to push the mass of the unphysical mode to a sufficiently high value by a suitable choice of parameters. In such an approach the vector-meson scattering amplitudes need not be transverse. Once the propagation of longitudinal modes is suppressed, the longitudinal parts of the scattering amplitude are not relevant.

We illustrate this discussion with a simple calculation. To leading order with no interactions the vector-meson fields satisfy the Proca equation. We add the typical interaction terms required for the modelling of the vector-meson decay widths

$$\mathcal{L}_{int} = g_{\rho\pi\pi} \vec{\rho}^\mu ((\partial_\mu \vec{\pi}) \times \vec{\pi}) + 2 \frac{g_{\rho\omega\pi}}{m_\omega} \epsilon^{\alpha\beta\mu\nu} (\partial_\nu \omega_\beta) (\partial_\mu \vec{\rho}_\alpha) \vec{\pi}. \quad (27)$$

Of course there may be more terms, which however are not relevant for the present discussion. Consider the lowest-order contribution to the ρ -meson polarization tensor $\Pi_{\mu\nu}^{(\rho)}(q)$, which in d dimensions is given by

$$\Pi_{\mu\nu}^{(\rho)}(q) = -i \frac{g_{\rho\pi\pi}^2}{\mu^{d-4}} \int \frac{d^d l}{(2\pi)^d} (2l - q)_\mu (2l - q)_\nu D_\pi(l) D_\pi(l - q)$$

$$= \Pi_T^{(\rho)}(q^2) \left(g_{\mu\nu} - \frac{q_\mu q_\nu}{q^2} \right) + \Pi_L^{(\rho)}(q^2) \frac{q_\mu q_\nu}{q^2} . \quad (28)$$

The contribution of the second term in (27) to the ρ -meson self energy is small, and we neglect it. However, for the self energy of the ω meson, which we discuss below, it plays a crucial role. The transverse and longitudinal components can be expressed in terms of the logarithmically divergent master loop function $I_{\pi\pi}(q^2)$ and the tadpole I_π

$$\begin{aligned} \Pi_T^{(\rho)}(q^2) &= \frac{g_{\rho\pi\pi}^2}{1-d} \left((q^2 - 4m_\pi^2) (I_{\pi\pi}(\sqrt{q^2}) - I_{\pi\pi}(0)) \right. \\ &\quad \left. + \left(\frac{q^2}{2m_\pi^2} (2-d) - 2(1-d) \right) I_\pi \right), \\ \Pi_L^{(\rho)}(q^2) &= -2g_{\rho\pi\pi}^2 I_\pi, \end{aligned} \quad (29)$$

where

$$\begin{aligned} I_{\pi\pi}(q^2) &= -\frac{i}{\mu^{d-4}} \int \frac{d^d l}{(2\pi)^d} D_\pi(l) D_\pi(q-l), \\ I_\pi &= \frac{i}{\mu^{d-4}} \int \frac{d^d l}{(2\pi)^d} D_\pi(l), \quad I_{\pi\pi}(0) = \frac{2-d}{2m_\pi^2} I_\pi. \end{aligned} \quad (30)$$

In our model, the ρ -meson polarization tensor does, according to (29), exhibit a longitudinal component. In contrast to that, the longitudinal polarization would be identically zero in a formulation, in which the ρ meson couples to a conserved current. We observe, however, that in our scheme the ρ -meson propagator is also well behaved supporting exclusively the propagation of transverse modes for any choice of parameters. This is a consequence of the fact that the longitudinal polarization $\Pi_L^{(\rho)}(q^2)$ is a constant (see (26)). It is clear that if additional interaction terms would lead to a contribution of the form $\Pi_L^{(\rho)}(q^2) = c_\rho q^2$, which gave rise to unphysical propagation of longitudinal modes with mass squared of m_ρ^2/c_ρ , an appropriate counter term $-c_\rho (\partial^\mu \rho_\mu) (\partial^\nu \rho_\nu)$ could be designed to exactly cancel this troublesome contribution. This has some similarity to the Stückelberg mechanism [27].

The renormalization of the simple model (27) is performed by absorbing the tadpole terms in (29) into the bare parameters \tilde{m}_ρ^2 and $\tilde{\zeta}_\rho^{(0)}$

$$\tilde{m}_\rho^2 = \tilde{m}_\rho^2 + 2g_{\rho\pi\pi}^2 I_\pi, \quad \tilde{\zeta}_\rho = \zeta_\rho^{(0)} - \frac{g_{\rho\pi\pi}^2}{2m_\pi^2} \frac{2-d}{1-d}. \quad (31)$$

After the renormalization (31) is implied the limit $d \rightarrow 4$ can be performed smoothly. All together we arrive at the renormalized propagator

$$\begin{aligned}
D_{\mu\nu}^{(\rho)}(q) &= \left(g_{\mu\nu} - \frac{q_\mu q_\nu}{q^2} \right) D_T^{(\rho)}(q^2) + \frac{q_\mu q_\nu}{q^2} D_L^{(\rho)}(q^2), \quad D_L^{(\rho)}(q^2) = \frac{1}{\tilde{m}_\rho^2}, \\
D_T^{(\rho)}(q^2) &= \frac{1}{\zeta_\rho (q^2 - m_\rho^2) + \frac{1}{3} g_{\rho\pi\pi}^2 (q^2 - 4m_\pi^2) (I_{\pi\pi}(\sqrt{q^2}) - \Re I_{\pi\pi}(m_\rho))} \quad (32)
\end{aligned}$$

where we performed an additional finite renormalization introducing the physical ρ -mass parameter $m_\rho \simeq 779$ MeV and the wave-function renormalization parameter ζ_ρ . The explicit form of the master-loop function $I_{\pi\pi}(q^2)$ follows from the expression $I_{\pi N}(\sqrt{q^2})$ given already in (20) if the formal limit $m_N \rightarrow m_\pi$ is applied. The coupling constant $g_{\rho\pi\pi} \simeq 5.79$ and $\zeta_\rho \simeq 1$ follow if the model (27) is used to reproduce the p-wave $\pi\pi$ scattering phase shift [28].

For later convenience it is useful to represent the ρ -meson propagator in terms of its spectral function $\rho_\rho(q^2)$,

$$\rho_\rho(q^2) = \Im D_T^{(\rho)}(q^2) \Theta(\Lambda_\rho^2 - q^2), \quad \int_{4m_\pi^2}^{\Lambda_\rho^2} \frac{dm^2}{\pi} \rho_\rho(m^2) = 1, \quad (33)$$

where the cutoff Λ_ρ is required if one demands a normalized spectral function. The spectral density $\rho_\rho(m^2)$ is normalized to π by the choice $\Lambda_\rho \simeq 1.34$ GeV. It is convenient to work with a normalized spectral function because that will avoid a particular class of divergent terms which would otherwise arise if the dressed ρ -meson propagator is used inside loop integrals. From a physical point of view this is well justified because the simple model (27) is certainly incorrect at invariant masses q^2 much larger than the squared ρ -meson mass.

We turn to the ω meson. The interaction vertex given in (27) leads to the following expression for the transverse and longitudinal polarization functions $\Pi_{L,T}^{(\omega)}(q^2)$

$$\begin{aligned}
\Pi_T^{(\omega)}(q^2) &= \frac{i 4 g_{\omega\rho\pi}^2}{m_\omega^2 \mu^{4-d}} \frac{3d-6}{1-d} \int \frac{d^d l}{(2\pi)^d} (q^2 l^2 - (l \cdot q)^2) D_T^{(\rho)}(l) D_\pi(l-q), \\
\Pi_L^{(\omega)}(q^2) &= 0, \quad (34)
\end{aligned}$$

where we consider the effect of a dressed ρ -meson propagator in the loop integral [29]. Since for the ω meson the interaction terms (27) lead to a vanishing longitudinal polarization tensor, the ω -meson propagator is well behaved supporting transverse modes only. The loop integration is most economically performed applying the spectral representation of the ρ -meson propagator. We write

$$\Pi_T^{(\omega)}(q^2) = \int_{\frac{4m_\pi^2}{\Lambda_\rho^2}}^{\Lambda_\rho^2} dm^2 \rho_\rho(m^2) \Pi_T^{(\omega)}(q^2, m^2), \quad (35)$$

where we use the normalized spectral function introduced in (32, 33). The integral kernel in (35) is evaluated in space-time dimension d ,

$$\begin{aligned} \Pi_T^{(\omega)}(q^2, m_\rho^2) = & \frac{4 g_{\omega\rho\pi}^2}{m_\omega^2 \mu^{4-d}} \frac{3d-6}{1-d} \left(\frac{1}{2} q^2 I_\pi + \frac{1}{4} q^2 (q^2 - m_\pi^2 - 3m_\rho^2) I_{\pi\rho}(0, m_\rho^2) \right. \\ & \left. + \left(\frac{1}{4} (q^2 + m_\rho^2 - m_\pi^2)^2 - q^2 m_\rho^2 \right) (I_{\pi\rho}(q^2, m_\rho^2) - I_{\pi\rho}(0, m_\rho^2)) \right), \quad (36) \end{aligned}$$

where we encounter exclusively the master-loop function $I_{\pi\rho}(q^2, m_\rho^2)$ and the tadpole terms I_π and I_ρ . At $d = 4$ the loop function $I_{\pi\rho}(q^2, m_\rho^2)$ can be inferred from the analogous expression $I_{\pi N}(\sqrt{q^2})$ given in (20). Note that here we make explicit the dependence of the master-loop function $I_{ab}(\sqrt{q^2}) \rightarrow I_{ab}(q^2, m_b^2)$ on the mass parameter m_b . The expression for the ω -meson polarization is renormalized by absorbing the diverging terms proportional to q^2 and $(q^2)^2$ into appropriate wave-function renormalization terms. For the renormalized polarization function $\Pi_{T,R}^{(\omega)}(q^2, m_\rho^2)$ we use

$$\begin{aligned} \Pi_{T,R}^{(\omega)}(q^2, m_\rho^2) = & -4 \frac{g_{\omega\rho\pi}^2}{m_\omega^2} \left((q^2 + m_\rho^2 - m_\pi^2)^2 - 4q^2 m_\rho^2 \right) \\ & \times (I_{\pi\rho}(q^2, m_\rho^2) - \Re I_{\pi\rho}(m_\omega^2, m_\rho^2)), \quad (37) \end{aligned}$$

where we performed a subtraction at the physical mass $m_\omega \simeq 782$ MeV for convenience. This permits the identification $\tilde{m}_\omega = m_\omega$ in (25). The parameter $g_{\omega\rho\pi} \simeq 7.57$ is adjusted to reproduce the hadronic decay width of the ω meson with $\Gamma_\omega \simeq 8.4$ MeV where we assume here $\zeta_\omega = 1$ for simplicity. By analogy with the ρ -meson spectral function (see (33)) we introduce a cutoff $\Lambda_\omega \simeq 821$ MeV. This leads to the correct normalization of the ω -meson spectral function $\rho_\omega(m^2)$, which is defined by (37,26).

3.1 Projector approach for vector mesons

We construct the relativistic vector-meson production amplitudes with total angular momentum $J = \frac{1}{2}$ and $J = \frac{3}{2}$ by specifying the appropriate projectors introduced in (13). It is sufficient to present the projectors $[Y_{n,\mu}^{(\pm)}]_{13}$, $[Y_{n,\mu}^{(\pm)}]_{31}$ and $[Y_{n,\mu\nu}^{(\pm)}]_{33}$ of the inelastic ρN channel for the isospin $I = \frac{1}{2}$ states. The remaining projectors follow then by analogy. For example in the isospin $1/2$ channel it holds $[Y_n^{(\pm)}]_{x3} = [Y_n^{(\pm)}]_{x4}$. The $J = \frac{1}{2}$ projectors are:

$$\begin{aligned}
[Y_{0,\mu}^{(+)}(\bar{q}, q; w)]_{31} &= -\frac{1}{2\sqrt{3}} \left(\gamma_\mu - \frac{w_\mu}{w^2} \psi \right) \left(1 - \frac{\psi}{\sqrt{w^2}} \right) i \gamma_5 , \\
[Y_{0,\mu}^{(+)}(\bar{q}, q; w)]_{13} &= +\frac{1}{2\sqrt{3}} i \gamma_5 \left(1 - \frac{\psi}{\sqrt{w^2}} \right) \left(\gamma_\mu - \frac{w_\mu}{w^2} \psi \right) , \\
[Y_{0,\mu\nu}^{(+)}(\bar{q}, q; w)]_{33} &= \frac{1}{6} \left(\gamma_\mu - \frac{w_\mu}{w^2} \psi \right) \left(1 - \frac{\psi}{\sqrt{w^2}} \right) \left(\gamma_\nu - \frac{w_\nu}{w^2} \psi \right) . \quad (38)
\end{aligned}$$

The $J = \frac{3}{2}$ projectors are:

$$\begin{aligned}
[Y_{1,\mu}^{(-)}(\bar{q}, q; w)]_{31} &= -\frac{\sqrt{3}}{2} \left(1 + \frac{\psi}{\sqrt{w^2}} \right) \left(q_\mu - \frac{w \cdot q}{w^2} w_\mu \right) i \gamma_5 \\
&\quad + \frac{1}{2\sqrt{3}} \left(\gamma_\mu - \frac{w_\mu}{w^2} \psi \right) \left(1 - \frac{\psi}{\sqrt{w^2}} \right) \left(\not{q} - \frac{w \cdot q}{w^2} \psi \right) i \gamma_5 , \\
[Y_{1,\mu}^{(-)}(\bar{q}, q; w)]_{13} &= +\frac{\sqrt{3}}{2} i \gamma_5 \left(1 + \frac{\psi}{\sqrt{w^2}} \right) \left(\bar{q}_\mu - \frac{\bar{q} \cdot w}{w^2} w_\mu \right) \\
&\quad - \frac{1}{2\sqrt{3}} i \gamma_5 \left(\not{\bar{q}} - \frac{\bar{q} \cdot w}{w^2} \psi \right) \left(1 - \frac{\psi}{\sqrt{w^2}} \right) \left(\gamma_\mu - \frac{w_\mu}{w^2} \psi \right) , \\
[Y_{1,\mu\nu}^{(-)}(\bar{q}, q; w)]_{33} &= \frac{1}{2} \left(1 + \frac{\psi}{\sqrt{w^2}} \right) \left(g_{\mu\nu} - \frac{w_\mu w_\nu}{w^2} \right) \\
&\quad - \frac{1}{6} \left(\gamma_\mu - \frac{w_\mu}{w^2} \psi \right) \left(1 - \frac{\psi}{\sqrt{w^2}} \right) \left(\gamma_\nu - \frac{w_\nu}{w^2} \psi \right) . \quad (39)
\end{aligned}$$

It is a straightforward exercise to verify that the projectors (38,39) have indeed the acclaimed property (14,15), provided that tadpole contributions are dropped systematically. We emphasize that the property (15) is sufficient as to prove that the projectors must carry good total angular momentum J . This is evident because only states with good total angular momentum J may decouple the Bethe-Salpeter equation. Note that the $J = \frac{3}{2}$ projectors couple to additional projectors, which probe the vector-meson nucleon state with angular momentum $L > 0$. In general the projectors for the vector mesons acquire an additional 3×3 matrix structure which simply reflects the various angular momenta L accessible at given J . For the case $J = \frac{1}{2}$ that matrix collapses to a 2×2 matrix describing the coupling of the two states $|\rho^{(T)} N, \lambda = \frac{1}{2}, J = \frac{1}{2}\rangle$ and $|\rho^{(L)} N, \lambda = \frac{1}{2}, J = \frac{1}{2}\rangle$ or alternatively the coupling of a s-wave and d-wave state. A third state $|\rho^{(T)} N, \lambda = \frac{1}{2}, J = \frac{3}{2}\rangle$ existed only for $J > \frac{1}{2}$. That follows because a transverse vector meson, $\rho^{(T)}$, cannot couple to a nucleon forming a helicity $\lambda = \frac{3}{2}$ state if the vector meson and nucleon sit in a relative s-wave. In the $J = \frac{1}{2}$ channel the matrix structure of the projectors is defined with respect to specific linear combinations of helicity states $|J = \frac{1}{2}; 1\rangle$ and $|J = \frac{1}{2}; 2\rangle$ defined as follows,

$$\begin{aligned} |J=\frac{1}{2}; 1\rangle &= |\rho^{(T)} N, \lambda=\frac{1}{2}, J=\frac{1}{2}\rangle + \frac{1}{\sqrt{2}}\sqrt{1+\vec{q}^2/m_\rho^2} |\rho^{(L)} N, \lambda=\frac{1}{2}, J=\frac{1}{2}\rangle, \\ |J=\frac{1}{2}; 2\rangle &= |\rho^{(L)} N, \lambda=\frac{1}{2}, J=\frac{1}{2}\rangle, \end{aligned} \quad (40)$$

where \vec{q} is the vector meson's three momentum. We point out that the particular form of the linear combination is unique in the sense that only with respect to the $|J=\frac{1}{2}; 1\rangle$ and $|J=\frac{1}{2}; 2\rangle$ states it is possible to construct an associated covariant projector algebra P_{ij} with $i, j = 1, 2$. For other linear combinations there are kinematic singularities which prohibit a covariant interpretation of the helicity states defined in the center of mass frame only. We observe that the coupling of the P_{11} to the P_{22} projector is kinematically suppressed by the phase space factor $p_{\rho N}^2$. In other words the associated loop functions J_{ij} with $i, j = 1, 2$ have the threshold property $\Im J_{11} \sim p_{\rho N}$, $\Im J_{12} = \Im J_{21} \sim p_{\rho N}^3$ and $\Im J_{22} \sim p_{\rho N}^5$. It is evident that the transformation (40) leads to non-diagonal loop functions because it is not a unitary transformation. In more physical terms the transformation (40) is required because both helicity states $|\rho^{(T)} N, \frac{1}{2}, \frac{1}{2}\rangle$ and $|\rho^{(L)} N, \frac{1}{2}, \frac{1}{2}\rangle$ carry non-zero s-wave components. The projectors given in (38) correspond to the leading $|J=\frac{1}{2}; 1\rangle$ state.

Similarly the implicit matrix structure of the projectors of the $J = \frac{3}{2}$ channel are defined with respect to the three states $|J=\frac{3}{2}; i\rangle$ with $i = 1, 2, 3$ reflecting the presence of one s-wave but two d-wave states. We find the unique transformation

$$\begin{aligned} |J=\frac{3}{2}; 1\rangle &= |\rho^{(T)} N, \frac{3}{2}, \frac{3}{2}\rangle + \sqrt{\frac{2}{3}}\sqrt{1+\vec{q}^2/m_\rho^2} |\rho^{(L)} N, \frac{1}{2}, \frac{3}{2}\rangle + \frac{1}{\sqrt{3}} |\rho^{(T)} N, \frac{1}{2}, \frac{3}{2}\rangle, \\ |J=\frac{3}{2}; 2\rangle &= |\rho^{(L)} N, \frac{1}{2}, \frac{1}{2}\rangle + \frac{1}{\sqrt{2}}\sqrt{1+\vec{q}^2/m_\rho^2} |\rho^{(T)} N, \frac{1}{2}, \frac{3}{2}\rangle, \\ |J=\frac{3}{2}; 3\rangle &= |\rho^{(T)} N, \frac{1}{2}, \frac{3}{2}\rangle, \end{aligned} \quad (41)$$

which leads to well defined associated covariant projectors P_{ij} with $i, j = 1, 2, 3$. The projectors given in (39) correspond to the leading $|J=\frac{3}{2}; 1\rangle$ state. In this work we neglect the contribution of the P_{ij} projectors with $i, j \neq 1$ since their contributions are suppressed close to the vector-meson nucleon threshold by at least the phase space factor $p_{\rho N}^2$. To reliably describe the behavior away from threshold to order $p_{\rho N}^2$ would require the systematic inclusion of p-wave projectors also.

The leading angular momentum L of a given projector $Y_n^{(\pm)}$ follows in a straightforward manner by inspecting the threshold behavior of its associated loop function (see (15)). The required loop functions are first specified in the limit of zero-width vector mesons. In this approximation the loop functions of the ρN channels are

$$J_{33}^{(I+)}(\sqrt{s}, 0) = N_{\rho N}(\sqrt{s}) I_{\rho N}(\sqrt{s}), \quad J_{33}^{(I-)}(\sqrt{s}, 1) = J_{33}^{(I+)}(\sqrt{s}, 0),$$

$$N_{\rho N} = \left(1 + \frac{p_{\rho N}^2}{3 m_\rho^2}\right) \left(\frac{\sqrt{s}}{2} + \frac{m_N^2 - m_\rho^2}{2 \sqrt{s}} + m_N\right), \quad (42)$$

where $\sqrt{s} = \sqrt{m_N^2 + p_{\rho N}^2} + \sqrt{m_\rho^2 + p_{\rho N}^2}$. The master-loop function $I_{\rho N}(\sqrt{s})$ is defined at hand of the pion-nucleon loop function $I_{\pi N}(\sqrt{s})$ in (20). The form of the loop functions in (42) at threshold indeed confirm that the considered vector-meson nucleon channels are s-wave like with $L = 0$. It is understood that $I_{\rho N}(\sqrt{s} = 0) = 0$ holds. Our final vector-meson loop functions are obtained by folding the result (42) with the normalized vector-meson spectral functions $\rho_\rho(q^2)$ and $\rho_\omega(q^2)$ as specified in (32,33,37). This is analogous to the folding performed when evaluating the ω -meson polarization tensor (35). Our final loop functions follow with

$$J_{33}^{(I+)}(\sqrt{s}, 0) \rightarrow \int_{4 m_\pi^2}^{\infty} \frac{d q^2}{\pi} \rho_\rho(q^2) J_{33}^{(I+)}(\sqrt{s}, 0), \quad (43)$$

where the integral in (43) extends over the implicit dependence of $J_{33}^{(I+)}(\sqrt{s}, 0)$ on the vector-meson mass $m_\rho^2 \rightarrow q^2$. The analogous folding is assumed for the $J = \frac{3}{2}$ loop function. The loop functions of the ωN channels are given by complete analogy with (42) and (43).

In order to have a convenient notation for the pion-induced vector-meson production cross sections it is useful to generalize (22) and introduce corresponding partial-wave amplitudes $f^{(IJ\pm)}(\sqrt{s})$. For example in the isospin $\frac{1}{2}$ channel we write:

$$\begin{aligned} f_{\pi N \rightarrow \rho N}^{(\frac{1}{2}\frac{1}{2}+)}(\sqrt{s}) &= \frac{\sqrt{N_{\pi N}^{(+)} N_{\rho N}}}{8 \pi \sqrt{s}} M_{31}^{(\frac{1}{2}+)}(\sqrt{s}, 0), \\ f_{\pi N \rightarrow \rho N}^{(\frac{1}{2}\frac{3}{2}-)}(\sqrt{s}) &= \frac{\sqrt{N_{\pi N}^{(-)} N_{\rho N}}}{8 \pi \sqrt{s}} p_{\pi N} M_{31}^{(\frac{1}{2}-)}(\sqrt{s}, 1). \end{aligned} \quad (44)$$

We derive the vector-meson production cross section in terms of the partial-wave amplitudes in (44). In the zero-width approximation one finds

$$\begin{aligned} \sigma_{\pi^- p \rightarrow \rho^0 n} &= 4 \pi \frac{p_{\rho N}}{p_{\pi N}} \frac{2}{9} \left(\left| f_{\pi N \rightarrow \rho N}^{(\frac{1}{2}\frac{1}{2}+)} - f_{\pi N \rightarrow \rho N}^{(\frac{3}{2}\frac{1}{2}+)} \right|^2 \right. \\ &\quad \left. + 2 \left| f_{\pi N \rightarrow \rho N}^{(\frac{1}{2}\frac{3}{2}-)} - f_{\pi N \rightarrow \rho N}^{(\frac{3}{2}\frac{3}{2}-)} \right|^2 \right), \end{aligned}$$

$$\begin{aligned}\sigma_{\pi^+ p \rightarrow \rho^+ p} &= 4\pi \frac{p_{\rho N}}{p_{\pi N}} \left(\left| f_{\pi N \rightarrow \rho N}^{(\frac{3}{2}\frac{1}{2}+)} \right|^2 + 2 \left| f_{\pi N \rightarrow \rho N}^{(\frac{3}{2}\frac{3}{2}-)} \right|^2 \right), \\ \sigma_{\pi^- p \rightarrow \omega n} &= 4\pi \frac{p_{\omega N}}{p_{\pi N}} \frac{2}{3} \left(\left| f_{\pi N \rightarrow \omega N}^{(\frac{1}{2}\frac{1}{2}+)} \right|^2 + 2 \left| f_{\pi N \rightarrow \omega N}^{(\frac{1}{2}\frac{3}{2}-)} \right|^2 \right).\end{aligned}\quad (45)$$

We include the energy-dependent width of the vector mesons by folding the cross section with the appropriate spectral functions. For example the ρ -meson width is included by the replacement,

$$\sigma_{\pi N \rightarrow \rho N} \rightarrow \int_{4m_\pi^2}^{\infty} \frac{dq^2}{\pi} \rho_\rho(q^2) \sigma_{\pi N \rightarrow \rho N}, \quad (46)$$

where the integrals in (46) extends over the implicit dependence of the bare cross section $\sigma_{\pi N \rightarrow \rho N}$ on the vector-meson mass $m_\rho^2 \rightarrow q^2$. We observe that the folding integral in (46) and (43) are closely related, which basically reflects the unitarity condition. This is clearly illustrated if the cross sections are written in terms of the original amplitudes M rather than the reduced amplitudes f . For instance one may rewrite the ρ^+ production cross section in (45) as follows:

$$\begin{aligned}\sigma_{\pi^+ p \rightarrow \rho^+ p} &= 4\pi \frac{\Im J_{\pi N}^{(1/2)} \Im J_{\rho N}^{(1/2)}}{p_{\pi N}^2} \left| M_{\pi N \rightarrow \rho N}^{(1/2)} \right|^2 \\ &+ 8\pi \frac{\Im J_{\pi N}^{(3/2)} \Im J_{\rho N}^{(3/2)}}{p_{\pi N}^2} \left| M_{\pi N \rightarrow \rho N}^{(3/2)} \right|^2,\end{aligned}\quad (47)$$

where $M_{\pi N \rightarrow \rho N}^{(1/2)}(\sqrt{s}) = M_{31}^{(3/2,+)}(\sqrt{s}, 0)$ and $M_{\pi N \rightarrow \rho N}^{(3/2)}(\sqrt{s}) = M_{31}^{(3/2,-)}(\sqrt{s}, 0)$. Similarly we write identify the loop functions $J_{\rho N}^{(1/2)}(\sqrt{s}) = J_{\rho N}^{(3/2)}(\sqrt{s}) = J_{33}^{(3/2,+)}(\sqrt{s}, 0)$ (see (15)).

4 Photon-induced meson production

We wish to generalize our model to describe electromagnetic processes as to constrain our model parameters by data from photon-induced meson production off the nucleon. Provided that all hadronic amplitudes of the previous sections are well determined by the available hadronic data set a generalized vector-meson dominance assumption would predict a huge amount of electromagnetic processes. Conversely, given a vector-meson dominance assumption the photon-induced reaction data may be used as a consistency check of the hadronic model. In this work we follow a mixed strategy in the sense that we use the ample data on the photon-induced meson production off the nucleon

to further constrain our hadronic reaction amplitudes. This is advantageous because we found out that the present day hadronic data set does not completely determine our hadronic model parameters⁷. Moreover, following this strategy avoids the fitting of some data over-precisely. One should not forget that the hadronic model constructed in the previous sections is rather crude and approximative. Thus it would be misleading to fix part of the model parameters by fitting some precise data point with small error bars that are much smaller than those expected from the accuracy level of the model. We emphasize that there still remains a strong predictive power of our scheme to the extent that many channels for which good data are not available so far, or which are unlikely to be measured, will be predicted.

It is useful to describe the framework within which we consider electromagnetic interactions and construct a generalized vector-meson dominance in our scheme. We will generalize Sakurai's vector meson dominance conjecture by assuming that the electromagnetic quasi-local 4-point interaction vertices of our model are directly proportional to corresponding vertices involving the ρ - and ω -meson fields. The photon field A_μ must be included in a gauge invariant manner. For instance the kinetic term of the photon field,

$$\mathcal{L}_{kin} = -\frac{1}{4} F_{\mu\nu} F^{\mu\nu}, \quad (48)$$

is expressed in terms of the field strength tensor $F_{\mu\nu} = \partial_\mu A_\nu - \partial_\nu A_\mu$. Since in our approach the vector-meson fields do not couple exclusively to conserved vector currents, an interaction vertex $A^\mu \rho_\mu^{(0)}$ or $A^\mu \omega_\mu$ suggested by Sakurai [25] would be in conflict with electromagnetic gauge invariance. We introduce the gauge invariant interaction terms instead

$$\begin{aligned} \mathcal{L}_{int} = & i e A_\mu \rho_\nu^{(-)} (\partial_\mu \rho_\nu^{(+)} - \partial_\nu \rho_\mu^{(+)}) - i e A_\mu \rho_\nu^{(+)} (\partial_\mu \rho_\nu^{(-)} - \partial_\nu \rho_\mu^{(-)}) \\ & - e^2 (A \cdot A) (\rho^{(+)} \cdot \rho^{(-)}) + e^2 (A \cdot \rho^{(+)}) (A \cdot \rho^{(-)}) \\ & + \frac{f_\rho}{2m_\rho^2} F^{\mu\nu} (\partial_\mu \rho_\nu^{(0)} - \partial_\nu \rho_\mu^{(0)}) + \frac{f_\omega}{2m_\omega^2} F^{\mu\nu} (\partial_\mu \omega_\nu - \partial_\nu \omega_\mu) + \dots, \end{aligned} \quad (49)$$

where we use

$$\rho_\mu^{(0)} = \rho_\mu^{(3)}, \quad \rho_\mu^{(\pm)} = \frac{1}{\sqrt{2}} (\rho_\mu^{(1)} \pm i \rho_\mu^{(2)}). \quad (50)$$

One observes that the terms in (49) proportional to f_ρ and f_ω induce a vector-meson dominance type behavior for virtual photons giving the photon hadronic $\rho_\mu^{(0)}$ and ω_μ components as suggested by phenomenology. The

⁷ In view of this we question our preliminary results, which did not consider the photon induced reactions systematically, presented in [30].

parameters f_ω and f_ρ are determined by the $e^+ e^-$ decay widths of the vector mesons

$$\begin{aligned} m_\rho \Gamma_{\rho \rightarrow e^- e^+} &= \frac{\alpha f_\rho^2}{3 m_\rho^4} \sqrt{1 - \frac{4 m_e^2}{m_\rho^2}} (2 m_e^2 + m_\rho^2) , \\ m_\omega \Gamma_{\omega \rightarrow e^- e^+} &= \frac{\alpha f_\omega^2}{3 m_\omega^4} \sqrt{1 - \frac{4 m_e^2}{m_\omega^2}} (2 m_e^2 + m_\omega^2) , \end{aligned} \quad (51)$$

where $\alpha = e^2/(4\pi) \simeq 1/137.04$. The empirical decay widths $\Gamma_{\omega \rightarrow e^+ e^-} = 0.60 \pm 0.02$ keV and $\Gamma_{\rho_0 \rightarrow e^+ e^-} = 6.77 \pm 0.32$ keV lead to the values

$$f_\rho \simeq 0.0357 \text{ GeV}^2, \quad f_\omega \simeq 0.0109 \text{ GeV}^2 . \quad (52)$$

On the other hand, it is evident that the terms proportional to f_ρ or f_ω do not contribute to reactions involving real photons. Therefore in our present approach, in which we do not consider explicit hadronic 3-point vertices but only quasi-local two-body interaction terms, we need to introduce effective 4-point vertices which involve the electromagnetic field tensor $F_{\mu\nu}$ explicitly. Only then the scheme is capable to describe the process of photon-induced meson production. We show a few typical examples we have in mind

$$F^{\mu\nu} \bar{N} \gamma_\mu \vec{\tau} \partial_\nu (N \vec{\pi}), \quad F^{\mu\nu} \bar{N} \gamma_\mu \vec{\tau} N \vec{\rho}_\nu, \quad \dots . \quad (53)$$

It is instructive to discuss such quasi-local two-body interaction terms (53) in view of the vector-meson dominance picture. In the vector-meson dominance approach one insists that the photon couples to hadronic states exclusively via its hadronic components. Interaction terms as given in (53) are typically not considered. Rather they would effectively be generated by corresponding hadronic vertices of the generic form

$$\omega^\mu \bar{N} \gamma_\mu \vec{\tau} N \vec{\pi}, \quad \omega^\mu \bar{N} \vec{\tau} N \vec{\rho}_\mu, \quad \dots . \quad (54)$$

According to the original conjecture of Sakurai [25] the vector-meson converts into a real photon via the interaction terms $A^\mu \rho_\mu^{(0)}$ and $A^\mu \omega_\mu$. In our scheme the terms $A^\mu \rho_\mu^{(0)}$ and $A^\mu \omega_\mu$ are not allowed. In order to implement the successful vector-meson dominance assumption it is therefore natural to directly relate the strength of the $\gamma N \rightarrow X$ and $\rho^{(0)} N \rightarrow X$, $\omega N \rightarrow X$ vertices, where X is any hadronic final state. Note that our construction has similarities with the construction of Kroll, Lee and Zumino [26] only that here we refrain from insisting that the vector mesons couple to conserved currents only.

We specify the generalized form of the vector-meson dominance conjecture as applied for the direct photon-induced production vertices $K_{\gamma N \rightarrow X}^{(I),\mu}(\bar{q}, q; w)$:

$$\begin{aligned} \frac{1}{2} \left(K_{\gamma p \rightarrow X}^{(\frac{1}{2}),\mu} + K_{\gamma n \rightarrow X}^{(\frac{1}{2}),\mu} \right) (\bar{q}, q; w) &= e K_{\nu, \omega N \rightarrow X}^{(\frac{1}{2})} (\bar{q}, q; w) \Gamma_S^{\nu\mu}(q; w), \\ \frac{1}{2} \left(K_{\gamma p \rightarrow X}^{(\frac{1}{2}),\mu} - K_{\gamma n \rightarrow X}^{(\frac{1}{2}),\mu} \right) (\bar{q}, q; w) &= \frac{e}{\sqrt{3}} K_{\nu, \rho N \rightarrow X}^{(\frac{1}{2})} (\bar{q}, q; w) \Gamma_V^{\nu\mu}(q; w), \\ K_{\gamma p \rightarrow X}^{(\frac{3}{2}),\mu} (\bar{q}, q; w) &= e \sqrt{\frac{2}{3}} K_{\nu, \rho N \rightarrow X}^{(\frac{3}{2})} (\bar{q}, q; w) \Gamma_V^{\nu\mu}(q; w), \\ K_{\gamma n \rightarrow X}^{(\frac{3}{2}),\mu} (\bar{q}, q; w) &= e \sqrt{\frac{2}{3}} K_{\nu, \rho N \rightarrow X}^{(\frac{3}{2})} (\bar{q}, q; w) \Gamma_V^{\nu\mu}(q; w), \end{aligned} \quad (55)$$

where X stands for any hadronic two-body final state with isospin I . The transverse isoscalar $\Gamma_S^{\mu\nu}(q; w)$ and isovector $\Gamma_V^{\mu\nu}(q; w)$ objects are to be specified transition tensors. Note that the factors $1/\sqrt{3}$ and $\sqrt{2/3}$ in the ρ -meson contribution follow from the definition of the isospin state in (8). We emphasize that our generalized vector-meson dominance assumption is defined with respect to the unique projector algebra introduced in the previous section. As is evident from (55) we rely on a particular off-shell interpretation of the hadronic production vertex, which is given by the form of the projectors. For the transition tensor $\Gamma_{S(V)}^{\nu\mu}(q; w)$ we make the most general ansatz,

$$\begin{aligned} \Gamma_{S(V)}^{\mu\nu}(q; w) &= \Gamma_{S(V)}^{\mu\nu,+}(q; w) + \Gamma_{S(V)}^{\mu\nu,-}(q; w), \\ \Gamma_{S(V)}^{\mu\nu,\pm}(q; w) &= \frac{g_{S(V),1}^{(\pm)}}{m_\omega} \frac{1}{2} \left(1 \pm \frac{\psi}{\sqrt{w^2}} \right) \left(\left(\not{q} - \frac{w \cdot q}{w^2} \psi \right) g^{\mu\nu} - q^\mu \left(\gamma^\nu - \frac{w^\nu}{w^2} \psi \right) \right) \\ &\quad + \frac{g_{S(V),2}^{(\pm)}}{m_\omega} \frac{1}{2} \left(1 \pm \frac{\psi}{\sqrt{w^2}} \right) \left(\frac{w \cdot q}{\sqrt{w^2}} g^{\mu\nu} - \frac{q^\mu w^\nu}{\sqrt{w^2}} \right) \\ &\quad + \frac{g_{S(V),3}^{(\pm)}}{m_\omega^2} \frac{1}{2} \left(1 \pm \frac{\psi}{\sqrt{w^2}} \right) \left(q^2 g^{\mu\nu} - q^\mu q^\nu \right), \end{aligned} \quad (56)$$

that is compatible with a vertex involving the field strength tensor $F_{\mu\nu}$ (see (53)). We note that we can not exclude the possibility that the coupling constants $g_{S,i}^{(\pm)}$ and $g_{V,i}^{(\pm)}$ are weakly dependent on the total energy \sqrt{s} in some polynomial fashion. We emphasize, however, that any further possible term in (56) would either renormalize the already existing terms or be in conflict with gauge invariance. Here we exploit the fact that our model does not consider any of the hadronic 3-point interaction vertices explicitly. Such interaction terms are supposed to be integrated out with their effect being absorbed into the quasi-local 2-body interaction terms. As a direct consequence the photon can couple to hadrons in $K_{\gamma N \rightarrow X}$ exclusively via the electromagnetic field strength tensor $F_{\mu\nu}$. The parameters $g_{S,i}^{(\pm)}$ and $g_{V,i}^{(\pm)}$ will be determined by the photon-induced meson production data. In fact the coupling constants $g_{S(V),3}^{(\pm)}$ do not contribute in processes with real photons obviously. The ratios $\sqrt{3} g_{S,i}^{(\pm)} / g_{V,i}^{(\pm)}$

may be identified with $f_\omega/f_\rho \simeq 0.3$ naively. In our scheme we consider all parameters $g_{S(V),i}^{(\pm)}$ as free, because we would like to avoid the poorly controlled extrapolation from virtual photon kinematics with $q^2 \simeq m_\omega^2$ down to the real photon point at $q^2 = 0$.

The generalized vector-meson dominance conjecture (55) leads to the γ -induced production amplitudes, $T_{\gamma N \rightarrow X}^{(I),\mu}(\bar{q}, q; w)$,

$$\begin{aligned} \frac{1}{2} \left(T_{\gamma p \rightarrow X}^{(\frac{1}{2}),\mu} + T_{\gamma n \rightarrow X}^{(\frac{1}{2}),\mu} \right) (\bar{q}, q; w) &= e T_{\nu, \omega N \rightarrow X}^{(\frac{1}{2})} (\bar{q}, q; w) \Gamma_S^{\nu\mu}(q; w), \\ \frac{1}{2} \left(T_{\gamma p \rightarrow X}^{(\frac{1}{2}),\mu} - T_{\gamma n \rightarrow X}^{(\frac{1}{2}),\mu} \right) (\bar{q}, q; w) &= \frac{e}{\sqrt{3}} T_{\nu, \rho N \rightarrow X}^{(\frac{1}{2})} (\bar{q}, q; w) \Gamma_V^{\nu\mu}(q; w), \\ T_{\gamma p \rightarrow X}^{(\frac{3}{2}),\mu} (\bar{q}, q; w) &= e \sqrt{\frac{2}{3}} T_{\nu, \rho N \rightarrow X}^{(\frac{3}{2})} (\bar{q}, q; w) \Gamma_V^{\nu\mu}(q; w), \\ T_{\gamma n \rightarrow X}^{(\frac{3}{2}),\mu} (\bar{q}, q; w) &= e \sqrt{\frac{2}{3}} T_{\nu, \rho N \rightarrow X}^{(\frac{3}{2})} (\bar{q}, q; w) \Gamma_V^{\nu\mu}(q; w), \end{aligned} \quad (57)$$

that are directly proportional to the corresponding vector-meson induced production amplitudes. This is a consequence of the generalized vector-meson dominance conjecture (55) and the particular form of the interaction kernel (12).

Given the generalized vector-meson dominance assumption (55) we can now derive photon-induced meson production cross sections in terms of the hadronic reaction amplitudes of the previous sections. In analogy to (44, 45) we express the production cross sections in terms of reduced reaction amplitudes, $f_{h,\gamma N \rightarrow X}^{(IJ\pm)}$, where the lower index h specifies their helicity projection and the signature \pm their parity. We provide explicit expressions of meson-production cross sections for reactions where multipole amplitudes are not established so far,

$$\begin{aligned} \sigma_{\gamma p \rightarrow \eta p} &= 4\pi \frac{p_{\eta N}}{p_{\gamma N}} \left| f_{\frac{1}{2}, \gamma p \rightarrow \eta N}^{(\frac{1}{2}\frac{1}{2}+)} \right|^2, & \sigma_{\gamma p \rightarrow K^+ \Lambda} &= 4\pi \frac{p_{K\Lambda}}{p_{\gamma N}} \left| f_{\frac{1}{2}, \gamma p \rightarrow K\Lambda}^{(\frac{1}{2}\frac{1}{2}+)} \right|^2, \\ \sigma_{\gamma p \rightarrow K^+ \Sigma^0} &= 4\pi \frac{p_{K\Sigma}}{p_{\gamma N}} \frac{1}{3} \left| f_{\frac{1}{2}, \gamma p \rightarrow K\Sigma}^{(\frac{1}{2}\frac{1}{2}+)} + \sqrt{2} f_{\frac{1}{2}, \gamma p \rightarrow K\Sigma}^{(\frac{3}{2}\frac{1}{2}+)} \right|^2, \\ \sigma_{\gamma p \rightarrow K^0 \Sigma^+} &= 4\pi \frac{p_{K\Sigma}}{p_{\gamma N}} \frac{1}{3} \left| \sqrt{2} f_{\frac{1}{2}, \gamma p \rightarrow K\Sigma}^{(\frac{1}{2}\frac{1}{2}+)} - f_{\frac{1}{2}, \gamma p \rightarrow K\Sigma}^{(\frac{3}{2}\frac{1}{2}+)} \right|^2. \end{aligned} \quad (58)$$

The reduced amplitudes, $f_{h,\gamma N \rightarrow X}^{(IJ\pm)}$, are determined by the invariant amplitudes $M_{i3}^{(I\pm)}(\sqrt{s}; J - \frac{1}{2})$ in the isovector and $M_{i4}^{(I\pm)}(\sqrt{s}; J - \frac{1}{2})$ in the isoscalar channel. The helicity index h is required for the $J = \frac{3}{2}$ channel because the invariant amplitudes introduced in (13) couples to two distinct multipole amplitudes. The helicity projection is $h = \frac{1}{2}$ for $J = \frac{1}{2}$ but $h = \frac{1}{2}, \frac{3}{2}$ for $J = \frac{3}{2}$. Note that, if we were to consider the effect of the kinematical suppressed states in (40, 41) an analogous index would be needed for the hadronic amplitudes. We

illustrate our notation at hand of the πN channels,

$$\begin{aligned}
\frac{1}{2} \left(f_{\frac{1}{2}, \gamma p \rightarrow \pi N}^{(\frac{1}{2}\frac{1}{2}+)}(\sqrt{s}) + f_{\frac{1}{2}, \gamma n \rightarrow \pi N}^{(\frac{1}{2}\frac{1}{2}+)}(\sqrt{s}) \right) &= \frac{\sqrt{N_{\pi N}^{(+)} N_{\frac{1}{2}, \gamma N}^{(S+)}}}{8\pi\sqrt{s}} M_{14}^{(\frac{1}{2}+)}(\sqrt{s}; 0) , \\
f_{\frac{1}{2}, \gamma p \rightarrow \pi N}^{(\frac{3}{2}\frac{1}{2}+)}(\sqrt{s}) &= \frac{\sqrt{N_{\pi N}^{(+)} N_{\frac{1}{2}, \gamma N}^{(V+)}}}{8\pi\sqrt{s}} \sqrt{\frac{2}{3}} M_{13}^{(\frac{3}{2}+)}(\sqrt{s}; 0) , \\
\frac{1}{2} \left(f_{h, \gamma p \rightarrow \pi N}^{(\frac{1}{2}\frac{3}{2}-)}(\sqrt{s}) + f_{h, \gamma n \rightarrow \pi N}^{(\frac{1}{2}\frac{3}{2}-)}(\sqrt{s}) \right) &= \frac{\sqrt{N_{\pi N}^{(-)} N_{h, \gamma N}^{(S-)}}}{8\pi\sqrt{s}} p_{\pi N} M_{14}^{(\frac{1}{2}-)}(\sqrt{s}; 1) , \\
f_{h, \gamma p \rightarrow \pi N}^{(\frac{3}{2}\frac{3}{2}-)}(\sqrt{s}) &= \frac{\sqrt{N_{\pi N}^{(-)} N_{h, \gamma N}^{(V-)}}}{8\pi\sqrt{s}} p_{\pi N} \sqrt{\frac{2}{3}} M_{13}^{(\frac{3}{2}-)}(\sqrt{s}; 1) . \tag{59}
\end{aligned}$$

The difference of proton and neutron production amplitudes not specified in (59) follows by analogy with (57). The normalization factor $N_{\pi N}^{(\pm)}$ for the pseudo-scalar channel was introduced already in (23). It remains to specify the normalization factors $N_{h, \gamma N}^{(S(V)\pm)}$ for the initial state,

$$\begin{aligned}
\sqrt{2\sqrt{s} N_{\frac{1}{2}, \gamma N}^{(S(V)+)}} &= e \frac{p_{\gamma N}}{\sqrt{3}} \left(2 \frac{\sqrt{s} - m_N}{m_\omega} g_{S(V),1}^{(+)} + \frac{\sqrt{s} + m_N}{m_\omega} g_{S(V),2}^{(+)} \right) , \\
\sqrt{2\sqrt{s} N_{\frac{1}{2}, \gamma N}^{(S(V)-)}} &= e \frac{p_{\gamma N}}{2\sqrt{3}} \left(-\frac{\sqrt{s} - m_N}{m_\omega} g_{S(V),1}^{(+)} + \frac{\sqrt{s} + m_N}{m_\omega} g_{S(V),2}^{(+)} \right) , \\
\sqrt{2\sqrt{s} N_{\frac{3}{2}, \gamma N}^{(S(V)-)}} &= e \frac{p_{\gamma N}}{2} \left(\frac{\sqrt{s} - m_N}{m_\omega} g_{S(V),1}^{(+)} + \frac{\sqrt{s} + m_N}{m_\omega} g_{S(V),2}^{(+)} \right) . \tag{60}
\end{aligned}$$

Note that the normalization factors (60) do not involve the vector-meson dominance parameters $g_{S(V),i}^{(-)}$. The reliable determination of the latter parameters requires the study of further multipole amplitudes, which couple to πN states not considered in this work. We imply a notation analogous to (59, 60) for the $K\Lambda$, $K\Sigma$ and ηN channels.

For photon-induced pion production it is more appropriate to compare with the multipole analysis [31]. We identify the electric and magnetic multipole amplitudes $E_{l\pm}^{(p,n)}$ and $M_{l\pm}^{(p,n)}$ (see e.g. [32,33]) by

$$\begin{aligned}
E_{0+}^{(p)}(S_{11}) &= f_{\frac{1}{2}, \gamma p \rightarrow \pi N}^{(\frac{1}{2}\frac{1}{2}+)}(\sqrt{s}) , \quad E_{0+}^{(n)}(S_{11}) = f_{\frac{1}{2}, \gamma n \rightarrow \pi N}^{(\frac{1}{2}\frac{1}{2}+)}(\sqrt{s}) , \\
E_{2-}^{(p)}(D_{13}) - 3 M_{2-}^{(p)}(D_{13}) &= 2 f_{\frac{1}{2}, \gamma p \rightarrow \pi N}^{(\frac{1}{2}\frac{3}{2}-)}(\sqrt{s}) , \\
E_{2-}^{(n)}(D_{13}) - 3 M_{2-}^{(n)}(D_{13}) &= 2 f_{\frac{1}{2}, \gamma n \rightarrow \pi N}^{(\frac{1}{2}\frac{3}{2}-)}(\sqrt{s}) ,
\end{aligned}$$

$$\begin{aligned}
E_{2-}^{(p)}(D_{13}) + M_{2-}^{(p)}(D_{13}) &= \frac{2}{\sqrt{3}} f_{\frac{3}{2}, \gamma p \rightarrow \pi N}^{(\frac{1}{2}\frac{3}{2}-)}(\sqrt{s}), \\
E_{2-}^{(n)}(D_{13}) + M_{2-}^{(n)}(D_{13}) &= \frac{2}{\sqrt{3}} f_{\frac{3}{2}, \gamma n \rightarrow \pi N}^{(\frac{1}{2}\frac{3}{2}-)}(\sqrt{s}), \\
E_{0+}^{(p)}(S_{31}) &= f_{\frac{1}{2}, \gamma p \rightarrow \pi N}^{(\frac{3}{2}\frac{1}{2}+)}(\sqrt{s}), \\
E_{2-}^{(p)}(D_{33}) - 3 M_{2-}^{(p)}(D_{33}) &= 2 f_{\frac{1}{2}, \gamma p \rightarrow \pi N}^{(\frac{3}{2}\frac{3}{2}-)}(\sqrt{s}), \\
E_{2-}^{(p)}(D_{33}) + M_{2-}^{(p)}(D_{33}) &= \frac{2}{\sqrt{3}} f_{\frac{3}{2}, \gamma p \rightarrow \pi N}^{(\frac{3}{2}\frac{3}{2}-)}(\sqrt{s}). \tag{61}
\end{aligned}$$

The matching of the multipole amplitudes in (61) is determined only up to an overall phase reflecting a particular convention for the production amplitude. The phase ambiguity reduces to a sign ambiguity if we insist on the reality of the interaction kernel $V^{(\pm)}(\sqrt{s}; n)$ in (16). In our present scheme the overall sign of a given off-diagonal hadronic amplitude with fixed isospin and total angular momentum may be flipped by a simultaneous sign change of all off-diagonal coupling constants in that channel without affecting any hadronic reaction cross section considered in this work. It is evident that precise differential hadronic production cross sections and polarization data, not available in most cases, could eliminate any phase ambiguity at least in principle. We emphasize that in our scheme all phases of the hadronic amplitudes are determined unambiguously once we incorporate the constraints from the photon-induced pion production data as parameterized conveniently in terms of the multipole amplitudes.

Finally we present the cross sections for photon-induced vector-meson production. We emphasize that these production processes, once they are studied experimentally in sufficient detail, offer the most stringent consistency test of the hadronic $VN \rightarrow VN$ scattering amplitudes. It would be desirable to establish a multipole analysis of the photon-induced vector-meson production data. This offers a powerful means to verify or disprove any type of vector-meson dominance assumption and permits in the former case a detailed consistency check of the various hadronic amplitudes with different angular momenta. At present there are basically only total cross sections available, for which we present explicit expressions,

$$\begin{aligned}
\sigma_{\gamma p \rightarrow \rho^0 p} &= 4\pi \frac{p_{\rho N}}{p_{\gamma N}} \frac{1}{3} \left(\left| f_{\frac{1}{2}, \gamma p \rightarrow \rho N}^{(\frac{1}{2}\frac{1}{2}+)} + \sqrt{2} f_{\frac{1}{2}, \gamma p \rightarrow \rho N}^{(\frac{3}{2}\frac{1}{2}+)} \right|^2 \right. \\
&\quad + 2 \left| f_{\frac{1}{2}, \gamma p \rightarrow \rho N}^{(\frac{1}{2}\frac{3}{2}-)} + \sqrt{2} f_{\frac{1}{2}, \gamma p \rightarrow \rho N}^{(\frac{3}{2}\frac{3}{2}-)} \right|^2 \\
&\quad \left. + 2 \left| f_{\frac{3}{2}, \gamma p \rightarrow \rho N}^{(\frac{1}{2}\frac{3}{2}-)} + \sqrt{2} f_{\frac{3}{2}, \gamma p \rightarrow \rho N}^{(\frac{3}{2}\frac{3}{2}-)} \right|^2 \right),
\end{aligned}$$

$$\begin{aligned}
\sigma_{\gamma p \rightarrow \rho^+ n} &= 4\pi \frac{p_{\rho N}}{p_{\gamma N}} \frac{1}{3} \left(\left| \sqrt{2} f_{\frac{1}{2}, \gamma p \rightarrow \rho N}^{(\frac{1}{2}\frac{1}{2}+)} - f_{\frac{1}{2}, \gamma p \rightarrow \rho N}^{(\frac{3}{2}\frac{1}{2}+)} \right|^2 \right. \\
&\quad + 2 \left| \sqrt{2} f_{\frac{1}{2}, \gamma p \rightarrow \rho N}^{(\frac{1}{2}\frac{3}{2}-)} - f_{\frac{1}{2}, \gamma p \rightarrow \rho N}^{(\frac{3}{2}\frac{3}{2}-)} \right|^2 \left. \right) \\
&\quad + 2 \left| \sqrt{2} f_{\frac{3}{2}, \gamma p \rightarrow \rho N}^{(\frac{1}{2}\frac{3}{2}-)} - f_{\frac{3}{2}, \gamma p \rightarrow \rho N}^{(\frac{3}{2}\frac{3}{2}-)} \right|^2 \left. \right), \\
\sigma_{\gamma p \rightarrow \omega n} &= 4\pi \frac{p_{\omega N}}{p_{\gamma N}} \left(\left| f_{\frac{1}{2}, \gamma p \rightarrow \omega N}^{(\frac{1}{2}\frac{1}{2}+)} \right|^2 + 2 \left| f_{\frac{1}{2}, \gamma p \rightarrow \omega N}^{(\frac{1}{2}\frac{3}{2}-)} \right|^2 + 2 \left| f_{\frac{3}{2}, \gamma p \rightarrow \omega N}^{(\frac{1}{2}\frac{3}{2}-)} \right|^2 \right), \quad (62)
\end{aligned}$$

in terms of the reduced amplitudes. As is implicit in (62) the description of the $\gamma N \rightarrow VN$ process requires various multipole amplitudes even at energies close to the production threshold. In order to determine the amplitudes separately experiments with a polarized beam and target are required. We emphasize that our model predicts all multipole amplitudes of the $\gamma N \rightarrow VN$ process required to describe the vector-meson production process in any detail for energies close to the production threshold,

$$\begin{aligned}
\frac{1}{2} \left(f_{\frac{1}{2}, \gamma p \rightarrow \rho N}^{(\frac{1}{2}\frac{1}{2}+)}(\sqrt{s}) + f_{\frac{1}{2}, \gamma n \rightarrow \rho N}^{(\frac{1}{2}\frac{1}{2}+)}(\sqrt{s}) \right) &= \frac{\sqrt{N_{\rho N} N_{\frac{1}{2}, \gamma N}^{(S+)}}}{8\pi\sqrt{s}} M_{43}^{(\frac{1}{2}+)}(\sqrt{s}, 0), \\
f_{\frac{1}{2}, \gamma p \rightarrow \rho N}^{(\frac{3}{2}\frac{1}{2}+)}(\sqrt{s}) &= \frac{\sqrt{N_{\rho N} N_{\frac{1}{2}, \gamma N}^{(V+)}}}{8\pi\sqrt{s}} \sqrt{\frac{2}{3}} M_{33}^{(\frac{3}{2}+)}(\sqrt{s}; 0), \\
\frac{1}{2} \left(f_{h, \gamma p \rightarrow \rho N}^{(\frac{1}{2}\frac{3}{2}-)}(\sqrt{s}) + f_{h, \gamma n \rightarrow \rho N}^{(\frac{1}{2}\frac{3}{2}-)}(\sqrt{s}) \right) &= \frac{\sqrt{N_{\rho N} N_{h, \gamma N}^{(S-)}}}{8\pi\sqrt{s}} M_{43}^{(\frac{1}{2}-)}(\sqrt{s}, 1), \\
f_{h, \gamma p \rightarrow \rho N}^{(\frac{3}{2}\frac{3}{2}-)}(\sqrt{s}) &= \frac{\sqrt{N_{\rho N} N_{h, \gamma N}^{(V-)}}}{8\pi\sqrt{s}} \sqrt{\frac{2}{3}} M_{33}^{(\frac{3}{2}-)}(\sqrt{s}; 1). \quad (63)
\end{aligned}$$

5 Results

In this section we present the results of our fits to the data set. In accordance with the effective field theory approach introduced in the previous sections only data in an appropriate kinematical window is used in the analysis. The threshold for elastic scattering is at $\sqrt{s} \simeq 1.1$ GeV, while that for vector-meson production off a nucleon is at $\sqrt{s} \simeq 1.7$ GeV. Because we do not expect our scheme to be efficient close to the elastic pion-nucleon threshold, we fit only data in the energy range $1.4 \text{ GeV} \leq \sqrt{s} \leq 1.8 \text{ GeV}$. We use the ansatz (16) with energy independent interaction matrices $g_{0,1}^{(\pm)}$ that parameterize quasi-local two-body interaction vertices of defined isospin and total angular momentum. In the model we include four spin and isospin channels with $I = \frac{1}{2}, \frac{3}{2}$ and $J = \frac{1}{2}, \frac{3}{2}$. For each value of spin and isospin, channels with different mesons and baryons are coupled by the interaction matrices. In our scheme, an acceptable fit to the data in these channels requires that the s- and d-wave baryon resonances $N(1535)$, $N(1650)$, $N(1520)$, $\Delta(1620)$ and $\Delta(1700)$ are generated dynamically. This is in contrast to the more conventional approaches [34,15–17,35] where such resonances are already part of the interaction kernel. Our approach leads to loop functions (see e.g. (19)) and scattering amplitudes that are analytic and satisfy the expected dispersion-integral representation implied by micro causality of local quantum field theories.

The set of parameters is adjusted to describe the partial-wave pion-nucleon phase shifts including their inelasticity parameters. Furthermore the pion- and photon-induced production cross sections of pseudo-scalar meson and vector mesons are included in the fit. The production cross sections provide crucial information on the coupling to specific channels, which obviously cannot be extracted from the inelasticity parameters of the pion-nucleon phase shifts alone. Ideally one should try to fit the two-pion data directly rather than possibly model dependent production cross sections for the different sub channels. However, in the present scheme, which does not include e.g. the p-wave channels, this would not make sense because potentially important contributions to the total cross sections are missing. We point out that the relative distribution of the various inelastic channels is constrained by the ρN and $\pi \Delta$ production data because these data clearly prevent an overestimate of the inelasticity into the two-pion channel. Here we exploit the fact that the inelasticity parameters of the πN phase shifts define the total inelastic strength. We checked that the sum of the partial isobar-production cross sections of our fit does not exceed the measured total $\pi \Delta$ cross sections. Since for this channel differential cross sections are not available and since there is no reason to expect the production cross section to be dominated by s- and d-waves at the energies considered, we do not fit the isobar production cross sections directly. Moreover, we note that the angular distribution of the two-pion production data is to a large extend already encoded in the inelasticity parameters of the pion-nucleon phase

shifts, provided that the relative importance of the dominant inelastic two-pion channels ρN and $\pi\Delta$ are treated correctly.

In some of the data sets, like e.g. the total cross section for the reaction $\pi^- p \rightarrow \rho^0 n$, only a few points are included in the fit, while e.g. for the πN phase shifts about 25 data points per channel, with fairly small error bars, are considered. Consequently, if one naively sums up the chi-squared errors of all data sets, a poor overall agreement with a small data set would be punished by only a small increase of the total chi-squared. This would lead to an undesired imbalance between the large and small data sets. In order to obtain a uniform reproduction of all data sets, we therefore introduce weighting factors, which enhance the weight of small data sets, when otherwise a reasonable overall description could not be obtained. Moreover, for the production cross sections we reduce the upper limit of the fitting window down to values where we expect the cross section to be dominated by s-wave dynamics. In view of this it does not make too much sense to provide the final chi-squared of our fit. The parameter search is performed with the FORTRAN routine MINUIT [36]. The statistical error in the coupling constants of the fit are estimated in the standard way by using the MINUIT error analysis. For our final solution we find that one standard deviation corresponds to an error of typically one percent in the coupling constants. This is certainly an underestimate of the error for two reasons. First, the sample is not statistical due to the weighting procedure. Second, the systematic errors, due e.g. to approximations and model assumptions, are not accounted for. However, it is very difficult to estimate these errors. The expected errors obviously propagate into the resonance coupling constants discussed below. Thus, the relative statistical errors of these parameters are expected to be of similar magnitude. The reader may judge the quality of the fit by the detailed comparison of our model results with the data presented below.

The empirical pion- and photon-induced vector-meson production data are of crucial importance to our fit. Only when they are included it is possible to determine the vector-meson nucleon scattering amplitudes, the primary goal of this work. In Fig. 1 we compare the results of our model for the ρ - and ω -meson production cross sections with data. Only the first few data points are included in the fit, since one can expect s-wave dominance only close to threshold. Note that a reliable separation of the partial wave would require differential cross sections, which in many cases are not available. The deviation of our model from the empirical cross section at energies $\sqrt{s} \simeq 1.8$ GeV and above leaves room for the contribution from higher partial waves, in particular the p-waves, not included in our model.

The bumps in the ρ -meson production cross section at \sqrt{s} below 1.7 GeV are due to the coupling to resonances below the nominal threshold, like the $N(1535)$ and $\Delta(1620)$. This illustrates the important role these resonances

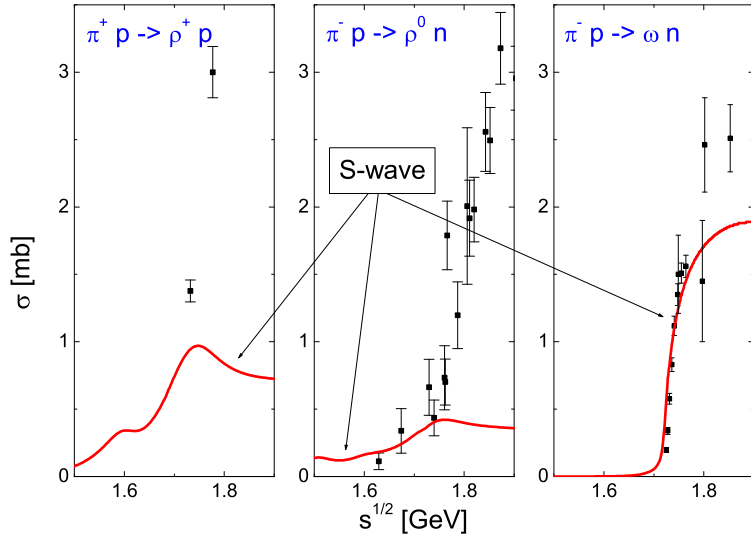


Fig. 1. Pion-induced vector-meson production. The data are taken from [37–39].

may play in the ρ -nucleon dynamics, in qualitative agreement with the findings of Manley and Saleski [19]. As compared to our previous analysis [30], where we did not consider the photon induced reactions systematically, we find a much reduced importance of the $N(1520)$ resonance for the subthreshold ρ^0 production cross section. Note that the very first data point which was questioned in [40] was not included in the fit.

The large discrepancy between the analysis of Manley *et al.* [19] and that of Brody *et al.* [37], as shown in [40], illustrates the ambiguity inherent in the extraction of the ρ -meson production cross section, in particular below the nominal threshold. Within our model we are able to find a consistent description of the ρ production cross section of Brody *et al.* and the E_{2-} and M_{2-} multipole amplitudes. Given the vector-meson dominance assumption, we find it difficult to accommodate a coupling of the $N(1520)$ to the ρN channel of the strength found by Manley *et al.* [19].

We find that the ω meson couples strongly to the $N(1520)$, $N(1535)$ and $N(1650)$ resonances. This is manifest in the ωN scattering amplitudes, presented in the subsequent sections. Due to the small width of the ω meson, the subthreshold resonances are not visible in the ω -meson production cross section shown in Fig. 1. Note that the production cross section was measured at fixed relative momentum in the final state[38] while the calculation is done at fixed energy. This leads to an uncertainty in the energy resolution close to the production threshold which is on the order of the ω -meson width. For a recent K-matrix analysis of this cross sections see [42].

In Fig. 2 we compare our photon-induced ρ - and ω -meson production cross

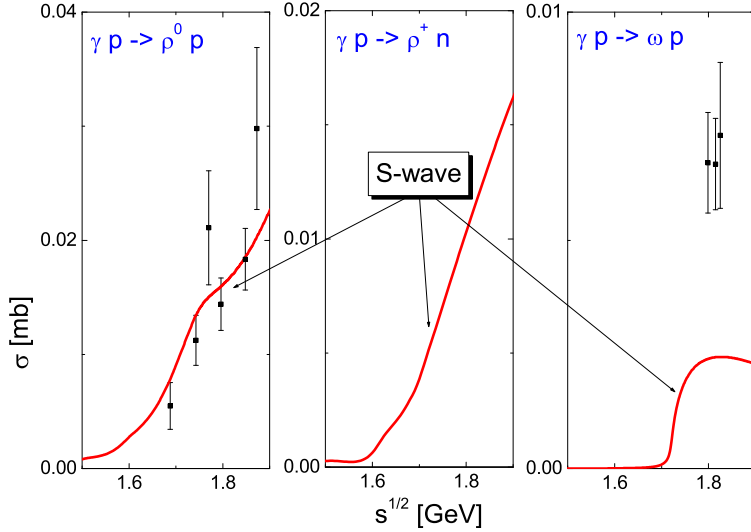


Fig. 2. Photon-induced vector-meson production. The data points are taken from [44].

sections with the data. Using the generalized vector-meson dominance conjecture (55,56), the photon-induced meson-production amplitudes are given in terms of the amplitudes for the corresponding vector-meson induced reaction and the four coupling constants, $g_{S,1}^{(+)}, g_{V,1}^{(+)}$ and $g_{S,2}^{(+)}, g_{V,2}^{(+)}$ specifying the vector-meson dominance assumption. Our best fit is obtained for

$$g_{S,1}^{(+)} = 0.083, \quad g_{V,1}^{(+)} = 0.469, \quad g_{S,2}^{(+)} = 0.000, \quad g_{V,2}^{(+)} = 0.241. \quad (64)$$

We recall that the deviation of $\sqrt{3} g_{S,i}^{(+)} / g_{V,i}^{(+)}$ from the ratio $f_\omega / f_\rho \simeq 0.3$ is a measure for the importance of an off-shell extrapolation from virtual photon kinematics at $q^2 \simeq m_\omega^2$ down to the photon point $q^2 = 0$. The parameters f_ω and f_ρ are determined by the decay of the vector mesons into lepton pairs and therefore correspond to virtual photons with $q^2 = m_\omega^2$ or $q^2 = m_\rho^2$. The fact that we find $\sqrt{3} g_{S,1}^{(+)} / g_{V,1}^{(+)} \simeq f_\omega / f_\rho$ but $\sqrt{3} g_{S,2}^{(+)} / g_{V,2}^{(+)} < f_\omega / f_\rho$ demonstrates that this off-shell extrapolation is quite non-trivial. Although the deviations from the naive vector-meson dominance expectation are strong for the $g_{S(V),2}$ parameters, the generic picture with $g_{S,2}^{(+)} < g_{V,2}^{(+)}$ is confirmed. In the fit we again include only the first few data points close to threshold, where one can expect the s-wave contribution to dominate. While our model describes the ρ^0 -meson production cross section reasonably well, it deviates strongly from the empirical ω -meson production cross section at $\sqrt{s} \simeq 1.8$ GeV where the data points start. On a qualitative level, the discrepancy may be understood if the ω -meson production cross section is dominated by the one-pion-exchange contribution, as suggested by one-boson-exchange models (see e.g. [43]). Since

the one-pion-exchange interaction is long ranged, this would imply that there are important contributions to the angle-averaged cross section from higher partial waves, which are not considered in our scheme at present. Note that the same argument applies for the pion-induced ρ -production cross sections of Fig. 1 which also allow for a t-channel one-pion-exchange contribution. On the other hand, it is evident that there is no one-pion-exchange contribution in the $\pi^- p \rightarrow \omega n$ reaction. The same holds for the $\gamma p \rightarrow \rho^0 p$ reaction provided that it is dominated by its isovector amplitude as suggested by (64). Consequently one expects the interaction in these channels to be short ranged and higher partial waves to be less important. The corresponding cross sections are described by our model fairly well up to higher energies suggesting that higher partial wave contributions are indeed small. In Fig. 2 we also show our prediction for the γ -induced ρ^+ -production cross section. At present there are no data available for this reaction close to the production threshold.

In the remainder of this section we discuss the results that are specific to the four spin- and isospin-channels. For a channel with given isospin I and angular momentum J we list the coupling constants $g_{J-\frac{1}{2}}^{(I\pm)}$, confront our model with the appropriate pion-nucleon phase shift and if available present further relevant data on inelastic reactions. The resulting scattering amplitudes are compared with a schematic resonance exchange model. The discussions are most detailed for the S_{11} and D_{13} channels and arguments which apply to all channels are not repeated.

5.1 $I J^P = \frac{1}{2} \frac{1}{2}^-$ channel

In the $I J^P = \frac{1}{2} \frac{1}{2}^-$ sector we include the πN , $\pi \Delta$, ρN , ωN , ηN , $K \Lambda$ and $K \Sigma$ channels. In order to reduce the number of parameters we impose a par-

| ij | 11 | 15 | 16 | 17 | 55 | 56 | 57 | 66 | 67 | 77 | 11 | 14 | 44 | | [1/ m_π] |
|----------------|----|----|----------------|----------------|---------------|----------------|----------------|---------------|----|----|----|----|----|-------|---------------|
| $c_{ij}^{(1)}$ | 2 | 0 | $-\frac{3}{2}$ | $\frac{1}{2}$ | 0 | $-\frac{3}{2}$ | $-\frac{3}{2}$ | 0 | 0 | 2 | -1 | -1 | -1 | h_1 | 2.62 |
| $c_{ij}^{(2)}$ | 2 | 0 | 0 | 0 | 2 | 0 | 0 | 2 | 0 | 2 | 2 | 0 | 2 | h_2 | 0.20 |
| $c_{ij}^{(3)}$ | 0 | 0 | 0 | 1 | 0 | 1 | 0 | 0 | 0 | 0 | 0 | 1 | 0 | h_3 | 8.79 |
| $c_{ij}^{(4)}$ | 1 | 1 | $-\frac{1}{2}$ | $-\frac{1}{2}$ | $\frac{5}{3}$ | $\frac{1}{6}$ | $-\frac{1}{2}$ | $\frac{5}{3}$ | 1 | 1 | 1 | 1 | 1 | h_4 | 1.76 |
| $c_{ij}^{(5)}$ | 1 | 1 | $-\frac{3}{2}$ | $\frac{1}{2}$ | -1 | $\frac{1}{2}$ | $\frac{1}{2}$ | 0 | 0 | -2 | 1 | -1 | 1 | h_5 | -4.03 |
| $c_{ij}^{(6)}$ | 0 | 0 | 0 | -1 | 0 | -1 | 0 | 0 | 0 | 0 | 0 | -1 | 0 | h_6 | 9.88 |

Table 1

Expansion coefficients $c_{ij}^{(k)}$ as defined in (65). The first 10 columns are the coefficients for the isospin one half channel, the proceeding columns provide the coefficients for the isospin three half channel. For the labelling of the channels see (8).

| $g_0^{(\frac{1}{2},+)} [m_\pi^{-\frac{n+m}{2}}]$ | $\pi N[n=1]$ | $\pi\Delta[n=3]$ | $\rho N[n=1]$ | $\omega N[n=1]$ | $\eta N[n=1]$ | $K\Lambda[n=1]$ | $K\Sigma[n=1]$ |
|--|--------------|------------------|---------------|-----------------|---------------|-----------------|----------------|
| $\pi N[m=1]$ | 3.35 | -30.55 | 6.36 | 9.78 | -2.29 | 1.24 | -2.66 |
| $\pi\Delta[m=3]$ | -30.55 | 0.00 | -10.98 | -14.02 | 15.48 | -19.36 | 14.35 |
| $\rho N[m=1]$ | 6.36 | -10.98 | 10.66 | 3.13 | -5.50 | 3.61 | 1.86 |
| $\omega N[m=1]$ | 9.78 | -14.02 | 3.13 | 16.36 | -9.35 | -9.16 | 8.56 |
| $\eta N[m=1]$ | -2.29 | 15.48 | -5.50 | -9.35 | 7.33 | -6.75 | -6.83 |
| $K\Lambda[m=1]$ | 1.24 | -19.36 | 3.61 | -9.16 | -6.75 | 3.30 | 1.75 |
| $K\Sigma[m=1]$ | -2.66 | 14.35 | 1.86 | 8.56 | -6.83 | 1.75 | 15.45 |

Table 2

Coupling constants in the $IJ^P = \frac{1}{2}\frac{1}{2}^-$ channel. We use $m_\pi = 139$ MeV.

tial SU(3) constraint on the coupling constants. The interaction strengths of the four pseudo-scalar channels $\pi N, \eta N, K\Lambda$ and $K\Sigma$ are given in terms of 6 parameters only, corresponding to the number of available SU(3) invariant tensors. This leaves us with all together 24 parameters in this channel. Note that in our present scheme it would not be justified to insist on SU(3) relations in the vector-meson nucleon channels, because some of the channels required in a SU(3) symmetric description like $K_\mu \Lambda$ and $\phi_\mu N$ are integrated out. In order to implement the SU(3) relations we decompose the coupling matrix for $i, j = 1, 5, 6, 7$ in SU(3) invariants

$$g_{0,ij}^{(\frac{1}{2},+)} = \sum_{k=1}^6 c_{ij}^{(k)} h_k. \quad (65)$$

The expansion coefficients $c_{ij}^{(k)}$ and the best-fit values of the parameters h_i are listed in Tab. 1. We note that the $k = 1$ term in (65) has the SU(3) tensor structure of the Weinberg-Tomozawa term. As shown by the sizable values of h_k for $k > 1$, we find that the flavor structure of the Weinberg-Tomozawa term is not sufficient to describe the data in the pseudo-scalar channels. This is not surprising because in our scheme the interaction kernel represents the scattering amplitude at $\sqrt{s} = 0$ where there is no reason to expect that the Weinberg-Tomozawa interaction dominates the amplitude. The complete coupling matrix $g_0^{(\frac{1}{2},+)}$ is given in Tab. 2. Since there are important components in basically all channels, it is difficult to select a dominating channel. In particular we find no reason to single out the pseudo-scalar channels.

The pion-nucleon phase shift and the inelasticity parameter are well reproduced by our model as demonstrated in Fig. 3. The phase shift and inelasticity parameter show characteristic structures at $\sqrt{s} \simeq 1535$ MeV and $\sqrt{s} \simeq 1650$ MeV, which correspond to the $IJ^P = \frac{1}{2}\frac{1}{2}^-$ baryon resonances $N(1535)$ and $N(1650)$. In contrast to the work of [47,48], where only the pseudoscalar channels were included, we find that both resonances can be generated by

coupled-channel dynamics. This illustrates the importance of the additional channels that are included in our model, in particular the ρN and ωN channels. Clearly a description of the scattering data at energies beyond $\sqrt{s} \simeq 1550$ MeV is impossible in a scheme where the second resonance, $N(1650)$, is missing.

We now turn to the multipole amplitudes of the γ -induced pion production process. Given the generalized vector-meson dominance conjecture, the multipole amplitudes $E_{0+}^{(p)}(S_{11})$ and $E_{0+}^{(n)}(S_{11})$, shown in Fig. 4, are related to the pion-induced vector-meson production amplitudes. Thus, the constraints provided by the multipole amplitudes are similar to those of the pion-induced vector-meson production data, however, the amplitudes are tested also at energies below the vector-meson production threshold. Furthermore, the multipole amplitudes correspond to combinations of the $\pi N \rightarrow \rho/\omega N$ amplitudes that differ from those probed in the pion-induced vector-meson production processes. In particular, there is interference between the isoscalar and isovector amplitudes which gives a handle on the relative phases of the amplitudes. The multipole amplitudes clearly reflect the presence of the s-wave nucleon resonances $N(1535)$ and $N(1650)$. Within the window of applicability $1.4 < \sqrt{s} < 1.8$ we obtain a satisfactory description of the multipole amplitudes. Close to the production threshold we do not expect our model to describe the multipole amplitudes well, in particular the real parts, because the strong energy dependence implied by the one-pion exchange contribution is not treated properly in our present scheme.

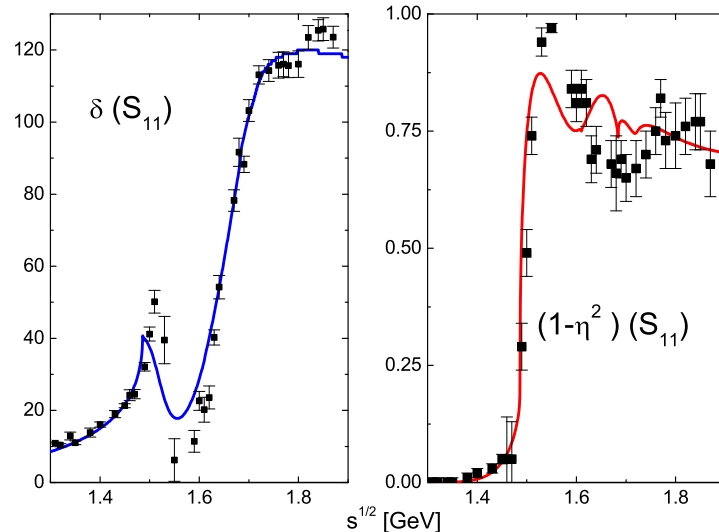


Fig. 3. Pion-nucleon scattering phase shift $\delta_{S_{11}}$ and inelasticity parameter $\eta_{S_{11}}$ of the S_{11} channel. Our results shown by solid lines are compared to the single energy solution SP98 of [45,46].

It is instructive to discuss the pseudo-scalar meson-baryon scattering lengths in some detail. A reliable extraction of a given scattering length from the data set requires that the model considers all rapid energy variations induced for example by the opening of inelastic channels or the presence of close by resonances. For instance the ηN threshold is quite close to the $N(1535)$ resonance. Thus a good value for the ηN scattering length should be based on a model describing the $N(1535)$ resonance in a realistic manner. Similarly we expect that it is important to consider the inelastic ρN and ωN channels when deriving the $K\Lambda$ and $K\Sigma$ scattering lengths, simply because the threshold values of those four channels are quite close to each other. Since we consider all above inelastic channels, we are convinced that our model permits reliable extractions of the pseudo-scalar meson baryon scattering lengths:

$$\begin{aligned} a_{\eta N}^{(\frac{1}{2})} &\simeq (0.43 + i 0.21) \text{ fm} , & a_{K\Lambda}^{(\frac{1}{2})} &\simeq (0.26 + i 0.10) \text{ fm} , \\ a_{K\Sigma}^{(\frac{1}{2})} &\simeq (-0.15 + i 0.09) \text{ fm} , & a_{K\Sigma}^{(\frac{3}{2})} &\simeq (-0.13 + i 0.04) \text{ fm} . \end{aligned} \quad (66)$$

We observe that our value for the eta-meson nucleon scattering length is quite consistent with previous analyses [34] with $a_{\eta N} \simeq (0.51 + i 0.21)$ fm, and [49] with $a_{\eta N} \simeq (0.55 + i 0.30)$. For a detailed discussion of the various analyses including a more complete collection of references we suggest the recent work by Green and Wychech [50]. Their latest scattering length, which favors

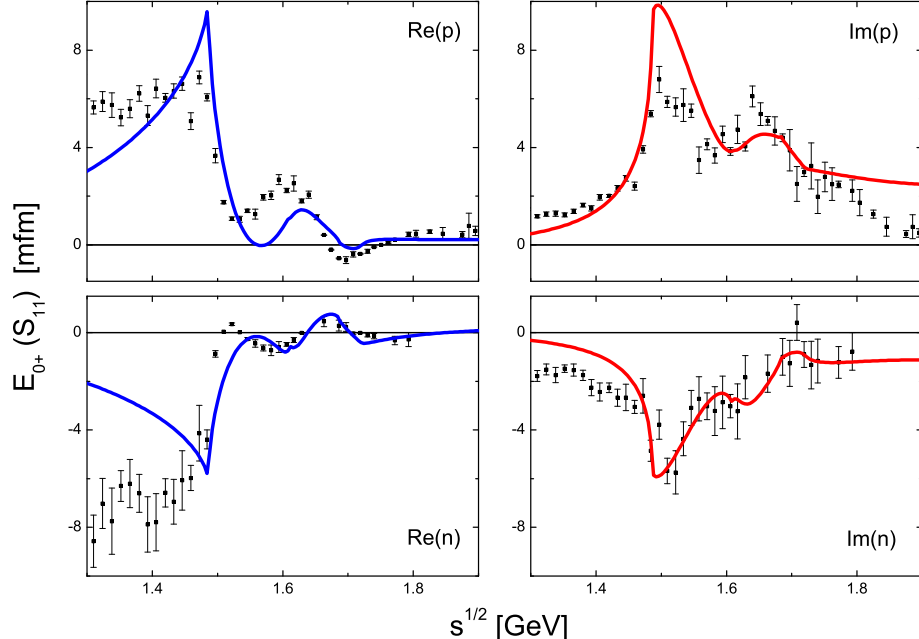


Fig. 4. Multipole amplitudes $E_{0+}^{(p)}(S_{11})$ and $E_{0+}^{(n)}(S_{11})$ of γ -induced pion production. Our amplitudes are confronted to those of the single energy analysis SM00 of [31,46]

a relatively large real part of about 1 fm, was obtained by a simultaneous analysis of the pion and photon induced eta production data. For the kaon-hyperon scattering lengths the existing literature is much more sparse. The value $a_{K\Lambda} \simeq (0.06 + i 0.03)$ fm was obtained recently in [51] in a coupled channel approach which does not consider the important ρN , ωN and $\pi\Delta$ channels (see also [15]). Their value differs from our result in (66) by about a factor four.

The values for the scattering lengths derived in our work are a particular interpretation of the pion- and photon-induced eta and kaon production data of Fig. 5. The pion- and γ -induced kaon production cross section with an associated Σ hyperon will be shown in the next section when presenting the s-wave dynamics in the isospin three half channel. The discrepancy of our model and some of the cross section data in Fig. 5 starting somewhat above threshold is expected since higher partial waves are not included in the analysis. The s-wave dominance for the considered reactions is confirmed qualitatively by available differential cross section data [52,54,55]. Note that there is no one-pion-exchange contribution in any of these cross sections. An improved treatment would profit from high quality differential production cross sections and polarization data not available for all reactions at present.

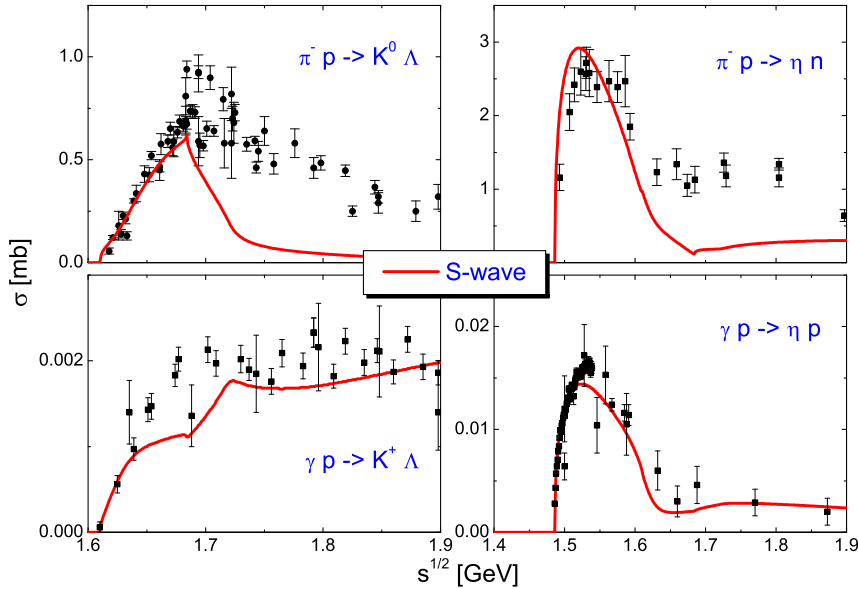


Fig. 5. Pion- and γ -induced ηN and $K\Lambda$ production cross sections. The data are taken from [52,53,39].

5.1.1 Scattering amplitudes

Our model analysis leads to well defined vector-meson production and vector-meson nucleon scattering amplitudes. These amplitudes constitute the central result of our work. In Fig. 6 we present the pion-induced vector-meson production amplitudes introduced in (133). The vector-meson nucleon scattering amplitudes are displayed in Fig. 7. The $N(1535)$ and $N(1650)$ resonances lead to peak structures in the imaginary parts of the subthreshold amplitudes. Those structures reflect the subthreshold strength seen in the ρ -meson production cross section of Fig. 1. It is convenient to represent the result in terms of the reduced scattering amplitudes $f_{VN \rightarrow VN}^{(IJ\pm)}(\sqrt{s})$,

$$\begin{aligned} f_{\rho N \rightarrow \rho N}^{(\frac{1}{2}\frac{1}{2}+)}(\sqrt{s}) &= \frac{N_{\rho N}(\sqrt{s})}{8\pi\sqrt{s}} M_{33}^{(\frac{1}{2}+)}(\sqrt{s}, 0), \\ f_{\omega N \rightarrow \omega N}^{(\frac{1}{2}\frac{1}{2}+)}(\sqrt{s}) &= \frac{N_{\omega N}(\sqrt{s})}{8\pi\sqrt{s}} M_{44}^{(\frac{1}{2}+)}(\sqrt{s}, 0), \end{aligned} \quad (67)$$

where the normalization factor $N_{\rho N}(\sqrt{s})$ and $N_{\omega N}(\sqrt{s})$ was introduced in (42). In $N_{\rho N}(\sqrt{s})$ we use the nominal ρ -meson mass $m_\rho = 779$ MeV as introduced in (32). The vector-meson nucleon s-wave scattering lengths with $I = J = \frac{1}{2}$ can be read of Fig. 7 at $\sqrt{s} = m_N + m_V$. It is evident from Fig. 7 that the repulsive ω -meson nucleon scattering length is a direct consequence of the close by $N(1650)$ resonance just below the ωN threshold. The ρ -meson nucleon scattering length is small and attractive in this channel because the

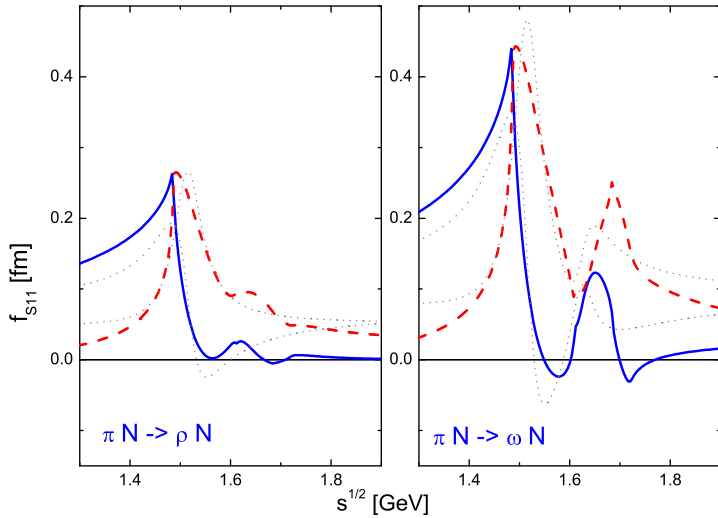


Fig. 6. Pion-induced vector-meson production amplitudes with $I = J = \frac{1}{2}$. The solid and dashed lines represent the real and imaginary parts of the amplitudes. The dotted lines follow from the schematic resonance exchange model defined in (69).

$N(1650)$ resonance couples weakly to the ρN channel and because the real part of the amplitude is strongly affected by an attractive background term effect. The scattering lengths are an important piece of information required for the study of vector-meson propagation in a dense nuclear environment,

$$\begin{aligned} a_{\rho N}^{(\frac{1}{2}\frac{1}{2})} &= f_{\rho N \rightarrow \rho N}^{(\frac{1}{2}\frac{1}{2}+)}(m_N + m_\rho) \simeq (0.17 + i 0.16) \text{ fm}, \\ a_{\omega N}^{(\frac{1}{2}\frac{1}{2})} &= f_{\omega N \rightarrow \omega N}^{(\frac{1}{2}\frac{1}{2}+)}(m_N + m_\omega) \simeq (-0.45 + i 0.31) \text{ fm}. \end{aligned} \quad (68)$$

We analyze the scattering amplitudes in more detail within a schematic resonance exchange model. The amplitudes can be represented in terms of the coupling constants $g_{\pi N}^{(R)}$, $g_{VN}^{(R)}$, the phases $\phi_{\pi V}^{(R)}$, $\phi_{\omega\rho}^{(R)}$, and the background parameters $b_{\pi N \rightarrow VN}^{(\frac{1}{2}\frac{1}{2})}$ and $b_{VN \rightarrow V'N}^{(\frac{1}{2}\frac{1}{2})}$,

$$f_{VN \rightarrow V'N}^{(\frac{1}{2}\frac{1}{2}+)}(\sqrt{s}) \simeq -\frac{e^{i\phi_{VV'}^{(1535)}} |g_{VN}^{(1535)}| |g_{V'N}^{(1535)}|}{\sqrt{s} - m_{1535} + \frac{i}{2}\Gamma_{1535}} - \frac{e^{i\phi_{VV'}^{(1650)}} |g_{VN}^{(1650)}| |g_{V'N}^{(1650)}|}{\sqrt{s} - m_{1650} + \frac{i}{2}\Gamma_{1650}} + b_{VN \rightarrow V'N}^{(\frac{1}{2}\frac{1}{2}+)},$$

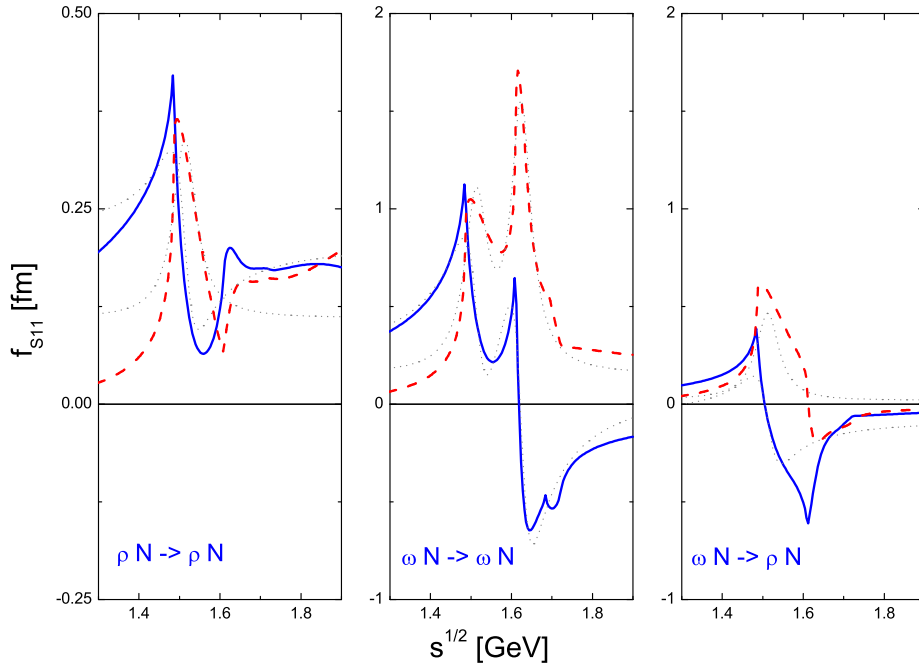


Fig. 7. Vector-meson nucleon scattering amplitude with $I = J = \frac{1}{2}$. Solid, dashed and dotted lines as in Fig. 6.

$$f_{\pi N \rightarrow VN}^{(\frac{1}{2}\frac{1}{2}+)}(\sqrt{s}) \simeq - \frac{e^{i\phi_{\pi V}^{(1535)}} |g_{\pi N}^{(1535)}| |g_{VN}^{(1535)}|}{\sqrt{s} - m_{1535} + \frac{i}{2}\Gamma_{1535}} - \frac{e^{i\phi_{\pi V}^{(1650)}} |g_{\pi N}^{(1650)}| |g_{VN}^{(1650)}|}{\sqrt{s} - m_{1650} + \frac{i}{2}\Gamma_{1650}} + b_{\pi N \rightarrow VN}^{(\frac{1}{2}\frac{1}{2}+)} . \quad (69)$$

Our amplitudes, as shown in Figs. 6, 7 by solid lines for the real parts and dashed lines for the imaginary parts, may be crudely interpreted in terms of the resonance parameters collected in Tab. 3. These parameters were obtained by fitting the amplitudes in the resonance region. Thus, the resonance mass and width parameters were fixed by fitting the elastic omega-meson nucleon amplitude. The coupling constants of the $N(1535)$ and $N(1650)$ resonances to the ρN channel were then determined from the $\omega N \rightarrow \rho N$ amplitude using the previously extracted resonance mass and width parameters. Similarly the coupling strength of the resonances to the πN channel were obtained in terms of previously determined parameters by adjusting $g_{\pi N}^{(R)}$ to the pion-induced ω -production amplitude of Fig. 6. We find particularly striking the quite different phase parameters $\phi_{\pi\omega}^{(R)}$ of $\simeq -9^\circ$ and $\simeq -90^\circ$ for the $N(1535)$ and $N(1650)$ resonances. Note that consistency of the resonance exchange picture requires the phase relation,

$$\phi_{\pi\omega}^{(R)} \simeq \phi_{\pi\rho}^{(R)} - \phi_{\omega\rho}^{(R)}, \quad (70)$$

which is reasonably well satisfied for the $N(1535)$ resonance. The background parameters, part of our schematic resonance exchange model, may be viewed as resonance-subtracted effective scattering lengths,

$$\begin{aligned} b_{+, \pi N \rightarrow \omega N}^{(\frac{1}{2}\frac{1}{2})} &\simeq (0.10 + i 0.09) \text{ fm}, & b_{+, \pi N \rightarrow \rho N}^{(\frac{1}{2}\frac{1}{2})} &\simeq (0.07 + i 0.05) \text{ fm}, \\ b_{+, \omega N \rightarrow \omega N}^{(\frac{1}{2}\frac{1}{2})} &\simeq (0.15 + i 0.15) \text{ fm}, & b_{+, \rho N \rightarrow \rho N}^{(\frac{1}{2}\frac{1}{2})} &\simeq (0.21 + i 0.11) \text{ fm}, \\ b_{+, \omega N \rightarrow \rho N}^{(\frac{1}{2}\frac{1}{2})} &\simeq (-0.07 + i 0.02) \text{ fm}, \end{aligned} \quad (71)$$

In Fig. 6 and 7 we included the result of the schematic model (69) for the vector-meson production and scattering amplitudes shown by thin dotted lines. As is clearly demonstrated the strong energy dependence induced by the nearby ηN and $K\Lambda$ thresholds prohibits a quantitative application of the resonance exchange model (69). In particular there is no unique interpretation of the $N(1650)$ resonance contributions in terms of simple coupling strengths to the πN , ρN channels. It is instructive to compare the background parameters $b_{VN \rightarrow VN}$ with the scattering lengths $a_{VN \rightarrow VN}$ given in (68). One concludes that a substantial fraction of the scattering length is a background term effect. We emphasize that such background term effects are crucial for the proper description of the in-medium propagation of vector mesons in nuclear matter. They act like an effective mean field which shifts the energy of the in-medium vector-meson state.

| | $g_{\pi N}$ | $g_{\omega N}$ | $g_{\rho N}$ | $\phi_{\pi\omega}$ [°] | $\phi_{\pi\rho}$ [°] | $\phi_{\omega\rho}$ [°] | m [MeV] | Γ [MeV] |
|-----------|-------------|----------------|--------------|------------------------|----------------------|-------------------------|-----------|----------------|
| $N(1535)$ | 0.19 | 0.39 | 0.20 | -8.5 | -7.5 | 2.7 | 1513 | 69 |
| $N(1650)$ | 0.04 | 0.45 | 0.00 | -89.3 | - | - | 1624 | 60 |

Table 3

Resonance and background parameters in the $IJ^P = \frac{1}{2} \frac{1}{2}^-$ channel .

We wish to make three points here. First, the schematic representation (69) of the amplitudes is respecting the unitarity condition only approximatively. In the presence of two resonances or a background term the 'unitarization' of the amplitudes is not unique. Since we aim at only a qualitative interpretation of our result we do not use a more complicated and necessarily less transparent representation of the amplitudes. In any case, the course of improving the representation (69) would ultimately lead us back to the original model or some improved version of it. Second we point out the importance of the background terms b in (69). It is clear that one may view the background terms as a particular model for the energy dependence of the resonance self energy. And third, even the most general off-shell behavior in the meson-baryon resonance vertex function, defines only a particular and incomplete model for the background term. One may always write down further 4-point interaction terms, in the spirit of effective field theory, which would alter the background term at will.

In the following subsection we will further study the schematic resonance coupling constants by relating the parameters of Tab. 3 to the most general and covariant 3-point interaction vertices describing the coupling of the on-shell resonances to the meson-baryon pairs. We will compare our results with recent values for the resonance coupling constants obtained by Brown and Riska [56] within the quark model.

5.1.2 Resonance coupling constants

The appropriate covariant interaction terms which couple the resonances $N(1535)$ and $N(1650)$ to the pion-nucleon channel are readily constructed,

$$\mathcal{L}_{\frac{1}{2} \frac{1}{2}^-}^{(\pi N)} = \frac{1}{\sqrt{3}} f_{\pi N}^{(1535)} \bar{N}_{1535} \vec{\pi} \cdot \vec{\tau} N + \frac{1}{\sqrt{3}} f_{\pi N}^{(1650)} \bar{N}_{1650} \vec{\pi} \cdot \vec{\tau} N + \text{h.c.}, \quad (72)$$

where we identify,

$$\begin{aligned} \left| f_{\pi N}^{(1535)} \right| &= \sqrt{\frac{8 \pi m_{1535}}{N_{\pi N}^{(+)}(m_{1535})}} \left| g_{\pi N}^{(1535)} \right| \simeq 0.85, \\ \left| f_{\pi N}^{(1650)} \right| &= \sqrt{\frac{8 \pi m_{1650}}{N_{\pi N}^{(+)}(m_{1650})}} \left| g_{\pi N}^{(1650)} \right| \simeq 0.19. \end{aligned} \quad (73)$$

Note that we do not consider further interaction terms in (72) which are redundant if the resonance, the nucleon and pion are strictly on-shell. As discussed above such terms do affect the background terms in the pion induced vector-meson production amplitudes of Fig. 6. Here we do not take up this issue since we believe that the reliable determination of any background parameter is possible only via a coupled channel analysis. The coupling constants $|f_{\pi N, BR}^{(1535)}| \simeq 3.6$ and $|f_{\pi N, BR}^{(1650)}| \simeq 2.5$ of Brown and Riska [56] differ significantly from our values given in (73). We use a subscript 'BR' to identify the coupling constants of [56]. On the other hand, our value for the N(1535) resonance coupling constant compares favorably with the analysis [34] where the value $|f_{\pi N}^{(1535)}| \simeq 1.2$, representative for various analyses, was obtained. The coupling constant $|f_{\pi N}^{(1650)}| \simeq 2.0$ of [34] is significantly larger than our result. This may reflect the fact that the $\pi\Delta$ and ρN channels, which are expected to be more important for the heavier resonance, were not explicitly included in [34]. Moreover, the extraction of the N(1650) resonance coupling strength to the πN channel from the πN partial-wave amplitude is obscured by a substantial background, which introduces a large ambiguity in the resonance width and coupling parameters. Note that we do not consider a possible phase parameter, $\phi_{\pi N}^{(R)}$, in the resonance coupling constant ⁸,

$$f_{\pi N}^{(R)} = e^{i\phi_{\pi N}^{(R)}} |f_{\pi N}^{(R)}|. \quad (74)$$

It is evident that only relative phases, like $\phi_{\pi\rho}^{(R)} = \phi_{\pi N}^{(R)} - \phi_{\rho N}^{(R)}$, are observable. That reflects the freedom to absorb for instance the phase $\phi_{\pi N}^{(R)}$ into the definition of the resonance field. Given that our model leads to resonance coupling constants which deviate strongly from those of the quark-model, we do not see much point to discuss the phase parameters in this section. The values of our relative phase parameters are given in Table 3.

We turn to the coupling constants of the resonances to the vector-meson nucleon channels. The most general on-shell vertex permits two independent interaction vertices parameterized by axial-vector, $f_{VN,A}^{(R)}$, and pseudo-scalar, $f_{VN,P}^{(R)}$, coupling constants,

$$\mathcal{L}_{\frac{1}{2} \frac{1}{2}^-}^{(VN)} = \frac{1}{3} f_{\rho N, A}^{(1535)} \bar{N}_{1535} \gamma_5 \gamma_\mu \vec{\rho}^\mu \cdot \vec{\tau} N + \frac{i}{3} f_{\rho N, P}^{(1535)} \bar{N}_{1535} \gamma_5 \vec{\rho}^\mu \cdot \vec{\tau} (\partial_\mu N)$$

⁸ The phase parameters discussed here are not directly related to the resonance and background phase parameters, ϕ_R and ϕ_B , frequently introduced at the level of the S -matrix, where one writes $S = e^{2i(\phi_B + \phi_R)}$ near the resonance pole. The background phase accounts for the contributions of the non-resonant background, which in the parameterization (69) is absorbed in the background parameters $b_{VN \rightarrow V'N}$ and $b_{\pi N \rightarrow VN}$.

$$\begin{aligned}
& + \frac{1}{\sqrt{3}} f_{\omega N, A}^{(1535)} \bar{N}_{1535} \gamma_5 \gamma_\mu \omega^\mu N + \frac{i}{\sqrt{3}} f_{\omega N, P}^{(1535)} \bar{N}_{1535} \gamma_5 \omega^\mu (\partial_\mu N) \\
& + \frac{1}{3} f_{\rho N, A}^{(1650)} \bar{N}_{1650} \gamma_5 \gamma_\mu \vec{\rho}^\mu \cdot \vec{\tau} N + \frac{i}{3} f_{\rho N, P}^{(1650)} \bar{N}_{1650} \gamma_5 \vec{\rho}^\mu \cdot \vec{\tau} (\partial_\mu N) \\
& + \frac{1}{\sqrt{3}} f_{\omega N, A}^{(1650)} \bar{N}_{1650} \gamma_5 \gamma_\mu \omega^\mu N + \frac{i}{\sqrt{3}} f_{\omega N, P}^{(1650)} \bar{N}_{1650} \gamma_5 \omega^\mu (\partial_\mu N) + \text{h.c.} .
\end{aligned} \tag{75}$$

The relative normalization factor of the ωN and ρN channels in (72) is motivated by the corresponding factors in (8). We illustrate the different effects of the axial-vector versus the pseudo-scalar term by evaluating the partial resonance-decay width,

$$\begin{aligned}
\Gamma_R^{(\rho N)}(\sqrt{s}) &= \frac{2}{3} (E_N + m_N) \left(2 \left(f_{\rho N, A}^{(R)} \right)^2 \right. \\
&\quad \left. + \left(\frac{\sqrt{s} - m_N}{m_\rho} f_{\rho N, A}^{(R)} - (E_N - m_N) \frac{\sqrt{s}}{m_\rho} f_{\rho N, P}^{(R)} \right)^2 \right) \frac{p_{\rho N}}{8\pi\sqrt{s}} ,
\end{aligned} \tag{76}$$

where $E_N^2 = m_N^2 + p_{\rho N}^2$. A folding with the ρ -meson spectral function (32) analogous to (43) is understood in (76). The width of the resonance in Breit-Wigner approximation is given with $\Gamma_R = \Gamma_R(m_R)$. The result (76) demonstrates that the axial-vector coupling term with $f_{\rho N, A}^{(R)}$ dominates the resonance-decay width. The pseudo-scalar contribution with $f_{\rho N, P}^{(R)}$ is suppressed by at least two powers of the phase-space factor $p_{\rho N}$. Note that the presence of two independent coupling constants in (76) reflects the two helicity states (40) a vector-meson nucleon pair with $J = \frac{1}{2}$ can occupy. Based on the leading projectors introduced in (38) we identify the coupling constants

$$\begin{aligned}
g_{VN}^{(R)} &= \sqrt{\frac{N_{VN}(m_R)}{8\pi m_R}} f_{VN, A}^{(R)}, \quad m_R f_{VN, P}^{(R)} = f_{VN, A}^{(R)}, \\
f_{\rho N, A}^{(1535)} &\simeq 0.97, \quad f_{\omega N, A}^{(1535)} \simeq 1.89, \quad f_{\rho N, A}^{(1650)} \simeq 0.00, \quad f_{\omega N, A}^{(1650)} \simeq 2.17 ,
\end{aligned} \tag{77}$$

where $R = (1535, 1650)$ and $V = (\rho, \omega)$ (see (69)). The reliable determination of the pseudo-scalar coupling constant $f_{\rho N, P}^{(R)}$ would require the consideration of subleading projectors not considered in this work. Taking our values for the resonance coupling constants in (77) we find partial ρN -decay widths of less than 1 MeV for the $N(1535)$ and $N(1650)$ resonance. We compare our resonance coupling constants with values of the recent work [56] derived within the quark model. We observe strong deviations for the vector meson coupling constants $|f_{\rho N, BR}^{(1535)}| \simeq 8.7$, $|f_{\omega N, BR}^{(1535)}| \simeq 7.8$ and $|f_{\rho N, BR}^{(1650)}| \simeq 2.2$, $|f_{\omega N, BR}^{(1650)}| \simeq 3.8$ from our values in (77). We should mention that the comparison of the vector-meson coupling constants is subtle. In [56] it is implied $f_{VN, P}^{(R)} = 0$ in conflict with our model. The quark model appears to suggest axial-vector type coupling constants $f_{VN, A}^{(R)}$ for which we recollect their values above. If we use

the value $|f_{\rho N, BR}^{(1535)}| \simeq 8.7$ together with the ρ -meson spectral density of (32) in (76) we obtain a partial ρN -decay width of 26 MeV for the N(1535) resonance. Moreover, we observe that this values is rather sensitive to the precise form of the ρ -meson spectral function. If we use a simple Breit-Wigner model with $m_\rho \simeq 770$ MeV and $\Gamma_\rho \simeq 150$ MeV, as applied in the analysis of Manley and Salesky [19], that partial decay widths becomes 143 MeV instead, clearly an unreasonable value. It was emphasized in [56] that only the ratios of the resonance coupling constants are expected to be reasonable because many-body quark operators not considered in [56] may change their results. However, even taking ratios only does not lead to a consistent matching of our values to those of the quark model. This is an interesting result which may help to discriminate the quark-model picture of resonances from the dynamical scenario in which all resonances except the baryon octet and decuplet ground states are considered to be generated by important coupled channel effects [20,35].

We discuss the coupling of the s-wave resonances to the photon-nucleon state as probed in the multipole amplitude. The most general gauge invariant interaction vertex as required for on-shell particles is readily constructed [57],

$$\mathcal{L}_{\frac{1}{2} \frac{1}{2}^-}^{(\gamma N)} = \frac{e}{4m_R} \bar{R} \gamma_5 \sigma_{\mu\nu} \left(f_{\gamma N, S}^{(R)} + f_{\gamma N, V}^{(R)} \tau_3 \right) N F^{\mu\nu} + \text{h.c.} \quad (78)$$

where e is the unit charge ($e^2/(4\pi) \simeq 1/137$). The isoscalar and isovector coupling constants $f_{\gamma N, S}^{(R)}$ and $f_{\gamma N, V}^{(R)}$ for a given resonance, R , are predicted by the generalized vector-meson dominance assumption (55) in terms of the hadronic coupling constants introduced in (75) and the channel independent parameters $g_{S(V),i}^{(\pm)}$ quantifying the generalized vector-meson dominance assumption. The effective interaction Lagrangian density describing the transition of the resonance into the γN state is identified⁹,

$$\begin{aligned} \mathcal{L}_{\frac{1}{2} \frac{1}{2}^-}^{(\gamma N)} = & e \bar{R} \gamma_5 \gamma^\mu \left(\frac{i}{\sqrt{3}} f_{\omega N, A}^{(R)} \Gamma_{S,\nu} + \frac{i}{3} f_{\rho N, A}^{(R)} \Gamma_{V,\nu} \tau_3 \right) \left(N F^{\mu\nu} \right) \\ & - e \bar{R} \gamma_5 \left(\frac{1}{\sqrt{3}} f_{\omega N, P}^{(R)} \Gamma_{S,\nu} + \frac{1}{3} f_{\rho N, P}^{(R)} \Gamma_{V,\nu} \tau_3 \right) \left((\partial^\mu N) F^{\mu\nu} \right) + \text{h.c.}, \end{aligned} \quad (79)$$

with the electromagnetic field strength tensor $F_{\mu\nu} = \partial_\mu A_\nu - \partial_\nu A_\mu$ and the transition operator $\Gamma_{S(V)}^\nu$,

$$\Gamma_{S(V),\nu} = \Gamma_{S(V),\nu}^{(+)} + \Gamma_{S(V),\nu}^{(-)},$$

⁹ The vector-meson dominance assumption is defined with respect to the covariant projector algebra. That implies a particular off-shell structure of the hadronic transition vertex. Here we apply the correct off-shell form as is probed by the leading projector, i.e. we assume that $m_R f_{V N, P}^{(R)} = f_{V N, A}^{(R)}$ holds strictly.

| | $f_{\gamma N,S}^{(1535)}$ | $f_{\gamma N,S}^{(1650)}$ | $f_{\gamma N,V}^{(1535)}$ | $f_{\gamma N,V}^{(1650)}$ |
|-----------|---------------------------|---------------------------|---------------------------|---------------------------|
| this work | 0.13 | 0.18 | 0.47 | 0.00 |
| [58] | 0.04-0.22 | 0.06-0.41 | 1.10-1.25 | 0.01-0.13 |

Table 4

Electromagnetic resonance coupling constants in the $IJ^P = \frac{1}{2} \frac{1}{2}^-$ channel .

$$\Gamma_{S(V),\nu}^{(\pm)} = \frac{m_R \pm i \gamma \cdot \partial}{2 m_R} \left(\frac{g_{S(V),2}^{(\pm)} \mp g_{S(V),1}^{(\pm)}}{m_R m_\omega} i \partial_\nu + \frac{g_{S(V),1}^{(\pm)}}{m_\omega} \gamma_\nu \right). \quad (80)$$

In (80) the transition tensor (56) is cast into a form that leads to the gauge invariant expressions (79). The linear dependence on the photon 4-momentum q_μ in $\Gamma_{(S,V)}^{\mu\nu}(q; w)$ is absorbed into the field strength tensor $F_{\mu\nu}$, explaining why (56) and (80) are Lorentz tensors of different degrees. We obtain the result:

$$\begin{aligned} f_{\gamma N,S}^{(R)} &= \frac{1}{\sqrt{3}} \left(2 g_{S,1}^{(+)} \frac{m_R - m_N}{m_\omega} + g_{S,2}^{(+)} \frac{m_R + m_N}{m_\omega} \right) f_{\omega N,A}^{(R)} \\ &\quad + \frac{1}{\sqrt{3}} g_{S,1}^{(-)} \frac{m_R + m_N}{m_\omega} \left(f_{\omega N,A}^{(R)} - m_R f_{\omega N,P}^{(R)} \right), \\ f_{\gamma N,V}^{(R)} &= \frac{1}{3} \left(2 g_{V,1}^{(+)} \frac{m_R - m_N}{m_\omega} + g_{V,2}^{(+)} \frac{m_R + m_N}{m_\omega} \right) f_{\rho N,A}^{(R)} \\ &\quad + \frac{1}{3} g_{V,1}^{(-)} \frac{m_R + m_N}{m_\omega} \left(f_{\rho N,A}^{(R)} - m_R f_{\rho N,P}^{(R)} \right). \end{aligned} \quad (81)$$

Our present scheme with (77) cannot determine the coupling constants $g_{S(V),i}^{(-)}$. These coupling constants should be derived studying photon-induced production of p-wave nucleon and isobar resonances. In Tab. 4 we compare the resulting electromagnetic resonance coupling constants with values obtained in a previous analysis [58]. We conclude that there is reasonable agreement given the quite large uncertainties in the coupling constants.

5.2 $IJ^P = \frac{3}{2} \frac{1}{2}^-$ channel

We proceed with the $IJ^P = \frac{3}{2} \frac{1}{2}^-$ sector where we include the four channels πN , $\pi \Delta$, ρN , and $K \Sigma$. Note that here the ωN channel does not contribute since we assume exact isospin conservation. The 10 parameters of this sector, determined by our best fit, are given in Tab. 5. As may be expected, the parameters, g_{11} , g_{14} and g_{44} describing the coupling strength in the πN and $K \Sigma$ channels do not satisfy the SU(3) constraint, given in terms of the h_i parameters specified in Tab. 1. In fact we find strong deviations from those values indicating that there are important SU(3) symmetry breaking effects in this sector, once part of the SU(3) dynamics, e.g. the $K_\mu \Sigma$ or $K \Sigma_\mu$ channels, is integrated out.

| $g_0^{(\frac{3}{2},+)} [m_\pi^{-\frac{n+m}{2}}]$ | $\pi N[n=1]$ | $\pi\Delta[n=3]$ | $\rho N[n=1]$ | $K\Sigma[n=1]$ |
|--|--------------|------------------|---------------|----------------|
| $\pi N[m=1]$ | -29.41 | 0.41 | -25.46 | 11.81 |
| $\pi\Delta[m=3]$ | 0.41 | 12.69 | 14.86 | -53.40 |
| $\rho N[m=1]$ | -25.46 | 14.86 | -26.44 | -5.77 |
| $K\Sigma[m=1]$ | 11.81 | -53.40 | -5.77 | 5.00 |

Table 5
Coupling constants in the $IJ^P = \frac{3}{2} \frac{1}{2}^-$ channel.

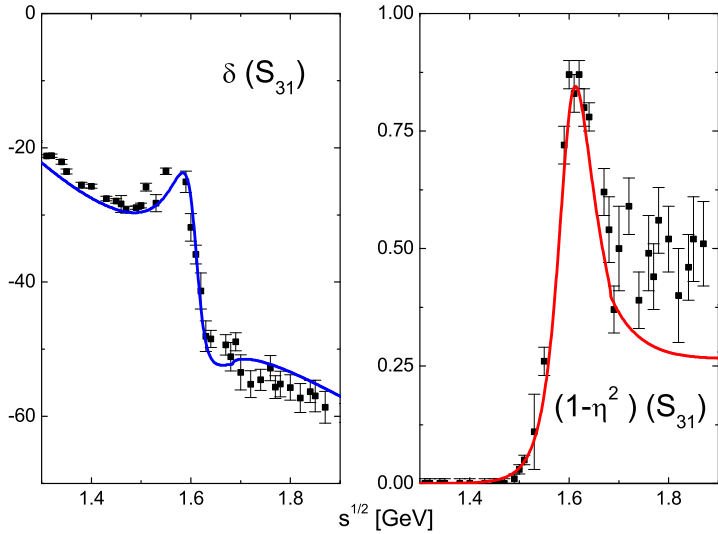


Fig. 8. Pion-nucleon scattering phase shift $\delta_{S_{31}}$ and inelasticity parameter $\eta_{S_{31}}$ of the S_{31} channel of our theory and of the single-energy analysis SP98 [45,46].

Our model reproduces the pion-nucleon phase shift and the inelasticity parameter nicely, as shown in Fig. 8. The rapid energy variation close to $\sqrt{s} \simeq 1620$ MeV reflects the presence of the isobar resonance $\Delta(1620)$ with quantum numbers $IJ^P = \frac{3}{2} \frac{1}{2}^-$. The fit is also constrained by the pion-induced $K^+\Sigma^+$, $K^+\Sigma^-$ and $K^0\Sigma^0$ production cross section shown in Fig. 9. For the $\pi^+p \rightarrow K^+\Sigma^+$ reaction data of good quality on the differential cross section is available. These were used in the partial-wave analysis of [62]. We utilize this, by fitting our model to the s-wave part of the production cross section, extracted in this analysis. In Fig. 9 the s-wave cross section, which is reasonably well reproduced by our model, is shown as open squares, while the total cross section is given by the filled squares. The difference between the total cross section and the s-wave part, starting at about $\sqrt{s} \simeq 1750$ MeV illustrates the importance of higher partial waves, not included in our model. In the case of the reactions $\pi^-p \rightarrow K^+\Sigma^-, K^0\Sigma^0$ the data set does not permit a reliable partial wave analysis. The few available data points [63,64] are consistent with s-wave dominance up to $\sqrt{s} \simeq 1.9$ GeV, as suggested by the

fit. Similar conclusions can be drawn in the γ -induced $K^+\Sigma^0$ and $K^0\Sigma^+$ production cross sections, also shown in Fig. 9. We find that our model provides a reasonable interpretation of the data, in particular in the $K^0\Sigma^+$ channel. The importance of higher partial waves in the $K^+\Sigma^0$ channel is, at least on a qualitative level, consistent with available differential cross sections [53], which show large non-isotropic contributions already at $p_{\text{lab}} = 1.5$ GeV.

We now turn to the γ induced production of pions. In Fig. 11 we compare the multipole amplitude $E_{0+}(S_{31})$ with the analysis of [31]. Given the simplicity of our model we obtain a reasonable description of the real and the imaginary part of $E_{0+}(S_{31})$ in the energy range of interest here. The discrepancy between our model and the empirical analysis may have several causes. First, the generalized vector-meson dominance assumption (55) for the electromagnetic interactions may be too restrictive. If other couplings, not related to the vector-meson amplitudes, play an important role, it is possible that our model does not have enough freedom to reproduce the data in the different partial waves and reaction channels simultaneously. On the other hand, it may be that the deficiencies of our model reflect the importance of inelastic channels, like the $K\Sigma_\mu$ or $K_\mu N$, which so far are not included. A further possible source of the discrepancy is the kinematically suppressed contributions from the ρN states (40), which are not included in the model. These define further contributions to the multipole amplitudes E_{0+} . However, since these

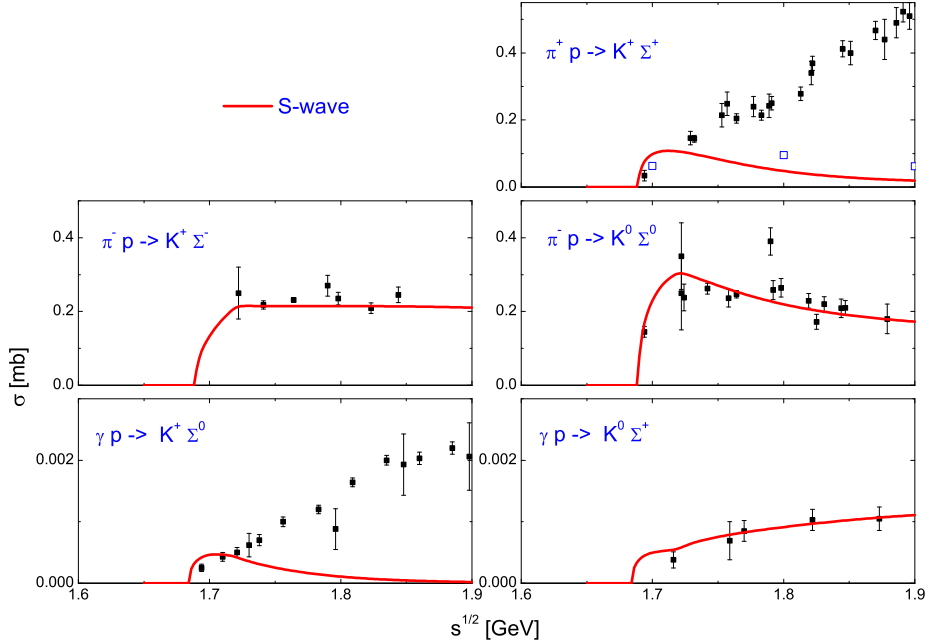


Fig. 9. Pion- and photon-induced $K\Sigma$ production cross sections. The data are taken from [59,53,60–62,39].

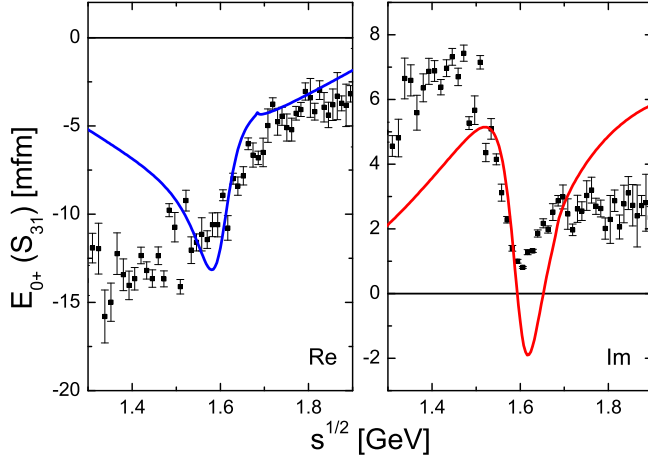


Fig. 10. Electric multipole amplitudes $E_{0+}(S_{31})$ of γ -induced pion production. We show the results of the single-energy solution SM00 [31,46].

contributions are suppressed by at least two powers of the phase space factor $p_{\gamma N} = (\sqrt{s} - m_N^2/\sqrt{s})/2$ they could play a role only if the corresponding coupling constants are anomalously large. The discrepancy at low energies is, as noted above, presumably related to the strong energy dependence of the one-pion exchange contribution, which is not treated properly in our scheme.

We now discuss the ρ -meson scattering and production amplitudes. In Fig. 11 we present the pion-induced ρ -meson production amplitude introduced in (44). and the ρ -meson nucleon scattering amplitude in the $I = \frac{3}{2}$ and $J = \frac{1}{2}$ sector. The presence of the $\Delta(1620)$ resonance leads to a peaked structure in the imaginary parts of the subthreshold amplitudes. Note we show the reduced amplitudes, which for elastic ρN scattering is given by

$$f_{\rho N \rightarrow \rho N}^{(\frac{3}{2}\frac{1}{2}+)}(\sqrt{s}) = \frac{N_{\rho N}}{8\pi\sqrt{s}} M_{33}^{(\frac{3}{2}+)}(\sqrt{s}, 0). \quad (82)$$

This means that the diagonal amplitude at threshold equals the ρ -meson nucleon s-wave scattering length

$$a_{\rho N}^{(\frac{3}{2}\frac{1}{2})} = f_{\rho N \rightarrow \rho N}^{(\frac{3}{2}\frac{1}{2}+)}(m_N + m_\rho) \simeq (-0.25 + i 0.09) \text{ fm}, \quad (83)$$

We find a repulsive s-wave scattering length in this channel, while in the isospin one-half channel we found an attractive one. The isospin averaged scattering length of the $J = \frac{1}{2}$ channel,

$$\bar{a}_{\rho N}^{(\frac{1}{2})} = \frac{1}{3} a_{\rho N}^{(\frac{1}{2}\frac{1}{2})} + \frac{2}{3} a_{\rho N}^{(\frac{3}{2}\frac{1}{2})} \simeq (-0.11 + i 0.11) \text{ fm}, \quad (84)$$

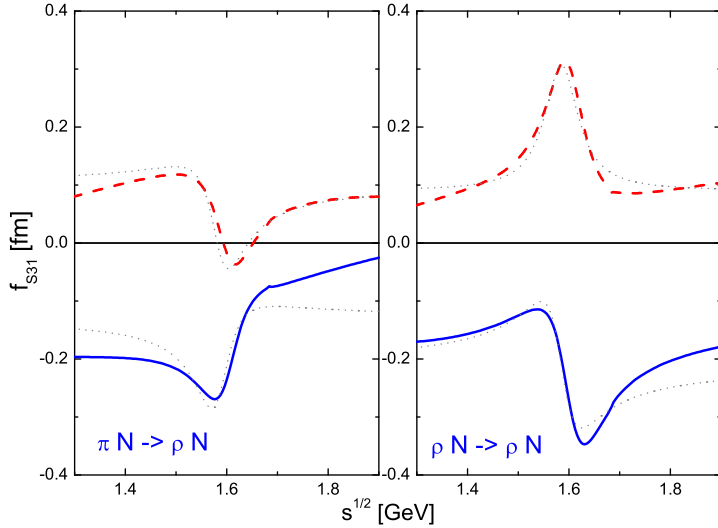


Fig. 11. Vector-meson production and scattering amplitude with $I = \frac{3}{2}$ and $J = \frac{1}{2}$. The solid and dashed lines show the real and imaginary parts of the amplitudes. The dotted lines are the result of the schematic resonance exchange model introduced in (85).

is therefore somewhat reduced.

We also analyze the production and scattering amplitudes in terms of a resonance model

$$\begin{aligned}
 f_{+, \rho N \rightarrow \rho N}^{(\frac{3}{2} \frac{1}{2})}(\sqrt{s}) &\simeq -\frac{|g_{\rho N}^{(1620)}|^2}{\sqrt{s} - m_{1620} + \frac{i}{2} \Gamma_{1620}} + b_{+, \rho N \rightarrow \rho N}^{(\frac{3}{2} \frac{1}{2})}, \\
 f_{+, \pi N \rightarrow \rho N}^{(\frac{3}{2} \frac{1}{2})}(\sqrt{s}) &\simeq -\frac{e^{i\phi_{\pi\rho}^{(1620)}} |g_{\pi N}^{(1620)}| |g_{\rho N}^{(1620)}|}{\sqrt{s} - m_{1620} + \frac{i}{2} \Gamma_{1620}} + b_{+, \pi N \rightarrow \rho N}^{(\frac{3}{2} \frac{1}{2})},
 \end{aligned} \tag{85}$$

with the coupling constants $g_{\pi N}^{(1620)}$, $g_{\rho N}^{(1620)}$, the relative phase $\phi_{\pi\rho}^{(1620)}$ and channel-dependent background terms $b_{\pi N \rightarrow \rho N}^{(\frac{3}{2} \frac{1}{2})}$ and $b_{\rho N \rightarrow \rho N}^{(\frac{3}{2} \frac{1}{2})}$. The resulting resonance parameters are given in Tab. 6. We obtain a fairly small decay width for the $\Delta(1620)$ resonance. Our value is about a factor two smaller than that given by the Particle Data Group [65], $\Gamma_{1620} \simeq 150$ MeV. This is possibly a consequence of the dynamic generation of the isobar resonance which typically introduces a pronounced energy dependence in the resonance self energy.

In Fig. 11 the amplitudes of the resonance-exchange model is shown by the dotted lines. Both amplitudes are fairly well represented by this simple model (85). We note, however, that it is crucial to allow for a strong, repulsive back-

ground contribution,

$$b_{-, \pi N \rightarrow \rho N}^{(\frac{3}{2} \frac{1}{2})} \simeq (-0.13 + i 0.10) \text{ fm}, \quad b_{-, \rho N \rightarrow \rho N}^{(\frac{3}{2} \frac{1}{2})} \simeq (-0.21 + i 0.09) \text{ fm}. \quad (86)$$

The sizeable imaginary part of the background parameters in (86) may be a reflection of our 'small' decay width of the resonance. By forcing all of the imaginary part of the amplitude into an effective width parameter, the total decay width is enhanced and approaches the value given by the Particle Data Group. In the subsequent section we compare these results with quark-model predictions for the coupling constants.

5.2.1 Resonance coupling constants

The interaction term which couples the resonances $\Delta(1620)$ to the pion-nucleon channel is readily constructed,

$$\begin{aligned} \mathcal{L}_{\frac{3}{2} \frac{1}{2}^-}^{(\pi N)} &= f_{\pi N}^{(1620)} \bar{\Delta}_{1620} \vec{\pi} \cdot \vec{T} N + \text{h.c.} \\ |f_{\pi N}^{(1620)}| &= \sqrt{\frac{8 \pi m_{1620}}{N_{\pi N}^{(+)}(m_{1620})}} |g_{\pi N}^{(1620)}| \simeq 0.19, \end{aligned} \quad (87)$$

where we used the results presented in the previous section and assumed on-shell kinematics. The corresponding value for the resonance coupling constant obtained from the quark model [56] is $|f_{\pi N, BR}^{(1620)}| \simeq 1.67$. Again we find a large deviation.

We turn to the coupling constants of the resonances to the vector-meson nucleon channels. The most general on-shell vertex permits two independent interaction terms parameterized by axial-vector, $f_{\rho N, A}^{(1620)}$, and pseudo-scalar, $f_{\rho N, P}^{(1620)}$, coupling constants,

$$\begin{aligned} \mathcal{L}_{\frac{3}{2} \frac{1}{2}^-}^{(\rho N)} &= \frac{1}{\sqrt{3}} f_{\rho N, A}^{(1620)} \bar{\Delta}_{1620} \gamma_5 \gamma_\mu \vec{\rho}^\mu \cdot \vec{T} N \\ &+ \frac{i}{\sqrt{3}} f_{\rho N, P}^{(1620)} \bar{\Delta}_{1620} \gamma_5 \vec{\rho}^\mu \cdot \vec{T} (\partial_\mu N) + \text{h.c.} \end{aligned} \quad (88)$$

We illustrate the different effects of the axial-vector versus the pseudo-scalar term by evaluating the partial decay width of the resonance:

| | $g_{\pi N}$ | $g_{\rho N}$ | $\phi_{\pi \rho}$ [°] | m [MeV] | Γ [MeV] |
|----------------|-------------|--------------|-----------------------|-----------|----------------|
| $\Delta(1620)$ | 0.17 | 0.21 | 130 | 1585 | 80 |

Table 6
Resonance parameters in the $IJ^P = \frac{3}{2} \frac{1}{2}^-$ channel .

$$\begin{aligned} \Gamma_{1620}^{(\rho N)}(\sqrt{s}) = & \frac{2}{3} \left(E_N + m_N \right) \left(2 \left(f_{\rho N, A}^{(1620)} \right)^2 \right. \\ & \left. + \left(\frac{\sqrt{s} - m_N}{m_\rho} f_{\rho N, A}^{(1620)} - \left(E_N - m_N \right) \frac{\sqrt{s}}{m_\rho} f_{\rho N, P}^{(1620)} \right)^2 \right) \frac{p_{\rho N}}{8\pi\sqrt{s}}, \end{aligned} \quad (89)$$

where $E_N^2 = m_N^2 + p_{\rho N}^2$. A folding with the ρ -meson spectral function (32) analogous to (43) is understood. The result (89) demonstrates that the pseudo-scalar contribution with $f_{\rho N, P}^{(1620)}$ is suppressed by at least two powers of the phase-space factor $p_{\rho N}$. We identify the coupling constants implied by the leading projectors introduced in (38),

$$\left| f_{\rho N, A}^{(1620)} \right| = \sqrt{\frac{8\pi m_{1620}}{N_{\rho N}(m_{1620})}} \left| g_{\rho N}^{(1620)} \right| \simeq 1.04, \quad m_{1620} f_{\rho N, P}^{(1620)} = f_{VN, A}^{(1620)}. \quad (90)$$

As in the S_{11} sector, a reliable determination of the pseudo-scalar coupling constant $f_{\rho N, P}^{(1620)}$ would require subleading projectors, which are not considered in this work. The axial-vector resonance coupling constant in (90) agrees reasonably well with the quark-model result $|f_{\rho N, BR}^{(1620)}| \simeq 1.52$ of [56]. Our value for this coupling constant implies a partial ρN -decay width for the $\Delta(1620)$ resonance of about 1 MeV when an energy dependent ρ -meson self energy (29) is employed.

We now discuss the electromagnetic interactions of the $\Delta(1620)$. The most general on-shell interaction vertex for the coupling of this resonance to the photon-nucleon state is of the form

$$\mathcal{L}_{\frac{3}{2} \frac{1}{2}^-}^{(\gamma N)} = \frac{e}{4m_R} f_{\gamma N, V}^{(1620)} \bar{\Delta}_{1620} T_3 \gamma_5 \sigma_{\mu\nu} N F^{\mu\nu} + \text{h.c.} \quad (91)$$

The coupling constant can be determined by analyzing the corresponding multipole amplitudes. By using the generalized vector-meson dominance assumption (55), we can relate the isovector coupling constant $f_{\gamma N, V}^{(1620)}$ to the hadronic coupling constants introduced in (88) and the channel independent parameters $g_{S(V), i}^{(\pm)}$, which quantifies the strength of the photon-vector meson conversion matrix element. It is then straightforward to construct the effective interaction Lagrangian density, which describes the transition of the resonance into the γN state

$$\begin{aligned} \mathcal{L}_{\frac{3}{2} \frac{1}{2}^-}^{(\gamma N)} = & i e \frac{1}{\sqrt{3}} f_{\rho N, A}^{(1620)} \bar{\Delta}_{1620} T_3 \gamma_5 \gamma^\mu \Gamma_{V, \nu} (N F^{\mu\nu}) \\ & - e \frac{1}{\sqrt{3}} f_{\rho N, P}^{(1620)} \bar{\Delta}_{1620} T_3 \gamma_5 \Gamma_{V, \nu} ((\partial^\mu N) F^{\mu\nu}) + \text{h.c.}, \end{aligned} \quad (92)$$

with the electromagnetic field strength tensor $F_{\mu\nu} = \partial_\mu A_\nu - \partial_\nu A_\mu$ and the transition operator Γ_V^ν given in (80). We then find:

$$f_{\gamma N, V}^{(1620)} = \frac{1}{\sqrt{3}} \left(2 g_{V,1}^{(+)} \frac{m_{1620} - m_N}{m_\omega} + g_{V,2}^{(+)} \frac{m_{1620} + m_N}{m_\omega} \right) f_{\rho N, A}^{(1620)} \simeq 0.93, \quad (93)$$

where (90) is strictly applied. Our value in (93) does not agree too well with the range of values $|f_{\gamma N, V}^{(1620)}| \simeq 0.01 - 0.45$ obtained in [58]. As was emphasized in [58] for the resonance $\Delta(1620)$ the coupling constants are not determined reliably.

5.3 $I J^P = \frac{1}{2} \frac{3}{2}^-$ channel

We continue with the $I J^P = \frac{1}{2} \frac{3}{2}^-$ sector where 10 parameters are required to account for the four channels πN , $\pi\Delta$, ρN , and ωN . The parameters of our best fit are given in Tab. 7. The inelastic channels are of almost the same importance in the coupled channel matrix, with roughly equal coupling strength to the πN channel. In particular there is no indication that it would be legitimate to integrate out the ωN channel.

| $g_1^{(\frac{1}{2}, -)} [m_\pi^{-\frac{n+m}{2}}]$ | $\pi N[n = 3]$ | $\pi\Delta[n = 1]$ | $\rho N[n = 1]$ | $\omega N[n = 1]$ |
|---|----------------|--------------------|-----------------|-------------------|
| $\pi N[m = 3]$ | 4.50 | 5.19 | 6.70 | 9.94 |
| $\pi\Delta[m = 1]$ | 5.19 | -11.90 | -7.37 | 24.72 |
| $\rho N[m = 1]$ | 6.70 | -7.37 | 5.26 | 23.88 |
| $\omega N[m = 1]$ | 9.94 | 24.72 | 23.88 | 24.65 |

Table 7
Coupling constants in the $I J^P = \frac{1}{2} \frac{3}{2}^-$ channel.

The pion-nucleon phase shift and its inelasticity parameter, presented in Fig. 8, are well reproduced by our model. The phase shift and inelasticity parameters clearly show the presence of the nucleon resonance $N(1520)$ with $I = \frac{1}{2}$ and $J = \frac{3}{2}$. The phase shift passes through 90 degree close to $\sqrt{s} \simeq 1520$ MeV. It is crucial to realize that the fit is constrained also by the vector-meson production cross section shown already in Fig. 1 and Fig. 2. Note that at present the pion-induced $\pi\Delta(1232)$ production does not constrain the model since differential production cross sections are not available. Of particular importance for the determination of the parameter set in Tab. 7 are the electric and magnetic multipole amplitudes $E_{2-}^{(p,n)}(D_{13})$ and $M_{2-}^{(p,n)}(D_{13})$ of the γ induced pion production process. One important remark is here in order. The neglected ρN and ωN states in (41) define further contributions to the multipole amplitudes $E_{2-}(D_{13})$ and $M_{2-}(D_{13})$. However, any contribution of those additional states is suppressed by at least two powers of the phase space factor $p_{\gamma N} = (\sqrt{s} - m_N^2/\sqrt{s})/2$. In view of this uncertainty we believe that Fig. 13 demonstrates a fair description of the resonance structures in the multipole amplitudes.

We now turn to the vector-meson scattering and production amplitudes. In Fig. 14 we present the pion-induced vector-meson production amplitudes $I = \frac{1}{2}$ and $J = \frac{3}{2}$ sector while the corresponding vector-meson nucleon scattering amplitudes are shown in Fig. 15. The presence of the $N(1520)$ resonance below threshold is clearly reflected in the reduced scattering amplitudes,

$$\begin{aligned} f_{\rho N \rightarrow \rho N}^{(\frac{1}{2}\frac{3}{2}-)}(\sqrt{s}) &= \frac{N_{\rho N}}{8\pi \sqrt{s}} M_{33}^{(\frac{1}{2}-)}(\sqrt{s}, 1), \\ f_{\omega N \rightarrow \omega N}^{(\frac{1}{2}\frac{3}{2}-)}(\sqrt{s}) &= \frac{N_{\omega N}}{8\pi \sqrt{s}} M_{44}^{(\frac{1}{2}-)}(\sqrt{s}, 1). \end{aligned} \quad (94)$$

The vector-meson nucleon s-wave scattering length in this sector corresponds to the value of the elastic amplitudes at threshold, i.e. $\sqrt{s} = m_N + m_V$

$$\begin{aligned} a_{\rho N}^{(\frac{1}{2}\frac{3}{2})} &= f_{+, \rho N \rightarrow \rho N}^{(\frac{1}{2}\frac{3}{2})}(m_N + m_\rho) \simeq (0.02 + i 0.15) \text{ fm}, \\ a_{\omega N}^{(\frac{1}{2}\frac{3}{2})} &= f_{+, \omega N \rightarrow \omega N}^{(\frac{1}{2}\frac{3}{2})}(m_N + m_\omega) \simeq (-0.43 + i 0.15) \text{ fm}. \end{aligned} \quad (95)$$

The ω -meson nucleon scattering length is repulsive reflecting a strong coupling of the subthreshold resonance $N(1520)$ to the ωN channel. The small imaginary part results from the various inelastic channels that are open at the ωN threshold. For the ρ -meson we find an imaginary part of similar size, but a very small, attractive, real part. Using the scattering lengths obtained in the S_{11} sector we can now compute the spin averaged ω -meson nucleon scattering

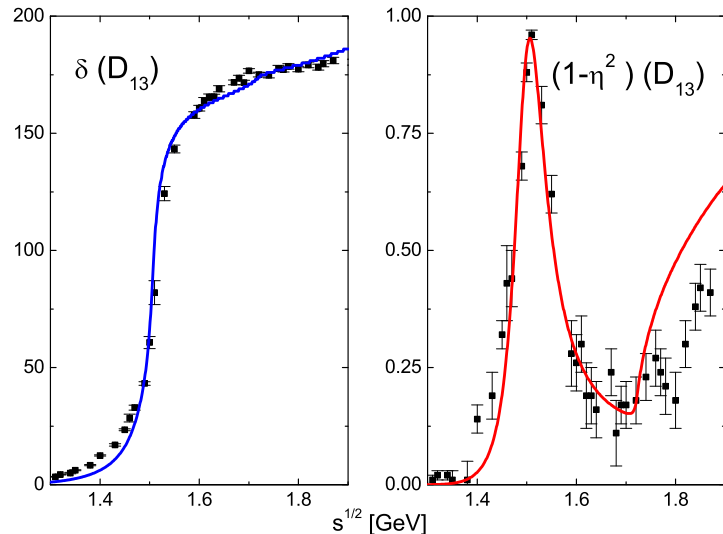


Fig. 12. Pion-nucleon scattering phase shift $\delta_{D_{13}}$ and inelasticity parameter $\eta_{D_{13}}$ of the D_{13} channel. We compare to the single-energy solution SP98 of [45,46]

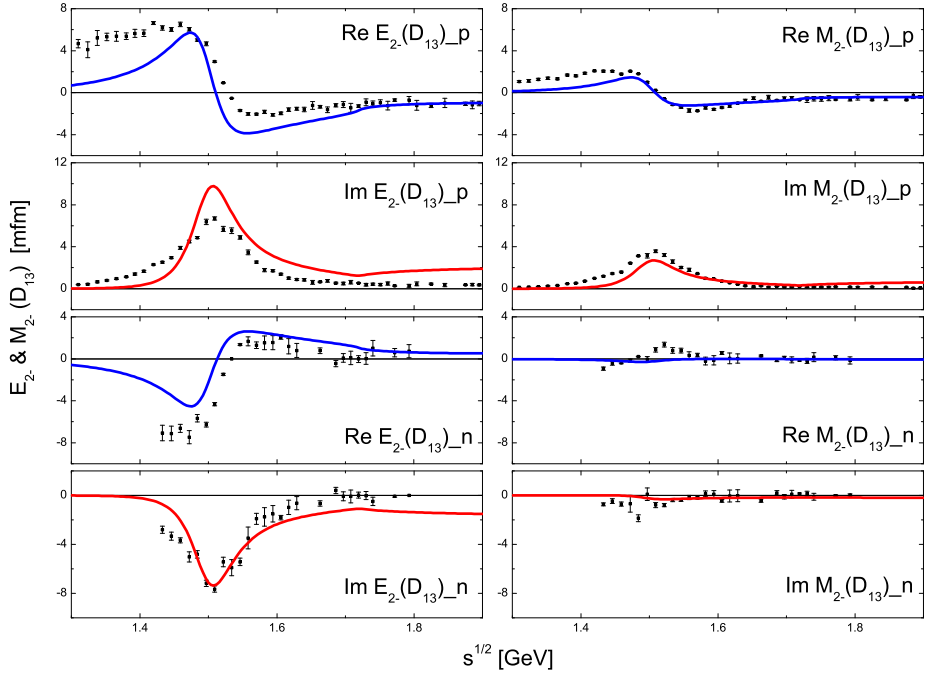


Fig. 13. Electric and magnetic multipole amplitudes $E_{2-}(D_{13})_{p,n}$ and $M_{2-}(D_{13})_{p,n}$ of photon-induced pion production (see (61)). It is shown the single energy solution SM00 [31,46]

length,

$$\bar{a}_{\omega N} = \frac{1}{3} a_{\omega N}^{(\frac{1}{2}\frac{1}{2})} + \frac{2}{3} a_{\omega N}^{(\frac{1}{2}\frac{3}{2})} \simeq (-0.44 + i 0.20) \text{ fm.} \quad (96)$$

This implies that an ω meson in low-density nuclear matter experiences a repulsive mass shift. This would rule out the existence of ω -mesic bound states at the nucleus surface. This is in contrast to the results of Klingl *et al.* [66] who find an attractive scattering length for the ω -meson, which would be conducive for ω -mesic atom states. However, it is possible that there are strong nonlinearities in the nuclear optical potential that lead to sufficient attraction at somewhat higher density and thus to deeply bound ω -mesic atom states. We return to this issue in section 6 when discussing the vector-meson spectral densities in nuclear matter.

It is useful to explore to what extend the production and scattering amplitudes may be represented in terms of a schematic resonance exchange model. We introduce a set of resonance coupling constants $g_{\pi N}^{(1520)}$ and $g_{VN}^{(1520)}$, phase parameters $\phi_{\pi V}$ and $\phi_{VV'}$, in terms of which we fit the resonance structure of the amplitudes,

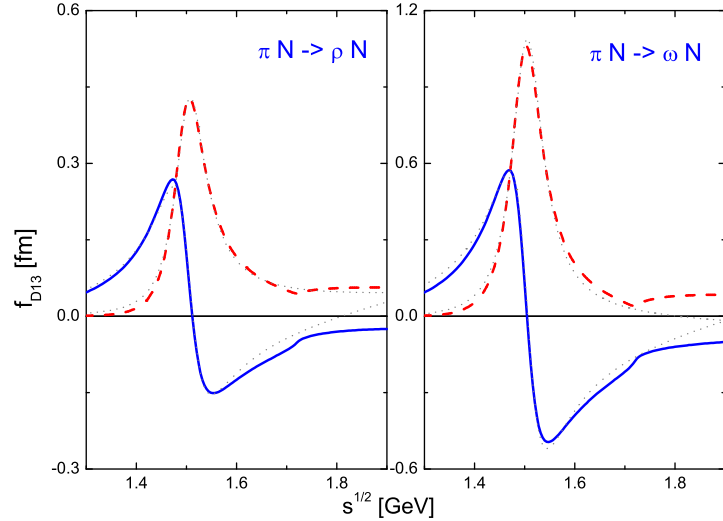


Fig. 14. Pion-induced vector-meson production amplitudes with $I = \frac{1}{2}$ and $J = \frac{3}{2}$. The real and imaginary parts of the amplitudes are shown by solid and dashed lines. The results of the schematic resonance exchange model (97) are represented by dotted lines.

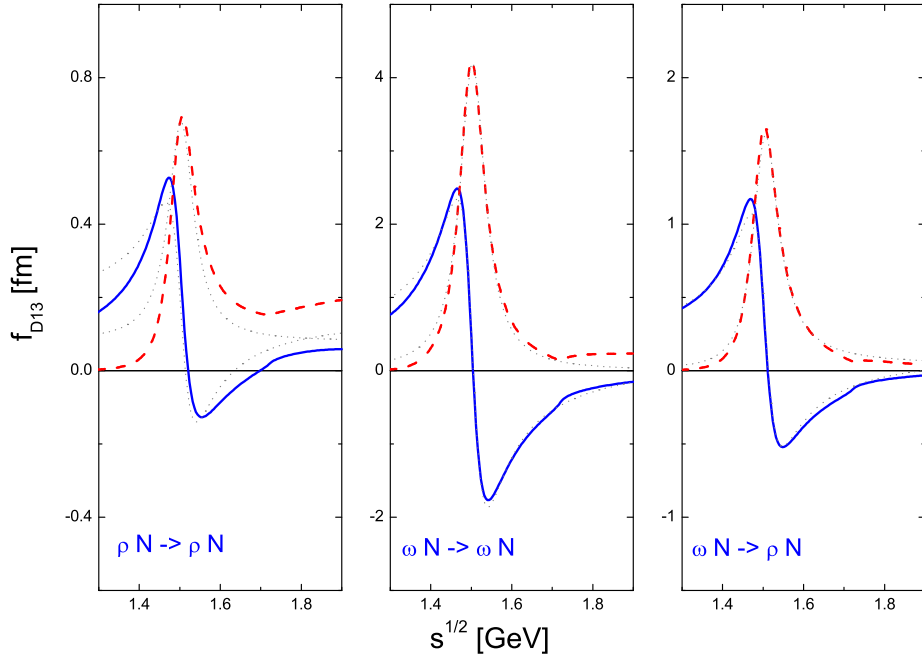


Fig. 15. Vector-meson nucleon scattering amplitude with $I = \frac{1}{2}$ and $J = \frac{3}{2}$. Solid, dashed and dotted lines as in Fig. 14.

| | $g_{\pi N}$ | $g_{\omega N}$ | $g_{\rho N}$ | $\phi_{\pi\omega}$ [°] | $\phi_{\pi\rho}$ [°] | $\phi_{\omega\rho}$ [°] | m [MeV] | Γ [MeV] |
|-----------|-------------|----------------|--------------|------------------------|----------------------|-------------------------|-----------|----------------|
| $N(1520)$ | 2.71 | 0.90 | 0.34 | 0.6 | -7.0 | -9.2 | 1503 | 76 |

Table 8

Resonance parameters in the $IJ^P = \frac{1}{2}\frac{3}{2}^-$ channel .

$$\begin{aligned}
f_{-, \pi N \rightarrow VN}^{(\frac{1}{2}\frac{3}{2})}(\sqrt{s}) &\simeq -\frac{e^{i\phi_{\pi V}} |g_{\pi N}^{(1520)}| |g_{VN}^{(1520)}| p_{\pi N}^2}{m_{1520}^2 (\sqrt{s} - m_{1520} + \frac{i}{2} \Gamma_{1520})} + \frac{p_{\pi N}^2}{m_{1520}^2} b_{-, \pi N \rightarrow VN}^{(\frac{1}{2}\frac{3}{2})} \\
f_{-, VN \rightarrow V'N}^{(\frac{1}{2}\frac{3}{2})}(\sqrt{s}) &\simeq -\frac{e^{i\phi_{V V'}} |g_{VN}^{(1520)}| |g_{V'N}^{(1520)}|}{\sqrt{s} - m_{1520} + \frac{i}{2} \Gamma_{1520}} + b_{-, VN \rightarrow V'N}^{(\frac{1}{2}\frac{3}{2})}.
\end{aligned} \quad (97)$$

Important background effects in the amplitudes are parameterized by the channel-dependent parameters $b_{X \rightarrow VN}^{(\frac{1}{2}\frac{3}{2})}$. In Fig. 14 and 15 we confront the schematic expressions (97) with our vector-meson production and scattering amplitudes. The dotted lines show real and imaginary parts of the amplitudes as given by the schematic resonance exchange model (97). The resonance parameters are collected in Tab. 8. The resonance exchange model leads to a fair reproduction of all but the elastic ρN amplitude provided the background terms,

$$\begin{aligned}
b_{-, \pi N \rightarrow \omega N}^{(\frac{1}{2}\frac{3}{2})} &\simeq (1.12 - i 0.18) \text{ fm}, \quad b_{-, \pi N \rightarrow \rho N}^{(\frac{1}{2}\frac{3}{2})} \simeq (0.57 + i 0.11) \text{ fm}, \\
b_{-, \omega N \rightarrow \omega N}^{(\frac{1}{2}\frac{3}{2})} &\simeq (0.24 + i 0.00) \text{ fm}, \quad b_{-, \rho N \rightarrow \rho N}^{(\frac{1}{2}\frac{3}{2})} \simeq (0.16 + i 0.08) \text{ fm}, \\
b_{-, \rho N \rightarrow \omega N}^{(\frac{1}{2}\frac{3}{2})} &\simeq (0.15 + i 0.03) \text{ fm},
\end{aligned} \quad (98)$$

are incorporated. Note that the coupling strength of the $N(1520)$ to the ρN state was extracted from the off diagonal $\omega N \rightarrow \rho N$ amplitude using the values of the resonance mass and width as obtained from the elastic ωN amplitude. The elastic ρN amplitude was then fitted in terms of only the background parameters. The discrepancy found for that amplitude reflects intrinsic limitations of the schematic resonance model which does not properly account for the energy dependence of the resonance self energy.

5.3.1 Discussion of $N(1520)$ resonance coupling constants

We compare the resonance coupling constants with the quark-model values found in [56]. Since that comparison has subtle aspects we do this in some detail. The d-wave nucleon resonance $N(1520)$ with $IJ^P = \frac{1}{2}\frac{3}{2}^-$ couples to the pion-nucleon channel in the following form:

$$\mathcal{L}_{\frac{1}{2}\frac{3}{2}^-}^{(\pi N)} = \frac{f_{\pi N}^{(1520)}}{m_\pi} \bar{R}_\mu (\partial^\mu \vec{\pi}) \cdot \vec{\tau} i \gamma_5 N + \text{h.c.}, \quad (99)$$

with $R_\mu = N_{1520,\mu}$, the nucleon field, N , and the pion field π . We identify

$$\left|f_{\pi N}^{(1520)}\right| = \frac{\sqrt{8\pi N_{\pi N}^{(+)}(m_{1520})}}{m_{1520}^{3/2}/m_\pi} \left|g_{\pi N}^{(1520)}\right| \simeq 1.44, \quad (100)$$

and conclude that our value compares favorably with the value $|f_{\pi N, BR}^{(1520)}| \simeq 1.71$, which was obtained in the quark model [56].

In contrast to the simple one-parameter structure of the pion-nucleon vertex the vector-meson nucleon vertices permit a much richer structure leading altogether to six coupling constants. We construct the most general on-shell interaction vertex,

$$\begin{aligned} \mathcal{L}_{\frac{1}{2}, \frac{3}{2}^-}^{(VN)} = & f_{\omega N, S}^{(1520)} \bar{R}_\mu N \omega^\mu + \frac{1}{\sqrt{3}} f_{\rho N, S}^{(1520)} \bar{R}_\mu \vec{\tau} N \vec{\rho}^\mu + i f_{\omega N, V}^{(1520)} \bar{R}_\mu \gamma_\alpha (\partial_\mu N) \omega^\alpha \\ & + \frac{i}{\sqrt{3}} f_{\rho N, V}^{(1520)} \bar{R}_\mu \vec{\tau} \gamma_\alpha (\partial_\mu N) \vec{\rho}^\alpha + i f_{\omega N, T}^{(1520)} \bar{R}_\mu \sigma_{\alpha\beta} (\partial_\mu \partial_\alpha N) \omega^\beta \\ & + \frac{i}{\sqrt{3}} f_{\rho N, T}^{(1520)} \bar{R}_\mu \vec{\tau} \sigma_{\alpha\beta} (\partial_\mu \partial_\alpha N) \rho^\beta + \text{h.c.}, \end{aligned} \quad (101)$$

describing the interaction of the vector meson fields ω_μ and ρ_μ . The three coupling constants f_S , f_V and f_T are independent quantities and need to be determined separately. In our work we evaluate only the scalar term, f_S ,

$$\begin{aligned} g_{VN}^{(1520)} &= \sqrt{\frac{N_{VN}(m_{1520})}{8\pi m_{1520}}} f_{VN, S}^{(1520)}, \quad f_{VN, V}^{(1520)} = f_{VN, T}^{(1520)} = 0, \\ \left|f_{\rho N, S}^{(1520)}\right| &\simeq 1.65, \quad \left|f_{\omega N, S}^{(1520)}\right| \simeq 4.35. \end{aligned} \quad (102)$$

We will demonstrate explicitly that the determination of f_V and f_T requires the control of terms suppressed by the phase space factor $p_{\rho N}^2$ or $p_{\omega N}^2$.

In our previous analyses [30], where we did not include constraints from the γ induced production data we obtained a significantly larger ratio $f_{\rho N}^{(1520)}/f_{\omega N}^{(1535)} \simeq 0.9$. We point out, however, that once the γ induced production data, in particular the electric and magnetic multipole amplitudes E_{2-} and M_{2-} describing the γ -induced pion production data, are considered (see Fig. 13), the coupling of the $N(1520)$ resonance to the ρN channel is reduced. Here we observe that the extraction of the coupling constant $f_{\rho N}^{(1520)}$ from the hadronic sector only appears rather model dependent. In fact this observation was in part our motivation for extending the analysis of [30]. Data on the dilepton production process $\pi^- p \rightarrow n e^+ e^-$ are expected to provide further constraints on the vector-meson coupling strengths to the subthreshold baryon resonances. In this reaction the subthreshold vector-meson nucleon production amplitudes,

required for the determination of $f_{\rho N}^{(1520)}$ and $f_{\omega N}^{(1520)}$ [68] are probed. We emphasize that any microscopic theory of the in-medium properties of vector mesons requires the information encoded in these coupling constants as input. This will be discussed in detail in section 6.

In order to illustrate the effect of the different coupling constants we evaluate the imaginary part of the reduced resonance self energy,

$$\begin{aligned} \Gamma_{1520}^{(\rho N)}(\sqrt{s}) = & 2 \left(\left(f_{\rho N, S}^{(1520)} \right)^2 + (E_N - m_N)^2 \left(f_{\rho N, V}^{(1520)} \right)^2 + \left(\frac{E_\rho}{m_\rho} f_{\rho N, S}^{(1520)} \right. \right. \\ & - \left(E_N - m_N \right) \left(\frac{\sqrt{s} + m_N}{m_\rho} f_{\rho N, V}^{(1520)} + \frac{s - m_\rho^2 - m_N^2}{2m_\rho} f_{\rho N, T}^{(1520)} \right) \left. \right)^2 \\ & \left. + \left(f_{\rho N, S}^{(1520)} - (E_N - m_N) f_{\rho N, V}^{(1520)} \right)^2 \right) (E_N + m_N) \frac{p_{\rho N}}{8\pi\sqrt{s}}, \quad (103) \end{aligned}$$

where a folding with the ρ -meson spectral function (32) analogous to (43) is understood. Also $\sqrt{s} = E_\rho + E_N$ and $E_N^2 = m_N^2 + p_{\rho N}^2$. A technical remark is in order here. The expression for the partial decay width in (103) is obtained by projecting the imaginary part of the polarization tensor for the d-wave $N(1520)$ resonance onto $J^P = \frac{3}{2}^-$. Clearly the contributions of the vector and tensor coupling constants $f_{\rho N, V}$ and $f_{\rho N, T}$ to the width are kinematically suppressed by the factor $p_{\rho N}^2$, compared to the contribution of the scalar coupling constant $f_{\rho N, S}$. This observation supports the reasoning in section 3.1, where we argued that the additional projectors for the ωN and ρN channels are kinematically suppressed. Therefore they are not considered in this work. Using our value for the resonance coupling constant we obtain a ρN -partial decay width of 2 MeV for a ρ -meson spectral function with an energy dependent, and 13 MeV with an energy-independent ρ -meson width. Thus, for a given value of the $\rho NN(1520)$ coupling constant, the ρN width of the $N(1520)$ depends crucially on the model for the ρ -meson spectral function.

As noted at the beginning of this section, the extraction of the ρ -production cross section and in particular the coupling of the $N(1520)$ to the ρN channel from hadronic reactions alone is model dependent. We attempt to remove this ambiguity by considering the additional constraints provided by the multipole amplitudes for the reaction $\gamma N \rightarrow \pi N$ within a generalized vector meson dominance model. Within this framework, we find a consistent description of the ρ production cross section of [37] and of the multipole amplitudes in all four channels.

The quantitative comparison with the result of [56] is more subtle since the quark model appears to favor vector- and tensor-type couplings of the $N(1520)$ to the ρN channel

$$\mathcal{L}_{BR} = i \frac{g_{BR}^{(\omega)}}{m_\omega^2} \bar{N} \sigma_{\mu\nu} R_\kappa (\partial^\nu \partial^\kappa \omega^\mu) + i \frac{g_{BR}^{(\rho)}}{m_\rho^2} \bar{N} \sigma_{\mu\nu} \vec{\tau} R_\kappa (\partial^\nu \partial^\kappa \vec{\rho}^\mu) + \text{h.c.} \quad (104)$$

while in our model the scalar coupling dominates. It is straightforward to identify the on-shell equivalent coupling constants,

$$\begin{aligned} f_{\rho N, T}^{(1520)} \Big|_{BR} &= 2\sqrt{3} \frac{g_{BR}^{(\rho)}}{m_\rho^2}, & f_{\omega N, T}^{(1520)} \Big|_{BR} &= 2 \frac{g_{BR}^{(\omega)}}{m_\omega^2} \\ f_{VN, S}^{(1520)} \Big|_{BR} &= 0, & f_{VN, V}^{(1520)} \Big|_{BR} &= -\frac{1}{2} (m_{1520} - m_N) f_{\omega N, T}^{(1520)} \Big|_{BR}, \end{aligned} \quad (105)$$

introduced in (101). Using the coupling constants obtained by Brown and Riska [56], $g_{BR}^{(\rho)} \simeq 4.5$ and $g_{BR}^{(\omega)} \simeq 7.7$, in (105), we find a ρN -decay width for the $N(1520)$ resonance of 0.04 MeV and 0.38 MeV for an energy dependent and energy independent ρ -meson width, respectively. Thus the partial width implied by the quark model results is much smaller than the partial widths, 2 MeV and 13 MeV, obtained in our model. This is by and large a consequence of the phase-space suppression, with $\Gamma_{1520}^{(\rho N)} \sim p_{\rho N}^3$ implied by the vertex (104).

It is instructive to express the coupling constants $f_{\omega N, S}$, $f_{\omega N, V}$ and $f_{\omega N, T}$ in terms of helicity matrix elements $h_{\omega N, h}^{(L, T)}$ where the upper index (L, T) refers to whether the matrix element involves a transverse or longitudinal vector meson,

$$\begin{aligned} f_{\omega N, S}^{(1520)} &= -h_{\omega N, 3/2}^{(T)}, \\ f_{\omega N, V}^{(1520)} &= \frac{\sqrt{3} E_N}{2 q^2} h_{\omega N, 1/2}^{(T)} - \frac{\sqrt{3} m_N^2}{2 q^2 m_{1520}} h_{\omega N, 1/2}^{(T)} - \frac{m_N + E_N}{2 q^2} h_{\omega N, 3/2}^{(T)} \\ &\quad + m_N \frac{E_N - E_\omega + m_N}{2 q^2 m_{1520}} h_{\omega N, 3/2}^{(T)} + \frac{\sqrt{6} m_\omega m_N}{2 m_{1520} q^2} h_{\omega N, 1/2}^{(L)}, \\ f_{\omega N, T}^{(1520)} &= -\frac{\sqrt{3} (m_{1520} + m_N)}{2 q^2 m_{1520}} h_{\omega N, 1/2}^{(T)} + \frac{E_N - E_\omega + m_N}{2 q^2 m_{1520}} h_{\omega N, 3/2}^{(T)} \\ &\quad + \frac{\sqrt{6} m_\omega}{2 m_{1520} q^2} h_{\omega N, 1/2}^{(L)}, \end{aligned} \quad (106)$$

where $E_N = (m_N^2 + q^2)^{1/2}$, $E_\omega = (m_\omega^2 + q^2)^{1/2}$ and $E_N + E_\omega = m_{1520}$. Analogous results hold for the coupling constants of the ρ meson. The expressions in (106) clearly demonstrate that the leading moments in q^2 of the helicity amplitudes are correlated. Only if

$$h_{\omega N, 3/2}^{(T)} = \sqrt{3} h_{\omega N, 1/2}^{(T)} = \sqrt{3} h_{\omega N, 1/2}^{(L)} / \sqrt{2}, \quad \text{at } q^2 = 0, \quad (107)$$

holds one obtains a finite result for $f_{\omega N, S}$, $f_{\omega N, V}$ and $f_{\omega N, T}$ in the limit of $q^2 \rightarrow$

0. Note that the various factors in (107) are in one to one correspondence to the coefficients given in (41) when defining the state $|J=\frac{3}{2}; 1\rangle$. This phenomenon illustrates a well known effect, namely that helicity amplitudes are subject to further constraint equations required as to avoid kinematical singularities. Nevertheless the helicity matrix elements are useful since they permit a more direct relation to corresponding matrix elements involving real photon states.

For the case of photons gauge invariance requires a transverse transition tensor. That leads to a correlation of the parameters in (101),

$$f_{\omega N, S}^{(1520)} = (m_{1520} - m_N) f_{\omega N, V}^{(1520)} + m_{1520} (E_N - m_N) f_{\omega N, T}^{(1520)}, \quad (108)$$

if applied to real photons. The fact that there are only two coupling constants left is readily understood because those two terms reflect the two helicity matrix elements $h_{\omega N, 3/2}^{(T)}$ and $h_{\omega N, 1/2}^{(T)}$. A longitudinal photon state does not exist implying $h_{\omega N, 1/2}^{(L)} = 0$ in the case of real photons. The most general on-shell vertex may be represented by [57],

$$\begin{aligned} \mathcal{L}_{\frac{1}{2} \frac{3}{2} -}^{(\gamma N)} = & \frac{e}{2 m_R} \bar{R}_\mu \gamma_\nu \left(i f_{\gamma N, S_1}^{(1520)} + i f_{\gamma N, V_1}^{(1520)} \tau_3 \right) N F^{\mu\nu} \\ & + \frac{e}{4 m_R^2} \bar{R}_\mu \left(f_{\gamma N, S_2}^{(1520)} + f_{\gamma N, V_2}^{(1520)} \tau_3 \right) (\partial_\nu N) F^{\mu\nu} + \text{h.c.} \end{aligned} \quad (109)$$

We derive the consequences of the generalized vector-meson dominance assumption (55,56). The effective interaction Lagrangian density describing the transition of the resonance into the γN state is:

$$\begin{aligned} \mathcal{L}_{\frac{1}{2} \frac{3}{2} -}^{(\gamma N)} = & e \bar{R}_\mu \left(i f_{\omega N, S}^{(1520)} \Gamma_{S, \nu}^{(+)} + \frac{i}{\sqrt{3}} f_{\rho N, S}^{(1520)} \Gamma_{V, \nu}^{(+)} \tau_3 \right) (N F^{\mu\nu}) + \text{h.c.}, \\ \Gamma_{S(V), \nu}^{(+)} = & \frac{m_{1520} + i \gamma \cdot \partial}{2 m_{1520}} \left(\frac{g_{S(V), 2}^{(+)} - g_{S(V), 1}^{(+)}}{m_{1520} m_\omega} i \partial_\nu + \frac{g_{S(V), 1}^{(+)}}{m_\omega} \gamma_\nu \right), \end{aligned} \quad (110)$$

where we do not consider effects from the vector and tensor coupling strength $f_{\rho N, V(T)}^{(1520)}$ and $f_{\omega N, V(T)}^{(1520)}$. The proper treatment of these terms requires a careful analysis of the suppressed ρN and ωN states in (41), in particular the off-shell structure of the associated projection operators. It is straightforward to match the on-shell parts of (109) and (110),

$$\begin{aligned} f_{\gamma N, V_1}^{(1520)} = & \frac{2}{\sqrt{3}} \frac{m_{1520}}{m_\omega} g_{V, 1}^{(+)} f_{\rho N, S}^{(1520)}, \quad f_{\gamma N, V_2}^{(1520)} = \frac{4}{\sqrt{3}} \frac{m_{1520}}{m_\omega} (g_{V, 1}^{(+)} - g_{V, 2}^{(+)}) f_{\rho N, S}^{(1520)} \\ f_{\gamma N, S_1}^{(1520)} = & 2 \frac{m_{1520}}{m_\omega} g_{S, 1}^{(+)} f_{\omega N, S}^{(1520)}, \quad f_{\gamma N, S_2}^{(1520)} = 4 \frac{m_{1520}}{m_\omega} (g_{S, 1}^{(+)} - g_{S, 2}^{(+)}) f_{\omega N, S}^{(1520)} \end{aligned} \quad (111)$$

| | $f_{\gamma N, S_1}^{(1520)}$ | $f_{\gamma N, S_2}^{(1520)}$ | $f_{\gamma N, V_1}^{(1520)}$ | $f_{\gamma N, V_2}^{(1520)}$ |
|-----------|------------------------------|------------------------------|------------------------------|------------------------------|
| this work | 7.84 | 7.63 | 1.72 | 1.67 |
| [58] | 2.9-4.5 | 4.3-5.8 | 3.1-5.3 | 1.1-4.4 |

Table 9

Electromagnetic resonance coupling constants in the $IJ^P = \frac{1}{2} \frac{3}{2}^-$ channel.

Finally we derive the isoscalar and isovector helicity matrix elements $h_{S(V),h}^{(T)}$ commonly used to parameterize the electromagnetic resonance decay $R \rightarrow \gamma N$,

$$\begin{aligned}
h_{S,3/2}^{(T)} &= -e f_{\omega N, S}^{(1520)} \frac{m_{1520}^2 - m_N^2}{2 m_{1520} m_\omega} \left(\frac{m_{1520} - m_N}{m_{1520} + m_N} g_{S,1}^{(+)} + g_{S,2}^{(+)} \right), \\
h_{S,1/2}^{(T)} &= \frac{e}{\sqrt{3}} f_{\omega N, S}^{(1520)} \frac{m_{1520}^2 - m_N^2}{2 m_{1520} m_\omega} \left(\frac{m_{1520} - m_N}{m_{1520} + m_N} g_{S,1}^{(+)} - g_{S,2}^{(+)} \right), \\
h_{S,1/2}^{(L)} &= 0.
\end{aligned} \tag{112}$$

Results for the isovector helicity matrix elements $h_{V,h}^{(T)}$ follow by analogy in terms of $\frac{1}{\sqrt{3}} f_{\rho N}^{(1520)}$ and $g_{V,i}^{(\pm)}$. In Table 9 we compare the electromagnetic resonance coupling constants with the estimates of [58]. We find deviations by almost a factor of two in some cases. Furthermore our estimates of the isoscalar coupling constants are systematically larger than the values of [58]. One may expect that the inclusion of the suppressed ρN and ωN channels (see 41) will lead to a more quantitative matching of the different approaches.

5.4 $IJ^P = \frac{3}{2} \frac{3}{2}^-$ channel

We now turn to the remaining $IJ^P = \frac{3}{2} \frac{3}{2}^-$ sector. Here we include the four channels πN , $\pi \Delta$, ρN and $\eta \Delta$. This leads all together to 10 parameters in this sector. The parameters of our best fit are given in Tab. 10.

| $g_1^{(\frac{3}{2}, -)} [m_\pi^{-\frac{n+m}{2}}]$ | $\pi N[n = 3]$ | $\pi \Delta[n = 1]$ | $\rho N[n = 1]$ | $\eta \Delta[n = 1]$ |
|---|----------------|---------------------|-----------------|----------------------|
| $\pi N[m = 3]$ | 0.36 | -2.47 | -3.68 | 2.24 |
| $\pi \Delta[m = 1]$ | -2.47 | 12.34 | 7.61 | -4.47 |
| $\rho N[m = 1]$ | -3.68 | 7.61 | 7.87 | -11.22 |
| $\eta \Delta[m = 1]$ | 2.24 | -4.47 | -11.22 | 12.02 |

Table 10

Coupling constants in the $IJ^P = \frac{3}{2} \frac{3}{2}^-$ channel.

The pion-nucleon phase shift and the inelasticity parameter are well reproduced by our model as demonstrated in Fig. 16. The phase shift and inelasticity parameter exhibit rapid changes at $\sqrt{s} \simeq 1700$ MeV signalling the presence

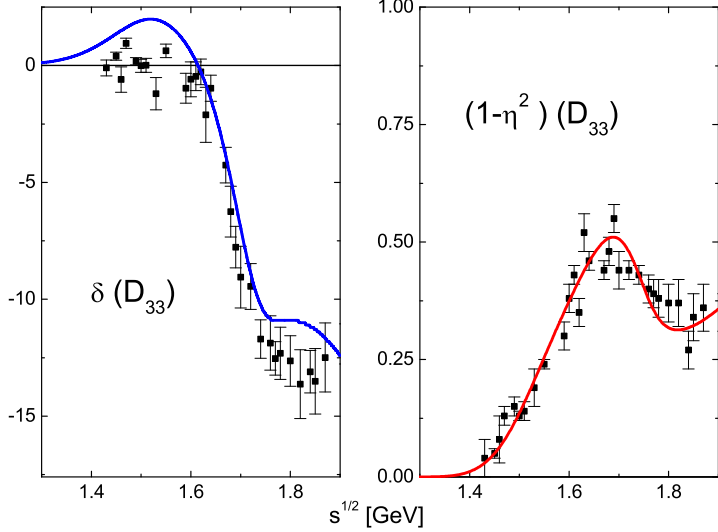


Fig. 16. Pion-nucleon scattering phase shift $\delta_{D_{33}}$ and inelasticity parameter $\eta_{D_{33}}$ of the D_{33} channel. We compare to the single-energy solution SP98 of [45,46].

of the baryon resonance $\Delta(1700)$ with quantum numbers $I J^P = \frac{3}{2} \frac{3}{2}^-$. The fit is constrained also by the vector-meson production cross section shown already in Fig. 1 and Fig. 2.

Further constraints are given by the electric and magnetic multipole ampli-

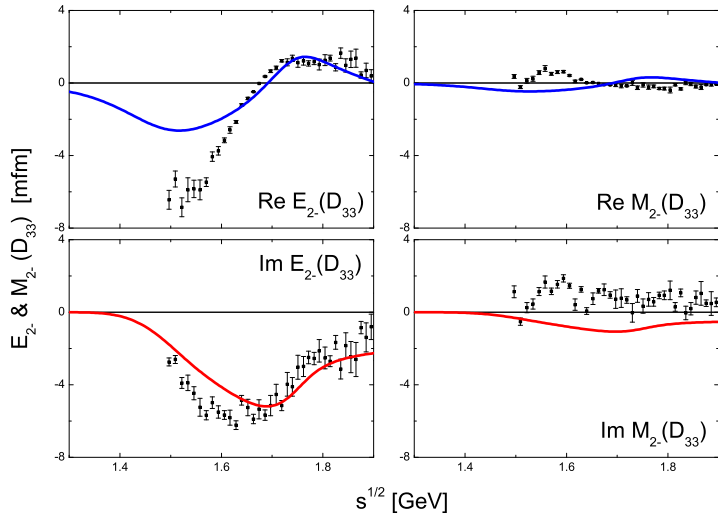


Fig. 17. Multipole amplitudes $E_{2-}(D_{33})$ and $M_{2-}(D_{33})$ of γ induced pion production (see (61)). Our results shown by solid lines are compared to those of the single-energy solution SM00 of [31,46].

tudes $E_{2-}(D_{33})$ and $M_{2-}(D_{33})$. In Fig. 17 we compare the appropriate electric and magnetic multipole amplitudes with the empirical SM00 analysis of [31,46]. We obtain a satisfactory description of the real and imaginary part, which indicates that the contributions we include are indeed the leading ones.

We turn to the ρ -meson scattering and production amplitudes. In Fig. 18 we present the pion-induced ρ -meson production amplitudes introduced in (133). The ρ -meson nucleon scattering amplitude with $I=\frac{3}{2}$ and $J=\frac{3}{2}$ is also shown in Fig. 18. The isobar $\Delta(1700)$ resonance leads to a peak structure in the imaginary parts of the subthreshold amplitudes. Again it is useful to introduce a reduced scattering amplitude,

$$f_{\rho N \rightarrow \rho N}^{(\frac{3}{2}\frac{3}{2}-)}(\sqrt{s}) = \frac{N_{\rho N}}{8\pi\sqrt{s}} M_{33}^{(\frac{3}{2}-)}(\sqrt{s}, 1),$$

$$a_{\rho N}^{(\frac{3}{2}\frac{3}{2})} = f_{\rho N \rightarrow \rho N}^{(\frac{3}{2}\frac{3}{2}-)}(m_N + m_\rho) \simeq (-0.13 + i 0.38) \text{ fm}, \quad (113)$$

which at threshold equals the scattering length. We find a repulsive scattering length consistent with the dominance of the $\Delta(1700)$ resonance in the $I J^P = \frac{3}{2} \frac{3}{2}^-$ amplitude. With (113) the collection of s-wave ρ -meson nucleon scattering lengths is complete, and we are ready to compute the spin and isospin averaged scattering length $\bar{a}_{\rho N}$,

$$\bar{a}_{\rho N} = \frac{1}{3} a_{\rho N}^{(\frac{1}{2})} + \frac{2}{3} a_{\rho N}^{(\frac{3}{2})} \simeq (-0.09 + i 0.24) \text{ fm}, \quad (114)$$

where $a_{\rho N}^{(\frac{1}{2})}$ is the isospin averaged $J = \frac{1}{2}$ scattering length given in (84) and $a_{\rho N}^{(\frac{3}{2})}$ the isospin averaged $J = \frac{3}{2}$ scattering length,

$$\bar{a}_{\rho N}^{(\frac{3}{2})} = \frac{1}{3} a_{\rho N}^{(\frac{1}{2}\frac{3}{2})} + \frac{2}{3} a_{\rho N}^{(\frac{3}{2}\frac{3}{2})} \simeq (-0.08 + i 0.30) \text{ fm}. \quad (115)$$

It is obvious that the scattering length $a_{\rho N}^{(\frac{3}{2}\frac{3}{2})}$, presented in this section, is of major importance for the spin and isospin averaged scattering length because it contributes with the relatively large weight factor 4/9. Our result for the averaged scattering length is in qualitative agreement with previous model calculations of the ρ -meson self energy [7,6,67] in nuclear matter if interpreted in terms of an effective scattering length. For dilute nuclear matter the isospin and spin averaged scattering $\bar{a}_{\rho N}$ of (114) leads to a considerable broadening but only a small mass shift for the ρ -meson. We return to the discussion of ρ -meson propagation in nuclear matter again in the next section where the influence of the nucleon and isobar resonances is discussed.

In Fig. 18 we show the vector-meson production and scattering amplitudes

obtained in our model as well as those of a schematic resonance exchange model, defined by,

$$\begin{aligned} f_{+, \pi N \rightarrow \rho N}^{(\frac{3}{2} \frac{3}{2})}(\sqrt{s}) &\simeq -\frac{e^{i\phi_{\pi\rho}^{(1700)}} |g_{\pi N}^{(1700)}| |g_{\rho N}^{(1700)}| p_{\pi N}^2}{m_{1700}^2 (\sqrt{s} - m_{1700} + \frac{i}{2} \Gamma_{1700})} + \frac{p_{\pi N}^2}{m_{1700}^2} b_{+, \pi N \rightarrow \rho N}^{(\frac{3}{2} \frac{3}{2})}, \\ f_{+, \rho N \rightarrow \rho N}^{(\frac{3}{2} \frac{3}{2})}(\sqrt{s}) &\simeq -\frac{|g_{\rho N}^{(1700)}|^2}{\sqrt{s} - m_{1700} + \frac{i}{2} \Gamma_{1700}} + b_{+, \rho N \rightarrow \rho N}^{(\frac{3}{2} \frac{3}{2})}, \end{aligned} \quad (116)$$

with the coupling constants $g_{\pi N}^{(1700)}$, $g_{\rho N}^{(1700)}$, a phase parameter $\phi_{\pi\rho}^{(1700)}$, and the background parameters $b_{\pi N \rightarrow \rho N}^{(\frac{3}{2} \frac{3}{2})}$, $b_{\rho N \rightarrow \rho N}^{(\frac{3}{2} \frac{3}{2})}$. The results of the schematic model are shown by the dotted lines. This simple model yields a reasonable description of the amplitudes. Note that in the model for the production amplitude in (116) we include a phase-space factor $p_{\pi N}^2$ which stems from the fact that the initial state is in a d-wave. The resonance parameters of our fit to the vector-meson production and scattering amplitudes are collected in Tab. 11. The background parameters are:

$$b_{-, \pi N \rightarrow \rho N}^{(\frac{3}{2} \frac{3}{2})} \simeq (-0.56 + i 0.32) \text{ fm}, \quad b_{-, \rho N \rightarrow \rho N}^{(\frac{3}{2} \frac{3}{2})} \simeq (0.06 - i 0.07) \text{ fm}. \quad (117)$$

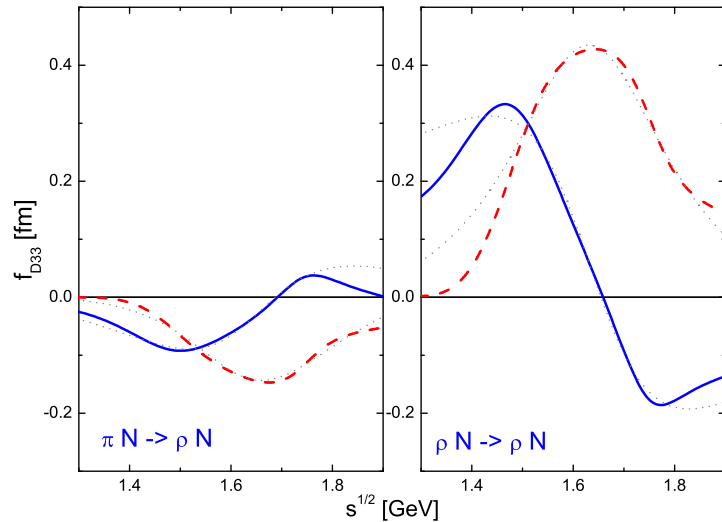


Fig. 18. Vector-meson production and scattering amplitude with $I = J = \frac{3}{2}$. The solid and dashed lines represent the real and imaginary parts of the amplitudes. The dotted lines follow from the schematic resonance exchange model defined in (116).

| | $g_{\pi N}$ | $g_{\rho N}$ | $\phi_{\pi\rho}$ [°] | m [MeV] | Γ [MeV] |
|----------------|-------------|--------------|----------------------|-----------|----------------|
| $\Delta(1700)$ | 2.29 | 0.71 | -175 | 1631 | 394 |

Table 11
Resonance parameters in the $IJ^P = \frac{3}{2} \frac{3}{2}^-$ channel .

5.4.1 Discussion of $\Delta(1700)$ resonance coupling constants

We compare the resulting resonance coupling constants with values of [56]. The d-wave isobar resonance $\Delta(1700)$ with $(I J)^P = (\frac{3}{2} \frac{3}{2})^-$ couples to the pion-nucleon and ρ -meson nucleon channels in the following form:

$$\begin{aligned} \mathcal{L}_{\frac{3}{2} \frac{3}{2}^-}^{(\pi N)} &= \left(f_{\pi N}^{(1700)} / m_\pi \right) \bar{\Delta}_{1700,\mu} (\partial^\mu \vec{\pi}) \cdot \vec{T} i \gamma_5 N + \text{h.c.}, \\ \mathcal{L}_{\frac{3}{2} \frac{3}{2}^-}^{(\rho N)} &= f_{\rho N,S}^{(1700)} \bar{\Delta}_\mu \vec{T} N \vec{\rho}^\mu + i f_{\rho N,V}^{(1700)} \bar{\Delta}_\mu \vec{T} \gamma_\alpha (\partial_\mu N) \vec{\rho}^\alpha \\ &\quad + i f_{\rho N,T}^{(1700)} \bar{\Delta}_\mu \vec{T} \sigma_{\alpha\beta} (\partial_\mu \partial_\alpha N) \vec{\rho}^\beta + \text{h.c.} \end{aligned} \quad (118)$$

The value $f_{\pi N, BR}^{(1700)} \simeq 2.66$ of [56] describing the strength with which the isobar resonance couples to the πN state, compares reasonably well with our result,

$$\left| f_{\pi N}^{(1700)} \right| = \sqrt{3} m_\pi \frac{\sqrt{8 \pi N_{\pi N}^{(+)}(m_{1700})}}{m_{1700}^{3/2}} \left| g_{\pi N}^{(1700)} \right| \simeq 1.89. \quad (119)$$

The three coupling constants f_S , f_V and f_T for the ρN channel, introduced in (118), are independent quantities. In our work we determined the scalar term only, which dominates the vertex, unless the vector and tensor coupling strengths are anomalously large,

$$\left| f_{\rho N,S}^{(1700)} \right| = \sqrt{\frac{8 \pi m_{1700}}{N_{\rho N}(m_{1700})}} \left| g_{\rho N}^{(1700)} \right| \simeq 3.42, \quad f_{\rho N,V}^{(1700)} = f_{\rho N,T}^{(1700)} = 0. \quad (120)$$

This should be compared with the quark-model results which imply a vanishing scalar coupling strength but finite values for the kinematically suppressed vector- and tensor-type vertices (see (105)). In order to facilitate the comparison with various models we evaluate the partial ρN -decay width of the isobar resonance,

$$\begin{aligned} \Gamma_{1700}^{(\rho N)}(\sqrt{s}) &= 2 \left(\left(f_{\rho N,S}^{(1700)} \right)^2 + (E_N - m_N)^2 \left(f_{\rho N,V}^{(1700)} \right)^2 + \left(\frac{E_\rho}{m_\rho} f_{\rho N,S}^{(1700)} \right. \right. \\ &\quad \left. \left. - (E_N - m_N) \left(\frac{\sqrt{s} + m_N}{m_\rho} f_{\rho N,V}^{(1700)} + \frac{s - m_\rho^2 - m_N^2}{2 m_\rho} f_{\rho N,T}^{(1700)} \right) \right)^2 \right) \end{aligned}$$

$$+ \left(f_{\rho N, S}^{(1700)} - (E_N - m_N) f_{\rho N, V}^{(1700)} \right)^2 \right) (E_N + m_N) \frac{p_{\rho N}}{8 \pi \sqrt{s}}, \quad (121)$$

in terms of the three coupling constants, $f_{S, V, T}^{(1700)}$, $\sqrt{s} = E_\rho + E_N$ and $E_N^2 = m_N^2 + p_{\rho N}^2$. In (121) a folding with the ρ -meson spectral function (32) analogous to (43) is understood. With our value for the resonance coupling constant we find a ρN -decay width of 71 MeV for an energy dependent, and 175 MeV for an energy independent width of the ρ -meson. Using the quark-model coupling constants instead [56], we obtain 0.03 MeV and 0.12 MeV, respectively, for the ρN partial widths of the $\Delta(1700)$.

Using the generalized vector-meson dominance assumption (55,56), the on-shell vertex may be represented by,

$$\begin{aligned} \mathcal{L}_{\frac{3}{2} \frac{3}{2}^-}^{(\gamma N)} &= \frac{e}{2 m_R} \bar{R}_\mu \gamma_\nu i f_{\gamma N, V_1}^{(1520)} T_3 N F^{\mu\nu} + \frac{e}{4 m_R^2} \bar{R}_\mu f_{\gamma N, V_2}^{(1520)} T_3 (\partial_\nu N) F^{\mu\nu} + \text{h.c.} \\ &= i e f_{\rho N, S}^{(1700)} \bar{\Delta}_\mu T_3 \Gamma_{V, \nu}^{(+)} (N F^{\mu\nu}) + \text{h.c.}, \end{aligned} \quad (122)$$

with the transition operator $\Gamma_{S(V)}^\nu$ specified in (110). We obtain values,

$$\left| f_{\gamma N, V_1}^{(1700)} \right| \simeq 3.23, \quad \left| f_{\gamma N, V_2}^{(1700)} \right| \simeq 3.14, \quad (123)$$

that are comparable with the values $f_{\gamma N, V_1}^{(1700)} \simeq 1.6 - 2.3$ and $f_{\gamma N, V_2}^{(1700)} \simeq 2.7 - 4.8$ suggested in [58].

6 Implications for vector-meson propagation in nuclear matter

In this section we present results for the propagators of the ρ and ω mesons at rest in nuclear matter, obtained with the scattering amplitudes presented in section 5, to leading order in density. The low-density theorem states that the self energy, $\Delta m_V^2(\omega)$, of a vector meson in nuclear matter is given by [70]

$$\Delta m_V^2(\omega) = - \frac{8 \pi \sqrt{s}}{N_{VN}(\sqrt{s})} f_{VN}(\sqrt{s}) \bigg|_{\sqrt{s}=\omega+m_N} \rho_N + \dots, \quad (124)$$

where ω is the energy of the vector meson and ρ_N the nucleon density. The normalization factor $N_{VN}(\sqrt{s}) \simeq 2 m_N$, was introduced in (42). In spin and isospin saturated nuclear matter, the shifts of the mass and width, given by $\Delta m_V^2(\omega)$, are in this approximation proportional to the spin and isospin averaged s-wave scattering amplitude,

$$\begin{aligned}
f_{\rho N}(\sqrt{s}) &= \frac{1}{9} f_{+, \rho N \rightarrow \rho N}^{(\frac{1}{2} \frac{1}{2})}(\sqrt{s}) + \frac{2}{9} f_{+, \rho N \rightarrow \rho N}^{(\frac{3}{2} \frac{1}{2})}(\sqrt{s}) \\
&\quad + \frac{2}{9} f_{-, \rho N \rightarrow \rho N}^{(\frac{1}{2} \frac{3}{2})}(\sqrt{s}) + \frac{4}{9} f_{-, \rho N \rightarrow \rho N}^{(\frac{3}{2} \frac{3}{2})}(\sqrt{s}), \\
f_{\omega N}(\sqrt{s}) &= \frac{1}{3} f_{+, \omega N \rightarrow \omega N}^{(\frac{1}{2} \frac{1}{2})}(\sqrt{s}) + \frac{2}{3} f_{-, \omega N \rightarrow \omega N}^{(\frac{1}{2} \frac{3}{2})}(\sqrt{s}).
\end{aligned} \tag{125}$$

In Fig. 19 we show the resulting propagators at the saturation density of nuclear matter, $\rho_0 = 0.17 \text{ fm}^{-3}$ and at $\rho = 2 \rho_0$. For the ρ meson we note an enhancement of the width, and a downward shift in energy, due to the mixing with the baryon resonances at $\sqrt{s} = 1.5 - 1.6 \text{ GeV}$. As the density is increased, the width of the ρ -like peak is amplified and more strength is shifted down to the resonance-hole region at lower energies. At nuclear saturation density the center of gravity of the energy-weighted sum rule is shifted down by about 3 % only. Compared to our previous preliminary result [30] we find much less attraction in the ρ -meson spectral function. This is a consequence of a significantly reduced coupling of the d-wave $N(1520)$ resonance to the ρN state. In the detailed discussions of the previous sections we linked this result to the fact that we now include the data on photon-induced reactions in a systematic fashion [1]. In previous analyses the photon-induced multipole amplitudes were not considered systematically in this context. In particular our spectral function for the ρ meson shows considerably less strength in the low-mass region as compared to previous works [71,69,72]. The in-medium propagator of the ω meson exhibits two distinct quasi-particles, an ω -meson like mode, which is shifted up somewhat in energy, and a resonance-hole like mode at low energies. This confirms our previous result [30] almost quantitatively. The low-lying mode carry about 15 % on the energy-weighted sum rule. The center-of-gravity is shifted down by $\simeq 4$ % at nuclear saturation density. However, we stress that the structure of the in-medium ω -meson spectral function clearly cannot be characterized by this number alone. Note that as compared to the recent work [73] we obtain a significantly stronger coupling of the ω meson to the $N(1520)$ nucleon-hole state leading to a much more pronounced effect of the resonance-hole state in the spectral function.

A simple estimate on the accuracy of the leading order result follows by investigating the size of the subleading term, which is due to the Pauli blocking of intermediate states. In order to compute the leading and subleading mass shifts of the ω meson we need only the s-wave scattering lengths $a_{\omega N}^{1/2} \simeq (-0.45 + i 0.31) \text{ fm}$ and $a_{\omega N}^{3/2} \simeq (-0.43 + i 0.15) \text{ fm}$. We obtain a model independent result, in complete analogy with the corresponding expression for the kaon [74,75],

$$\Delta m_\omega^2 = -4 \pi \left(1 + \frac{m_\omega}{m_N}\right) \left[\frac{1}{3} a_{\omega N}^{(\frac{1}{2})} + \frac{2}{3} a_{\omega N}^{(\frac{3}{2})} \right] \rho$$

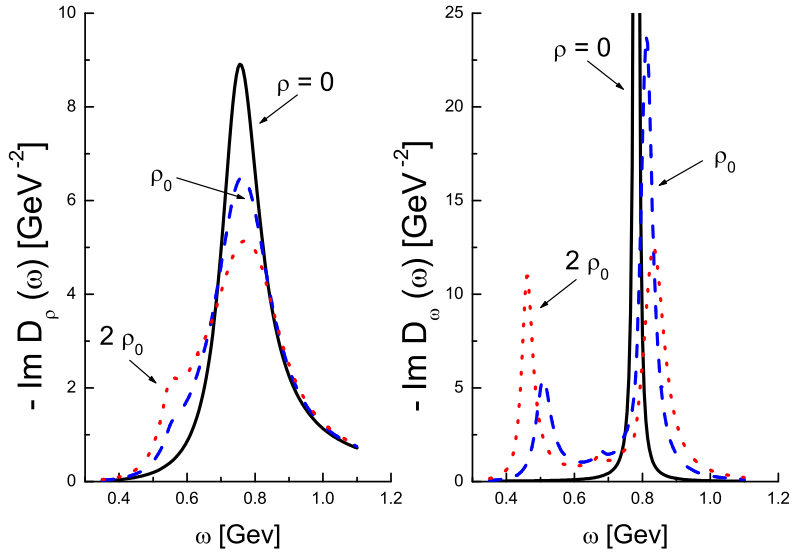


Fig. 19. Imaginary parts of the ρ -meson and ω -meson propagators in nuclear matter at $\rho = \rho_0$ and $\rho = 2 \rho_0$, compared to those in the vacuum.

$$+ \frac{4}{\pi^2} \frac{1 - x^2 + x^2 \log x^2}{(1 - x)^2} \left[\frac{1}{3} \left(a_{\omega N}^{(\frac{1}{2})} \right)^2 + \frac{2}{3} \left(a_{\omega N}^{(\frac{3}{2})} \right)^2 \right] k_F^4 + \mathcal{O}(k_F^5) \quad (126)$$

where $x = m_\omega/m_N$. At nuclear saturation density the correction term of order k_F^4 in (126) implies a further repulsive mass shift of about 1 MeV and increase of the decay width of 2 MeV for the ω meson. This should be compared to the leading order repulsive mass and width shift of 43 MeV and 39 MeV respectively. We expect that the results obtained with only the leading term in the low-density expansion are qualitatively correct at normal nuclear matter density. However, on a quantitative level, the spectral functions may change when higher order terms in the density expansion are included. For instance, we expect that the in-medium properties of the baryon resonances depend sensitively on the meson spectral functions. If this is the case, a self consistent calculation, which corresponds to a partial summation of terms in the density expansion, would have to be performed [74,76,69].

7 Summary and conclusion

In this work we have computed the scattering amplitudes that describe the s-wave scattering of the light vector mesons off nucleons. To leading order in a density expansion these amplitudes, in particular the subthreshold parts, determine the spectral functions of the ρ - and ω -meson in nuclear matter. Since there are no data on vector-meson nucleon scattering we constrained our

analysis by all relevant elastic and inelastic γN and πN data. The coupled channel unitarity condition together with covariance, the causality property of local quantum field theory and the data set then lead to fairly robust predictions for the vector-meson nucleon scattering amplitudes. We explored the possibility that the nucleon and isobar resonances, which do not belong to the large- N_c ground state of QCD, are generated by coupled channel dynamics [20]. The merit of this conjecture, which admittedly is rather extreme, consists in a significant reduction of the number of parameters, since such a scheme does not require any parameters describing the properties of bare resonances. Based on our analysis, where all relevant resonances in the channels considered were successfully generated by coupled channel dynamics, we see no indication that would disprove this conjecture [20].

In contrast to previous works which typically apply the K-matrix formalism, our coupled channel study is based on the covariant projector technique introduced in [20]. This leads to loop functions and scattering amplitudes which are consistent with a dispersion-integral representation. The known drawback of the K-matrix formalism, the violation of analyticity and causality, is avoided. We developed a generalization of the vector meson dominance assumption that is appropriate for an effective field theory formulated in terms of quasi-local two-body interaction terms only. Moreover, this work is the first study of the vector-meson nucleon scattering processes where the ρN , ωN and γN states were considered simultaneously. Altogether, in our approach we incorporate the γN , πN , $\pi\Delta$, ρN , ωN , ηN , $K\Lambda$ and $K\Sigma$ states. We allow for s- and d-wave states in the πN and $\pi\Delta$ channels since only those states couple to the s-wave vector-meson nucleon states. In the remaining hadronic channels we determine the strength of the leading s-wave states only. We approximate the three-body final state, $\pi\pi N$, by including the ρN and $\pi\Delta$ channels where we use energy dependent decay widths of the ρ meson and Δ isobar. The two-pion total cross section was not fitted directly, since our model is restricted to low angular momentum states. Furthermore, we did not include the σN channel explicitly. It would anyway be difficult to discriminate its effects from the $\pi\Delta$ channel, which in our scheme is only indirectly constrained by data. Hence, we consider the latter as an effective channel, which subsumes also the residual effect of the σN channel.

Since there is no model-independent partial-wave decomposition of the two-pion production data available, the σN channel was not considered. It would be extremely difficult to discriminate its effects from the $\pi\Delta$ channel in our present scheme. The latter channel, which is constrained in our scheme by data only rather indirectly, is considered as an effective channel in the sense that it is supposed to describe some residual effects of the σN channel also.

Due to the presence of nucleon and isobar resonances, the vector-meson nucleon scattering amplitudes show rapid energy variations. In particular we find

that the s-wave resonances $N(1535)$ and $N(1650)$ show a strong ωN component, which are required to simultaneously generate both resonances. On the other hand, only the $N(1535)$ but not the $N(1650)$ resonance appears to couple significantly to the ρN channel. Similarly striking is our result that the d-wave $N(1520)$ resonance couples strongly to the ωN channel but with only much reduced strength to the ρN channel. This result is a consequence of our systematic inclusion of the photon-induced scattering data not done previously. We extracted coupling constants of the nucleon and isobar resonances to the vector-meson nucleon states and compared those to predictions of the quark model. In some cases we find a strong disagreement.

It is gratifying to obtain a simultaneous description of all considered photon- and pion-induced production data. Production cross sections, for which a t-channel exchange of a single pion is dominantly contributing, are typically described well only at energies rather close to the production threshold. The long-ranged one-pion exchange contribution is expected to yield significant strength in higher partial waves, not considered in this work. The remaining empirical pion- and photon-induced production cross sections are fairly well described up to significantly higher energies, thus demonstrating s-wave dominance for those reactions.

An improved description of the considered electromagnetic multipole amplitudes as well as the production cross sections is expected once ρN and ωN states with subleading angular momentum characteristics are included in the analysis.

In nuclear matter our scattering amplitudes imply an ω -meson spectral functions with considerable support at energies smaller than the free-space mass representing resonance nucleon-hole type excitations. On the other hand, as an immediate consequence of the moderate coupling of the ρN channel to the $N(1520)$ d-wave resonance, the in-medium effects for the ρ meson are found to be significantly smaller as compared to previous calculations. We emphasize that the rigorous evaluation of the vector-meson spectral functions requires an approach in which the transformation of the scattering amplitudes from the center of mass system into the laboratory frame is well defined. This transformation can be quite non-trivial for states with high spin and angular momentum. Clearly, the covariant projector technique applied in this work fulfils this requirement. We anticipate that a realistic evaluation of the in-medium spectral functions of the light vector mesons requires a self consistent many-body approach, in particular when the nucleon and isobar resonances show important in-medium modifications [76].

The results presented in this paper are relevant for the experimental program at GSI. The HADES detector will help to further explore the properties of the light vector mesons in nuclear matter by measuring their dilepton final

state with high accuracy. Complementary experimental programs are pursued at Jefferson Lab [77], MAMI [78] and KEK [79] with photon and nucleon induced reactions off nuclei. To further substantiate the structure of the vector-meson nucleon scattering amplitudes it would be desirable to establish a more microscopic understanding of the effective interaction vertices employed in our work. We expect that a significant parameter reduction is feasible by a proper extension of the χ -BS(3) approach (chiral Bethe-Salpeter approach for the SU(3) flavor group) in [20] to include additional inelastic channels like $\pi\Delta$, ωN and ρN .

Acknowledgments

M.F.M.L. and B.F. acknowledge encouragement and fruitful discussions with M. Soyeur. Gy.W. was supported by the Hungarian research Foundation (OTKA) grants T 32038 and T 30855. We thank V. Koch for a critical reading of the manuscript.

8 Appendix A: Projector approach for Δ -isobars

We elaborate on the inclusion of the $\pi\Delta$ channel. The $J = \frac{1}{2}$ and $J = \frac{3}{2}$ projectors are

$$\begin{aligned} [Y_{0,\mu}^{(+)}(\bar{q}, q; w)]_{21} &= -3 P_{\mu\alpha}^{(-)}(w) \bar{q}^\alpha i \gamma_5, \\ [Y_{0,\mu}^{(+)}(\bar{q}, q; w)]_{12} &= +i \gamma_5 q^\alpha 3 P_{\alpha\mu}^{(-)}(w), \\ [Y_{0,\mu\nu}^{(+)}(\bar{q}, q; w)]_{32} &= \sqrt{3} P_{\mu\alpha}^{(-)}(w) \bar{q}^\alpha \left(\gamma_\nu - \frac{w_\nu}{w^2} \psi \right), \\ [Y_{0,\mu\nu}^{(+)}(\bar{q}, q; w)]_{23} &= \sqrt{3} \left(\gamma_\mu - \frac{w_\mu}{w^2} \psi \right) q^\alpha P_{\alpha\nu}^{(-)}(w), \\ [Y_{0,\mu\nu}^{(+)}(\bar{q}, q; w)]_{22} &= 9 P_{\mu\alpha}^{(-)}(w) \bar{q}^\alpha q^\beta P_{\beta\nu}^{(-)}(w), \end{aligned} \quad (127)$$

and

$$\begin{aligned} [Y_{1,\mu}^{(-)}(\bar{q}, q; w)]_{21} &= -\sqrt{3} P_{\mu\alpha}^{(+)}(w) q^\alpha i \gamma_5, & [Y_{1,\mu\nu}^{(-)}(\bar{q}, q; w)]_{32} &= P_{\mu\nu}^{(+)}(w), \\ [Y_{1,\mu}^{(+)}(\bar{q}, q; w)]_{12} &= +\sqrt{3} i \gamma_5 \bar{q}^\alpha P_{\alpha\mu}^{(+)}(w), & [Y_{1,\mu\nu}^{(-)}(\bar{q}, q; w)]_{23} &= P_{\mu\nu}^{(+)}(w), \\ [Y_{1,\mu\nu}^{(-)}(\bar{q}, q; w)]_{22} &= P_{\mu\nu}^{(+)}(w), \end{aligned} \quad (128)$$

where we introduced the auxiliary objects

$$\begin{aligned} P_{\mu\nu}^{(\pm)}(w) &= \frac{1}{2} \left(g_{\mu\nu} - \frac{w_\mu w_\nu}{w^2} \right) \left(1 \pm \frac{\psi}{\sqrt{w^2}} \right) \\ &\quad - \frac{1}{6} \left(\gamma_\mu - \frac{w_\mu}{w^2} \psi \right) \left(1 \mp \frac{\psi}{\sqrt{w^2}} \right) \left(\gamma_\nu - \frac{w_\nu}{w^2} \psi \right). \end{aligned} \quad (129)$$

Note that in the $J = \frac{3}{2}$ channel the projectors couple to further projectors not considered in this work. This amounts to neglecting contributions from the $\pi\Delta$ states with $J = \frac{3}{2}$ but $L = 2$. Finally we provide the loop functions of the $\pi\Delta$ channels. The loop functions are specified first in the zero-width approximation,

$$\begin{aligned} J_{22}^{(I+)}(\sqrt{s}, 0) &= N_{\pi\Delta}^{(+)}(\sqrt{s}) I_{\pi\Delta}(\sqrt{s}), & J_{22}^{(I-)}(\sqrt{s}, 1) &= N_{\pi\Delta}^{(-)}(\sqrt{s}) I_{\pi\Delta}(\sqrt{s}), \\ N_{\pi\Delta}^{(+)}(\sqrt{s}) &= \left(E_\Delta - m_\Delta \right) \frac{2}{3} \left(2 \frac{E_\Delta}{m_\Delta} - 1 \right)^2 p_{\pi\Delta}^2, \\ N_{\pi\Delta}^{(-)}(\sqrt{s}) &= \left(E_\Delta + m_\Delta \right) \left(\frac{5}{9} + \frac{2}{9} \frac{E_\Delta}{m_\Delta} + \frac{2}{9} \frac{E_\Delta^2}{m_\Delta^2} \right), \end{aligned} \quad (130)$$

with $\sqrt{s} = \sqrt{m_\Delta^2 + p_{\pi\Delta}^2} + \sqrt{m_\pi^2 + p_{\pi\Delta}^2}$ and $E_\Delta = \sqrt{m_\Delta^2 + p_{\pi\Delta}^2}$. The threshold behavior of the loop functions (130) confirms that in the $J = \frac{1}{2}$ channel the considered $\pi\Delta$ state has $L = 2$ but in the $J = \frac{3}{2}$ channel $L = 0$. The finite decay width is included by analogy with our treatment of the vector-meson loop functions in (43). For the isobar we use the spectral density

$$\begin{aligned} \rho_\Delta(q^2) &= -\Im \left(\zeta_\Delta(q^2 - m_\Delta^2) - \Pi_\Delta(q^2) \right)^{-1}, \\ \Pi_\Delta(q^2) &= -\frac{C^2}{3f^2} \left(m_N + \sqrt{m_N^2 + p_{\pi N}^2} \right) p_{\pi N}^2 \left(I_{\pi N}(\sqrt{q^2}) - \Re I_{\pi N}(m_\Delta) \right) \\ &\quad \times \left(\frac{\lambda_\Delta^2 + \bar{p}_{\pi N}^2}{\lambda_\Delta^2 + p_{\pi N}^2} \right)^2, \end{aligned} \quad (131)$$

with $\sqrt{q^2} = \sqrt{m_N^2 + p_{\pi N}^2} + \sqrt{m_\pi^2 + p_{\pi N}^2}$ and $m_\Delta = \sqrt{m_N^2 + \bar{p}_{\pi N}^2} + \sqrt{m_\pi^2 + \bar{p}_{\pi N}^2}$. The parameters are adjusted as to reproduce the pion-nucleon P_{33} phase shift. We use $f = 90$ MeV, $C \simeq 2.05$, $m_\Delta \simeq 1232$ MeV, $\zeta_\Delta \simeq 0.9$ and $\lambda_\Delta \simeq 316$ MeV. The incorporation of the dipole form factor in (131) leads to a quantitative description of the P_{33} phase up to about $\sqrt{s} \simeq 1.5$ GeV [80]. Finally the isobar spectral function is normalized by the cutoff $\Lambda_\Delta \simeq 1.78$ GeV where Λ_Δ is introduced by analogy with (33).

The pion-induced isobar production cross sections are:

$$\begin{aligned} \sigma_{\pi^- p \rightarrow \pi^- \Delta^+} &= 4\pi \frac{p_{\pi\Delta}}{p_{\pi N}} \frac{4}{9} \left(\left| \frac{1}{2} f_{\pi N \rightarrow \pi\Delta}^{(\frac{1}{2}\frac{1}{2}+)} - \sqrt{\frac{2}{5}} f_{\pi N \rightarrow \pi\Delta}^{(\frac{3}{2}\frac{1}{2}+)} \right|^2 \right. \\ &\quad \left. + 2 \left| \frac{1}{2} f_{\pi N \rightarrow \pi\Delta}^{(\frac{1}{2}\frac{3}{2}-)} - \sqrt{\frac{2}{5}} f_{\pi N \rightarrow \pi\Delta}^{(\frac{3}{2}\frac{3}{2}-)} \right|^2 \right), \\ \sigma_{\pi^- p \rightarrow \pi^+ \Delta^-} &= 4\pi \frac{p_{\pi\Delta}}{p_{\pi N}} \frac{1}{3} \left(\left| f_{\pi N \rightarrow \pi\Delta}^{(\frac{1}{2}\frac{1}{2}+)} + \sqrt{\frac{2}{5}} f_{\pi N \rightarrow \pi\Delta}^{(\frac{3}{2}\frac{1}{2}+)} \right|^2 \right. \\ &\quad \left. + 2 \left| f_{\pi N \rightarrow \pi\Delta}^{(\frac{1}{2}\frac{3}{2}-)} + \sqrt{\frac{2}{5}} f_{\pi N \rightarrow \pi\Delta}^{(\frac{3}{2}\frac{3}{2}-)} \right|^2 \right), \\ \sigma_{\pi^+ p \rightarrow \pi^+ \Delta^+} &= 4\pi \frac{p_{\pi\Delta}}{p_{\pi N}} \frac{2}{5} \left(\left| f_{\pi N \rightarrow \pi\Delta}^{(\frac{3}{2}\frac{1}{2}+)} \right|^2 + 2 \left| f_{\pi N \rightarrow \pi\Delta}^{(\frac{3}{2}\frac{3}{2}-)} \right|^2 \right), \\ \sigma_{\pi^+ p \rightarrow \pi^0 \Delta^{++}} &= \frac{3}{2} \sigma_{\pi^+ p \rightarrow \pi^+ \Delta^+}, \end{aligned} \quad (132)$$

where we introduced the partial-wave amplitudes $f^{(IJ\pm)}(\sqrt{s})$. For example in the isospin $\frac{1}{2}$ channel we write:

$$\begin{aligned}
f_{\pi N \rightarrow \pi \Delta}^{(\frac{1}{2}\frac{1}{2}+)}(\sqrt{s}) &= \frac{\sqrt{N_{\pi N}^{(+)} N_{\pi \Delta}^{(+)}}}{8 \pi \sqrt{s}} M_{21}^{(\frac{1}{2}+)}(\sqrt{s}, 0) , \\
f_{\pi N \rightarrow \pi \Delta}^{(\frac{1}{2}\frac{3}{2}-)}(\sqrt{s}) &= \frac{\sqrt{N_{\pi N}^{(-)} N_{\pi \Delta}^{(-)}}}{8 \pi \sqrt{s}} p_{\pi N} M_{21}^{(\frac{1}{2}-)}(\sqrt{s}, 1) .
\end{aligned} \tag{133}$$

The energy dependent width of isobar resonance is taken into account by folding the cross sections (132) with the spectral function (131).

References

- [1] R. Rapp and J. Wambach, *Adv. Nucl. Phys.* **25** (2000) 1.
- [2] CERES, G. Agakichiev *et al.*, *Phys. Rev. Lett.* **75** (1995) 1272; *Nucl. Phys. A* **610** (1996) 317c; A. Drees, *Nucl. Phys. A* **610** (1996) 536c.
- [3] G.E. Brown and M. Rho, *Phys. Rev. Lett.* **66** (1991) 2720.
- [4] C. Gale and Kapusta, *Nucl. Phys. B* **357** (1991) 65.
- [5] T. Hatsuda and S.H. Lee, *Phys. Rev. C* **46** (1992) R34.
- [6] G. Chanfray and P. Schuck, *Nucl. Phys. A* **545** (1992) 271c.
- [7] M. Herrmann, B. Friman and W. Nörenberg, *Nucl. Phys. A* **560** (1993) 411.
- [8] Gy. Wolf, W. Cassing and U. Mosel, *Nucl. Phys. A* **552** (1993) 549.
- [9] Gy. Wolf, *Heavy Ion Phys.* **5** (1997) 281.
- [10] G. Chanfray, R. Rapp and J. Wambach, *Phys. Rev. Lett.* **76** (1996) 368.
- [11] S. Leupold, W. Peters and U. Mosel, *Nucl. Phys. A* **628** (1998) 311.
- [12] S. Leupold, *Phys. Rev. C* **64** (2001) 015202.
- [13] B. Friman and H.J. Pirner, *Nucl. Phys. A* **617** (1997) 496.
- [14] M. Urban, M. Buballa, R. Rapp and J. Wambach, *Nucl. Phys. A* **673** (2000) 357.
- [15] T. Feuster and U. Mosel, *Phys. Rev. C* **58** (1998) 457.
- [16] T. Feuster and U. Mosel, *Phys. Rev. C* **59** (1999) 460.
- [17] T.P. Vrana, S.A. Dytman and T.-S. H. Lee, *Phys. Rept.* **328** (2000) 181.
- [18] S. Kondratyuk and O. Scholten, *Nucl. Phys. A* **677** (2000) 396.
- [19] D.M. Manley and E.M. Saleski, *Phys. Rev. D* **45** (1992) 4002; *Phys. Rev. D* **30** (1984) 904.
- [20] M.F.M. Lutz and E.E. Kolomeitsev, *Nucl. Phys. A* **700** (2002) 193.
- [21] C. Itzykson and J.-B. Zuber, *Quantum field theory*, McGraw-Hill 1980.
- [22] S. Kamefuchi, L. O'Raifeartaigh and A. Salam, *Nucl. Phys. B* **28** (1961) 529.
- [23] S. Scherer and H.W. Fearing, *Phys. Rev. D* **52** (1995) 6445; H.W. Fearing and S. Scherer, *Phys. Rev. C* **62** (2000) 034003.
- [24] S. Weinberg, *Phys. Rev.* **166** (1968) 1568; *Physica* **96 A** (1979) 327.
- [25] J.J. Sakurai, *Currents and Mesons* (University of Chicago Press, Chicago, 1969).

- [26] N.M. Kroll, T.D. Lee and B. Zumino, Phys. Rev. **157** (1967) 1376.
- [27] E.C.G. Stueckelberg, Helv. Phys. Acta **11** (1938) 226.
- [28] C.D. Froggatt and J.L. Petersen, Nucl. Phys. **B 129** (1977) 89.
- [29] M. Gell-Man, D. Sharp and W.G. Wagner, Phys. Rev. Lett. **8** (1962) 261.
- [30] M.F.M. Lutz, Gy. Wolf and B. Friman, Nucl. Phys. **A 661** (1999) 526c; B. Friman, M. Lutz and G. Wolf, in Proc. of Int. Workshop XXVIII on Gross Properties of Nuclei and Nuclear Excitations, Hirschegg, Austria, January 16-22, 2000.
- [31] R.A. Arndt, R. Workman, Z. Li and L.D. Roper, Phys. Rev. **C 42** (1990) 1853.
- [32] R.L. Walker, Phys. Rev. **182** (1969) 1729.
- [33] R.G. Moorhouse, H. Oberlack and A.H. Rosenfeld, Phys. Rev. **D 9** (1974) 1.
- [34] C. Sauerman, B. Friman and W. Nörenberg, Phys. Lett. **B 341** (1995) 261.
- [35] O. Krehl, C. Hanhart, S. Krewald and J. Speth, Phys. Rev. **C 62** (2000) 025207.
- [36] F. James, MINUIT functional minimization and error analysis, Version 94.1, CERN Program Library Long Writeup D506, CERN (1994).
- [37] A.D. Brody *et al.*, Phys. Rev. **D 4** (1971) 2693.
- [38] J. Keyne *et al.*, Phys. Rev. **D 14** (1976) 28; H. Karami *et al.*, Nucl. Phys. **B 154** (1979) 503.
- [39] A. Baldini, *et al.*, in Landolt-Börnstein, Vol. 12a, (Springer, Berlin, 1988).
- [40] M. Post, W. Peters and U. Mosel, Talk given at the 'XXXV International Winter Meeting on Nuclear Physics', Jan 25 - 29 (1999), Bormio.
- [41] W. Langgärtner *et al.*, Phys. Rev. Lett. **87** (2001) 052001-1.
- [42] G. Penner and U. Mosel, nucl-th/0111023.
- [43] B. Friman and M. Soyeur, Nucl. Phys. **A 600** (1996) 477.
- [44] Aachen-Berlin-Bonn-Hamburg-Heidelberg-München Collaboration, Phys. Rev. **175** (1968) 1669.
- [45] R.A. Arndt *et al.*, Phys. Rev. **C 52** (1995) 2120.
- [46] SAID on-line program, <http://gwdac.phys.gwu.edu/>.
- [47] J. Caro Ramon, N. Kaiser, S. Wetzel and W. Weise, Nucl. Phys. **A 672** (2000) 249.
- [48] N. Kaiser, P.B. Siegel and W. Weise, Nucl. Phys. **A 594** (1995) 325; N. Kaiser, T. Waas and W. Weise, Nucl. Phys. **A 612** (1997) 297; J.C. Nacher *et al.*, Nucl. Phys. **A 678** (2000) 187.

- [49] C. Wilkin, Phys. Rev. **C 47** (1993) 938.
- [50] A.M. Green and S. Wycech, Phys. Rev. **C 55** (1997) 2167; nucl-th/0009053.
- [51] J. Nieves and E.R. Arriola, nucl-th/104307.
- [52] B. Krusche et al., Phys. Rev. Lett. **74** (1995) 3736.
- [53] M.Q. Tran et al. (SAPHIR Collaboration), Phys. Lett. **B 445** (1998) 20.
- [54] R.M. Brown et al., Nucl. Phys. **B 153** (1979) 89.
- [55] R.D. Baker et al., Nucl. Phys. **B 141** (1978) 29. R.D. Baker et al., Nucl. Phys. **B 141** (1978) 29.
- [56] G.E. Brown and D.O. Riska, Nucl. Phys. **A 679** (2001) 577.
- [57] M. Benmerrouche, N.C. Mukhopadhyay and J.F. Zhang, Phys. Rev. **D 51** (1995) 3237.
- [58] T. Feuster and U. Mosel, Nucl. Phys. **A 612** (1997) 375.
- [59] M. Bockhorst et al. (SAPHIR Collaboration), Z. Phys. **C 63** (1994) 37.
- [60] S. Goers et al. (SAPHIR collaboration), Phys. Lett. **B 464** (1999) 331.
- [61] D.J. Candlin et al., Nucl. Phys. **B 226** (1983) 1.
- [62] D.J. Candlin et al., Nucl. Phys. **B 238** (1984) 477.
- [63] M.L. Good and R.R. Kofler, Phys. Rev. **183** (1969) 1142.
- [64] R.D. Baker et al., Nucl. Phys. **B 145** (1978) 402.
- [65] Particle Data Tables, Eur. Phys. J. **C 15** (2000) 1.
- [66] F. Klingl, T. Waas and W. Weise, Nucl. Phys. **A 650** (1999) 299.
- [67] F. Klingl, N. Kaiser and W. Weise, Nucl. Phys. **A 624** (1997) 527.
- [68] M. Soyeur, M.F.M. Lutz and B. Friman, in Proc. of Int. Workshop XXVIII on Gross Properties of Nuclei and Nuclear Excitations, Hirschegg, Austria, January 16-22,2000.
- [69] W. Peters et al., Nucl. Phys. **A 632** (1998) 109.
- [70] W. Lenz, Z. Phys. **56** (1929) 778; C.D. Dover, J. Hüfner and R.H. Lemmer, Ann. Phys. **66** (1971) 248; M. Lutz, A. Steiner and W. Weise, Nucl. Phys. **A 574** (1994) 755.
- [71] M. Post, S. Leupold and U. Mosel, Nucl. Phys. **A 689** (2001) 753.
- [72] Y. Kim, R. Rapp, G.E. Brown and M. Rho, Phys. Rev. **C 62** (2000) 015202.
- [73] M. Post and U. Mosel, Nucl. Phys. **A 688** (2001) 808.
- [74] M.F.M. Lutz, Phys. Lett. **B 426** (1998) 12.

- [75] M.F.M. Lutz, in Proceeding "APCTP Workshop on Astro-Hadron Physics", Seoul, 25.- 31. Oktober 1997, World Scientific 1999, 560.
- [76] M.F.M. Lutz and C. Korpa, Nucl. Phys. **A** **700** (2002) 309.
- [77] C. Djalali, M. Kossow, D. Weygand, Jefferson Lab experiment E-01-112
- [78] V. Metag, Acta Phys. Pol. **B** **31** (2000) 197.
- [79] K. Ozawa et al., Phys. Rev. Lett. **86** (2001) 5019.
- [80] J.H. Koch, E.J. Moniz and N. Ohtsuka, Ann. Phys. **154** (1984) 99.